

Cost-Effective and Optimized Optical Networks Based on Point to Multipoint Transceivers



Mohammad Mohammad Hosseini

Aston Institute Of Photonic Technologies
Aston University

This thesis is submitted for the degree of
Doctor of Philosophy

August 2023

© Mohammad Mohammad Hosseini, 2023

This copy of the thesis has been supplied on condition that anyone who consults it is understood to recognise that its copyright belongs to its author and that no quotation from the thesis and no information derived from it may be published without appropriate permission or acknowledgement.

I am deeply honored to dedicate this thesis to pillars of my life: my parents, my loving wife, our precious daughter, Diana, and all other cherished family members.

Declaration

I hereby declare that except where specific reference is made to the work of others, the contents of this thesis are original and have not been submitted in whole or in part for consideration for any other degree or qualification in this, or any other university. This thesis is my own work and contains nothing which is the outcome of work done in collaboration with others, except as specified in the text and Acknowledgements.

Mohammad Mohammad Hosseini
August 2023

Acknowledgements

I would like to express my gratitude and appreciation to my academic supervisors, Professor Sergei K. Turitsyn, and Dr. Jaroslaw E. Prilepsky for providing me with the opportunity to pursue a Ph.D. degree in a dynamic, and joyful atmosphere.

I also would like to thank my industry mentors, Dr. Joao Pedro, Dr. Antonio Napoli, and Dr. Nelson Costa for their invaluable help and support during my research. Their expertise and dedication have been instrumental in shaping my academic and personal growth.

I am deeply grateful to Aston University and the EU Horizon 2020 program (REAL-NET project) for their generous funding of my Ph.D., as well as to Infinera, Lisbon for kindly hosting me as an intern.

Finally, I want to express my sincere appreciation to my inspiring twin brother, Ali Mohammad Hosseini, all friends, and colleagues at Aston University.

Abstract

The rapid increase in internet traffic due to widespread internet access and technological advancements such as 5G, cloud computing, Internet of Things (IoT), and virtual reality has created a complex environment for network operators and internet service providers. To ensure profitability and improve user experience, these entities need to implement long-term strategies that optimize network planning, cost, and efficiency. These strategies should consider market demands, evolving technologies, and prioritize resource utilization, customer expansion, service quality, and cost reduction. The thesis mainly focuses on network design and optimization. It begins with a concise introduction to optical transport network elements and the primary motivations for networking. The use of dense wavelength division multiplexing (DWDM) systems is described, along with the conventional network problems associated with routing and wavelength assignment, as well as routing and spectrum assignment. The thesis also includes a brief discussion on the power consumption of the Internet, with a particular focus on routers as power-hungry network components. Next, the thesis delves into the digital subcarrier multiplexing point-to-multipoint (P2MP) transceiver, explaining its architecture and function. Several optimization frameworks based on integer linear Programming (ILP) are proposed to effectively deploy P2MP transceivers in both filtered and filterless scenarios. Different protection scenarios are also explored. Furthermore, the thesis investigates a comprehensive multi-period planning scenarios that take into account evolving traffic and transceiver technology. The results demonstrate that P2MP transceivers can reduce transceiver costs by up to 35% compared to traditional point-to-point transceivers. Finally, the thesis presents a comprehensive and optimized physical design for horseshoe networks, integrating the utilization of P2MP transceivers and a filterless architecture. This design approach offers a simplified and cost-effective solution while leveraging the savings offered by P2MP technology.

Table of contents

List of figures	xv
List of tables	xix
Nomenclature	xxi
1 Introduction	1
1.1 Optical Transport Networks	1
1.2 Motivation	4
1.3 Thesis Outline and Contributions	5
2 Network Resource Allocation and Optimization Methods	9
2.1 Introduction	9
2.2 A Brief History of DWDM Systems and Their Features	9
2.3 Optical Transport Network	11
2.4 Flex-grid DWDM Systems	11
2.5 Combinatorial Optimization	12
2.5.1 Minimum Cost Flow Problem	13
2.5.2 Simplex Method	14
2.5.3 Simplex Method Time Complexity	19
2.5.4 Integer Linear Programming Solving methods	20
2.6 Evolutionary Optimization Algorithms	21
2.6.1 Genetic Algorithms	22
2.7 Filterless Networks	24
2.8 Monte Carlo Simulations	25
2.9 Routing and Wavelength Assignment Analysis	25
2.9.1 Results and Discussions I	26
2.10 Routing and Spectrum Assignment	29
2.11 Routing Modulation Format and Spectrum Assignment	30

2.11.1	Network Scenario and Genetic Algorithm Formulation	31
2.11.2	Results and Discussion II	33
2.12	Power Consumption of the Internet	34
2.12.1	Network Power Consumption	35
2.12.2	Power consumption modelling	37
2.13	Conclusion	38
3	Point to Multipoint Communication	39
3.1	Introduction	39
3.2	Optical Transceiver Modules Evolution	40
3.3	Optical Transponder	42
3.4	Sliceable Bandwidth Variable Transponder	42
3.5	Digital Subcarrier Multiplexing Point to Multipoint Transceivers	44
3.5.1	Transceiver Architecture	45
3.6	Network Application Scenarios	46
3.7	P2MP Transceivers Deployment in ROADM-based Meshed Networks	47
3.7.1	Survivable Network Scenarios	47
3.7.2	Optimization Framework	49
3.7.3	Transceivers Cost Model	53
3.7.4	Results and Discussion I	53
3.8	Optimized Deployment of P2MP Transceivers in Filterless Networks	57
3.8.1	Survivability in Filterless Networks	58
3.8.2	ILP Optimization Framework	60
3.8.3	Results and Discussion II	63
3.9	Conclusion	68
4	Multi-period Planning Using Point to MultiPoint Transceivers	71
4.1	Introduction	71
4.2	Technology Evolution	72
4.3	Internet Traffic Characteristics	72
4.4	Long-term Cost-effectiveness of Point to Multipoint Transceivers	73
4.4.1	Optimization Framework	73
4.4.2	Results and Discussion I	76
4.5	Multiperiod Planning Scenarios	78
4.5.1	Optimization Framework	79
4.5.2	Results and Discussion II	82
4.6	Conclusion	86

5	Horseshoe Architecture For Point-to-Multipoint Transceivers Deployment	87
5.1	Introduction	87
5.2	Horseshoe Topology	88
5.3	Filterless Networks	89
5.3.1	Protection	90
5.3.2	Semi-Filterless Architectures	92
5.4	Optical Splitters/Combiners Technologies	93
5.5	Filterless Horseshoe Architecture	94
5.5.1	Link Length Statistical Model	96
5.5.2	Optimization Framework	97
5.5.3	Results and Discussion	100
5.5.4	Optical Signal to Noise Ratio	102
5.5.5	Constrained-Optimization Framework	105
5.5.6	Genetic Algorithms for Constrained-Optimization	106
5.6	Results and Discussion	109
5.7	Conclusion	112
6	Conclusion and Future Works	113
6.1	Review of Thesis	113
6.2	Future Work Direction	114
	References	119
	Appendix A How to Formulate ILP Problems Using GAMS	133
A.1	What is GAMS	133
A.2	Minimum Spanning Tree Problem	133
A.3	ILP formulation Using GAMS	134
A.4	Integer Linear Programming Techniques	137
A.4.1	sets	137
A.4.2	Variables	138
A.4.3	Constraints	138
A.4.4	Objective Function	139
A.5	Connecting MATLAB and GAMS	139

List of figures

1.1	A WDM link multiplexing five channels.	2
1.2	(a) A full meshed network comprising 5 nodes and 10 links and (b) a partially meshed network with 5 nodes and only 5 links.	2
1.3	The hierarchy architecture of current Internet infrastructure from access networks to core networks.	4
2.1	Conversion of different protocols to OTN protocol by a muxponder	11
2.2	Fixed grid DWDM system with (a) 100 GHz spacing and (b) 50 GHz spacing and (c) flex grid DWDM system with 12.5 GHz spacing.	12
2.3	A network of supply and demand nodes connected by a number of links with certain amount of capacity.	14
2.4	Graphical illustration of the an LP problem.	16
2.5	Graphical illustration of (a)Simplex, (b)Ellipsoid and (c)Interior point method for an IL problem.	20
2.6	Process of the first iteration of GA optimization starts with creating an initial population, then followed by cross-over, and ends with mutation.	23
2.7	NSFNET network	27
2.8	Blocking ratio of NSFNET network using ILP versus number of needed wavelength.	28
2.9	Blocking Ratio of RWA problem using shortest path and (a) First Fit and (b) Random Fit in NSFnet network.	29
2.10	(a) Blocking ratio of EON28 network using random ordering, shortest path, and first fit heuristic versus the number of needed wavelengths and (b) Network congestion in terms of used wavelength when the number requested wavelengths is 756 wavelengths.	30
2.11	Illustrative example of RSA in a 5-node network with 3 traffic demands.	31
2.12	Bandwidth-hop blocking ratio for three different heuristics, two-step GA and GA for ordering with and without using heuristics (a) $k = 2$, (b) $k = 3$	34

2.13	Routers power consumption in different capacities from three major producers.	38
3.1	(a) A tree Vs (b) a full meshed network connecting 5 nodes	40
3.2	A typical transceivers module with its sub-systems [1]	41
3.3	Nyquist Vs OFDM in time and frequency domains [2]	43
3.4	Optical transponder function evolution. [3]	44
3.5	DSCM P2MP transmitter architecture [4].	45
3.6	DSCM P2MP receiver architecture (note that Digital freq. Mux refers to Digital freq. DeMux). [4]	46
3.7	Implementation of communication links with (a) identical P2P transceivers, (b) P2MP transceivers deployment in a ring network, and (c) in a meshed network (dashed lines show logical connections while highlighted paths show optical paths) ([C2] © 2021 IEEE).	48
3.8	Illustration of the five network scenarios considered in this work over a reference mesh network: (a) single hub (SH), (b) single hub with link protection (SH-LP), (C) multi-hub (MH), (d) multi-hub with link protection (MH-LP), and (e) multi-hub with the link and hub protection (MH-LHP) ([C2] © 2021 IEEE).	50
3.9	Visual representation of cost profile versus data rate and possible cost decrease compared to linear cost scale.	53
3.10	Normalized interface cost calculated for SH scenario when the number of shortest paths increases from 1 to 8 ([C2] © 2021 IEEE).	55
3.11	Normalized interface cost ([C2] © 2021 IEEE).	56
3.12	Number of interfaces at the hub node(s) ([C2] © 2021 IEEE).	57
3.13	(a) P2P transceivers deployment using active ROADMs, (b) P2P transceivers deployment using passive optical splitters/combiners, (c) P2MP transceivers deployment using passive optical splitters/combiners (with permission from [J1] ©Optica Publishing Group).	59
3.14	(a) Topology A and (b) topology D defined by Telefónica (with permission from [J1] ©Optica Publishing Group).	64
3.15	(a) Normalized P2MP transceiver cost for topology A and corresponding savings compared to P2P approach, and (b) normalized P2MP transceiver cost for topology D and corresponding savings compared to P2P approach for optimistic cost profile (with permission from [J1] ©Optica Publishing Group).	66

3.16	Example of (a) working and (b) protection trees computed for topology A (with permission from [J1] ©Optica Publishing Group).	67
3.17	(a) Normalized P2MP transceiver cost for topology A and corresponding savings compared to the P2P approach, and (b) normalized P2MP transceiver cost for topology D and corresponding savings compared to the P2P approach for the conservative cost profile (with permission from [J1] ©Optica Publishing Group).	69
3.18	Normalized transceiver costs for different hub locations in topology A (with permission from [J1] ©Optica Publishing Group).	70
3.19	Number of P2P and P2MP transceivers in protected scenario versus traffic loads for topology A and optimistic cost profile (with permission from [J1] ©Optica Publishing Group).	70
4.1	Cost of transceivers deployed at (a) the hub and (b) the leaf nodes versus average traffic loads ([C5] © 2022 IEEE).	77
4.2	P2MP transceiver savings compared to (a) 100G P2P and (b) the combination of 100G and 400G P2P transceivers versus average traffic loads ([C5] © 2022 IEEE).	78
4.3	(a) P2MP transceiver cost for all-period, extended-period, and single-period planning, and (b) the amount of savings compared to the corresponding P2P transceiver approaches (with permission from [J2] © Optica Publishing Group).	84
4.4	(a) Cost reduction of the movable transceiver approach compared to unmovable transceivers for different planning strategies and (b) their number of visits to the leaf nodes (with permission from [J2] © Optica Publishing Group).	85
4.5	OpEx vs. CapEx relation in unmovable all-period planning for four traffic sets (with permission from [J2] © Optica Publishing Group).	86
5.1	Dual-band MAN with filtered C-band and filterless unamplified L-band [5].	88
5.2	Illustrative example of constructing two trees on top of 6-node topology or accommodating 5 demands [6].	89
5.3	4-node and 5-node topologies with their illustrative examples of two spanning trees.	91
5.4	An illustrative example of node 2 architecture in Fig. 5.2: (a) in the conventional ROADM network, (b) in the passive filterless network, and (c) node 3 and node 4 in the white box-based programmable filterless network architecture [6].	92
5.5	Technologies used for constructing optical couplers [7].	93

5.6	A 1 by 2 coupler made by a 2 by 2 coupler [8].	94
5.7	Illustration of DSCM-based P2MP transceiver in horseshoe topology using passive optical splitters/combiners (with permission from [J3] © Optica Publishing Group).	95
5.8	Log-normal distribution fitting the length of optical links from real networks (with permission from [J3] © Optica Publishing Group).	96
5.9	Minimum number of amplifiers and maximum power difference of SCs at Hub 2 Rx versus set of candidate splitter/combiner types used in horseshoe network with (a) 5 leaf nodes and (b) 10 leaf nodes (with permission from [J3] © Optica Publishing Group).	101
5.10	Characterization of losses and gains for an optimized instance of 10-leaf node network (optical fiber link directed from Hub1 to Hub2) for (a) Scenario1 and (b) Scenario4 (with permission from [J3] © Optica Publishing Group).	102
5.11	Average OSNR of signals from Hub 1 to leaf nodes and in 10-leaf horseshoe networks in different scenarios (with permission from [J3] © Optica Publishing Group).	104
5.12	Flowchart of the proposed GA.	108
5.13	Biased crossover approach, where one parent is an elite individual and the offspring inherits a greater number of genes from this parent [9].	109
5.14	(a) Average number of amplifiers using the ILP model and GA for three different splitters/combiners scenarios and 16-quadrature amplitude modulation (QAM) format, and (b) evolution of the fitness of the best individual of each generation and its components; objective-related term and the penalty for a single problem instance of Scenario1 ([C8] © 2023 IEEE).	111
5.15	(a) Average number of amplifiers for 50 networks optimized by the GA considering 8-QAM, 16-QAM and 32-QAM and (b) the average maximum DSC power difference ([C8] © 2023 IEEE).	112
A.1	An undirected graph and its MST	134

List of tables

2.1	Alcohol percentage and price of two different drinks.	16
2.2	The first tableau.	17
2.3	The second tableau.	18
2.4	The third tableau.	18
2.5	The fourth tableau.	19
2.6	Different heuristic approaches regarding request order, routing, and wave-length assignment for solving RWA problems.	28
2.7	(a) Demand characterization for a simple 4-node network, and (b) BBR and BHBR for two different demands ordering instances.	32
2.8	(a) Overview of the GA approach and (b) value of different GA parameters.	33
3.1	Input parameters of the ILP model	50
3.2	Decision variables of the ILP model	51
3.3	Scenarios based on auxiliary variables s_1 and s_2 values.	52
3.4	Total number of interfaces for a traffic load with an average of $4 \times 25\text{Gb/s}$ and their total costs for different scenarios ([C2] © 2021 IEEE).	56
4.1	Transceiver cost per data rate type (assuming $A = \frac{1}{4}$, $B = \frac{1}{2}$) ([C5] © 2022 IEEE)	73
4.2	Transceiver data rate scenarios ([C5] © 2022 IEEE).	76
4.3	Relative transceiver cost per data rate by year without considering cost discount (with permission from [J2] © Optica Publishing Group).	82
4.4	Number of transceivers added per type at leaf nodes in unmovable and movable transceivers approaches (with permission from [J2] © Optica Publishing Group).	85
5.1	List of 1:2 splitters/combiners as well as ports insertion losses in dB in ideal and realistic cases (with permission from [J3] © Optica Publishing Group).	100

5.2	Usage probability of the different splitter/combiner types in 10-leaf horseshoe networks obtained by 100 simulation (with permission from [J3] © Optica Publishing Group).	102
5.3	Average and standard deviation of the ILP model solving time for the Scenario1 and networks with 5, 10, and 15 leaf nodes (with permission from [J3] ©Optica Publishing Group).	105
5.4	Network parameters and their corresponding values considered in this study ([C8] © 2023 IEEE).	110
5.5	GA parameters and their corresponding values considered in this paper ([C8] © 2023 IEEE).	110

Nomenclature

Acronyms / Abbreviations

ACO Ant Colony Optimization

ASE Amplified Spontaneous Emission

BBR Bandwidth Blocking Ratio

BFS Breadth-first search

BHBR Bandwidth-Hob Blocking Ratio

BVT Bandwidth Variable Transponder

CapEx Capital Expenditure

CD Chromatic Dispersion

D&W Drop-and-Waste

DAC Digital to Analog Converter

DFS Depth-first search

DSCM Digital Subcarrier Coherent Multiplexing

DSP Digital Signal Processing

DWDM Dense Wavelength Division Multiplexing

EA Evolutionary Algorithm

EDFA Erbium-Doped Fiber Amplifier

FMN Filterless Metropolitan Network

FOADM	Fixed Optical Add/Drop Multiplexer
GA	Genetic Algorithm
ICT	information and communication technolog
ILP	Integer Linear Programming
IM-DD	Intensity Modulation Direct Detection
IoT	Internet of Things
ISP	Internet Service Provider
ITU	International Telecommunication Union
LPF	Longest Path First
LP	Linear Programming
MFD	Mode Field Diameter
MFD	Mode-Field Diameter
MILP	Mixed Integer Linear Programming
MSF	Most Spectrum First
MST	Minimum Spanning Tree
NWDM	Nyquist Wavelength Division Multiplexing
OFDM	Orthogonal Frequency Division Multiplexing
OpEx	Operational Expense
OTN	Optical Transport Network
OXC	Optical Cross Connect
P2MP	Point to Multipoint
P2P	Point to point
PON	Passive Optical Network
PSO	Particle Swarm Optimization

-
- QAM Quadrature Amplitude Modulation
- QPSK Quadrature Phase Shift Keying
- RMSA Routing, Modulation Format and Spectrum Assignment
- ROADM Re-configurable Add-Drop Multiplexers
- RSA Routing and Wavelength Assignment
- RWA Routing and Wavelength Assignment
- S-BVT Sliceable Bandwidth Variable Transponder
- SC Subcarrier
- SDM Spatial Division Multiplexing
- SE Spectral Efficiency
- SLA Service Level Agreement
- SP Shortest Path
- SSS Spectrum Selective Switch
- WDM Wavelength Division Multiplexing
- WSS Wavelength Selective Switch

Chapter 1

Introduction

1.1 Optical Transport Networks

Internet traffic demands are increasing at a rate between 25% and 80% [10]. The key factors driving such a steady and sharp increase are the Internet of Things (IoT), enhanced video calling, cloud applications, 5G development, and industry 4.0. The total number of IoT connections is forecasted to double between 2019 and 2025, reaching 24 billion [11]. Data transport networks play an essential role in the age of data by connecting data sources to data consumers. These networks try to deliver data as cheaply as possible and the highest quality of service hand-in-hand to the intended destination using unique hierarchies and architectures.

Optical fibers benefit from a substantial optical frequency spectrum and carry most of the internet traffic. This became possible due to several significant breakthroughs in managing optical fiber loss and optical spectrum. For instance, optical fibers' loss has decreased to as low as 0.2 dB/km. On the other hand, Erbium-Doped Fiber Amplifier (EDFA) was born in 1986, which makes long communication links possible. Electronic devices usually have far less bandwidth than C-band optical fiber spectrum (4.4 THz). With the advent of Coherent technology and Wavelength Division Multiplexing (WDM), the optical spectrum could be sliced into small partitions, each forming an independent optical channel. Dense Wavelength Division Multiplexing (DWDM) is the next generation of WDM technology, utilizing more channels. Besides, coherent transmission enables the use of higher modulation formats such as 16-QAM and QPSK. Figure 1.1 shows a single-direction point-to-point WDM link that multiplexes five wavelengths (channels) at the transmission side and demultiplexes at the end of the optical link. For interconnecting WDM links and building networks, standards and protocols are needed. International Telecommunication Union (ITU) regulates the standards

required for WDM links. For instance, initially, they divided the C-band spectrum into 40 channels with 100 GHz bandwidth each.

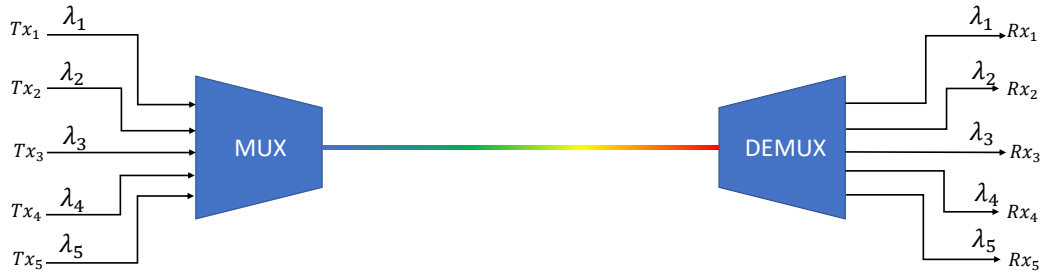


Fig. 1.1 A WDM link multiplexing five channels.

One of the networks primary goals is to interconnect some sites with minimum resources. In other words, a network facilitates sharing available resources between requested demands, and as a result reducing the total cost. However, it increases the complexity of design and management. Take Fig. 1.2(a) as an example; five nodes are connected with ten links (we describe networks using graph representation). Between each node pair, a direct link exists. This network is called a full-meshed network. Most of the time, there are better solutions for network planning. The network depicted in Fig. 1.2(b) has five links. Therefore, optical links must be shared between different source-destination connections. Note that the number of links increases exponentially with the number of nodes in full-meshed networks.

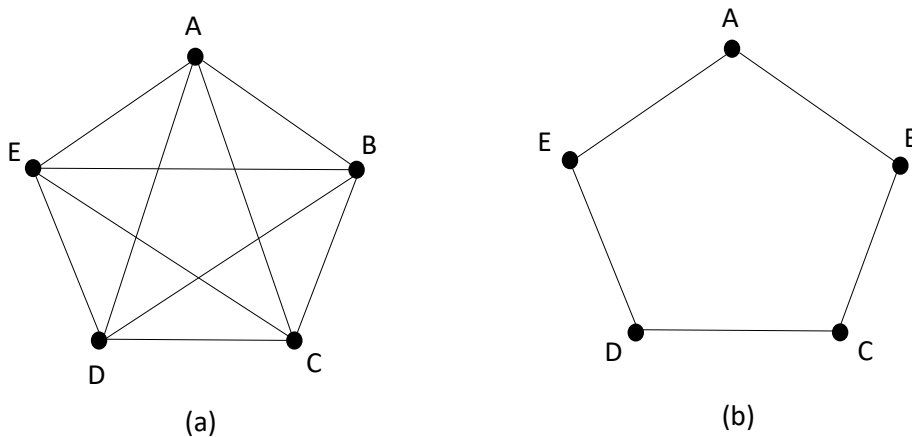


Fig. 1.2 (a) A full meshed network comprising 5 nodes and 10 links and (b) a partially meshed network with 5 nodes and only 5 links.

Network planning is accommodating traffic demands using the least resources while meeting the required quality conditions. The main challenges in network planning are:

- Evolution of technology,
- Dealing with legacies,
- Resource limitation,
- Unforeseen future (traffic growth uncertainty),
- Environmental issues (carbon footprint).

Technologies that are used in optical networks are changing consistently. For instance, spatial division multiplexing (SDM) and multiband technologies have received increasing attention and might be deployed widely soon. New technologies often need to be backward compatible in most cases, like brownfield planning, where an already deployed network is expected to be upgraded. Capital expenditure (CapEx), operational expenses (OpEx), spectrum, and fiber infrastructures must be carefully managed because they are scarce. In addition, uncertainty in the future adds difficulties to network planning. A notable example is uncertainties in future traffic demands. Besides, designs should be environmentally-friendly. Power consumption of the internet is one of the most concerning barriers to current and future internet growth. Based on an optimistic prediction [12], information and communication technology (ICT) can consume 8% of global electricity by 2030, while it may use up to 21% in the worst-case scenario.

As depicted in Fig 1.3, today's central Internet infrastructure can be considered mesh networks that connect various regions globally using unique networking protocols. The network nodes are connected with certain types of medium for the appropriate transport technology in each network domain. In fact, each network segment may have its own specific structure primarily based on the amount of traffic it carries and the historical evolution of technologies. The information is encrypted and modulated before being switched and routed toward the final destination. The core network is responsible for connecting major cities and countries, while metro networks usually provide connections inside cities. The IP layer and the optical layer are the two layers that make up the IP-over-WDM [13] network, as can be seen in Fig 1.3. A core IP router combines data traffic from low-end access routers at the IP layer and links to an optical switch node through short-reach interfaces. The optical layer provides the capacity needed for IP routers' communication. Each optical link may comprise many optical fibers that connect optical switch nodes. Access networks, which often are the closest segments to the customers, usually are in a passive form and are called passive optical networks (PON) [14].

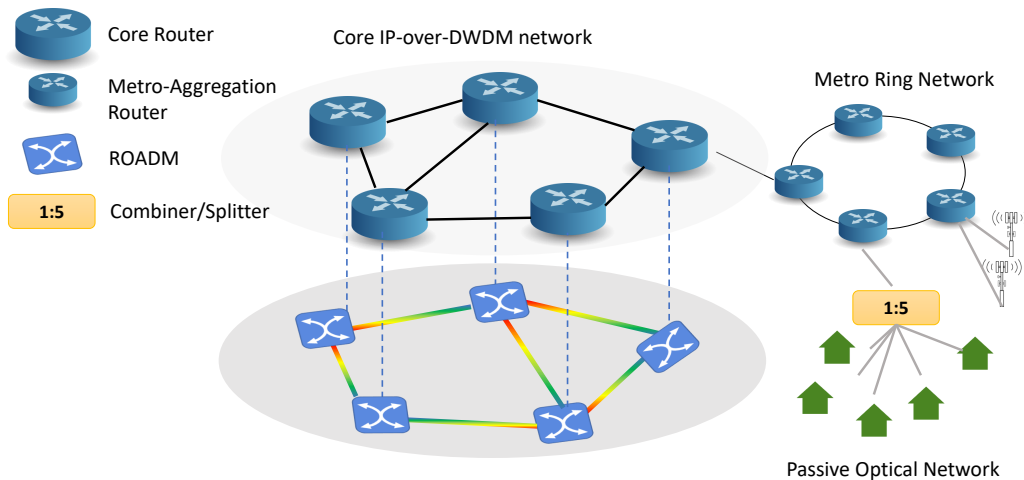


Fig. 1.3 The hierarchy architecture of current Internet infrastructure from access networks to core networks.

1.2 Motivation

As long as the decline in the underlying unit costs of carrying the internet traffic is faster than the increase in traffic, the internet traffic demand growth will likely continue. The telecommunication industry, directly and indirectly, contributes to the economy globally. For instance, only the mobile ecosystem generated about \$1.1 Trillion economic value in 2021 [15]. This cost decrease can be achieved by technological advances in individual components and deployment in cost-efficient scalable ecosystems. The leading network planning objectives can be maximizing network utilization, improving network operations, and eliminating complexity. Although ICT can bring economic growth, it likely has environmental effects that must be managed. In [16], links between economic growth, power consumption, and environmental damage are investigated for the Kingdom of Saudi Arabia from 1980 to 2019.

An effective cost-saving strategy involves resource sharing using Point-to-multipoint transceivers. They have the ability to share a single optical channel among multiple endpoints, simplifying network architectures management.

1.3 Thesis Outline and Contributions

The thesis's main technical contribution is presented in Chapters 2, 3, 4, and 5, and the thesis is concluded in Chapter 6. The following sections outline the thesis's organization and highlight the structure of each chapter at a high level.

- Chapter 2 provides a short introduction to optical network architectures such as DWDM systems. Some essential mathematics tools for network optimization, such as integer linear programming and genetic algorithms, are described. Next, some fundamental but important optical network problems are analyzed using these methods. Finally, power consumption, which directly affects the environment and operational expenses, is briefly discussed.
- Chapter 3 describes point-to-multipoint (P2MP) communication and its key enablers. A newly developed P2MP transceiver based on digital subcarrier multiplexing is introduced. Different network scenarios for deploying this transceiver are then defined and analyzed through extensive integer linear programming optimization (my published papers used in this chapter: [J1][C2]).
- Chapter 4 is dedicated to addressing the crucial problem of multi-period planning using P2MP transceivers. Technology evolution, price erosion, and Internet traffic characteristics are considered since these are critical to planning an optimized network for today and tomorrow. Additionally, the long-term cost-effectiveness of P2MP transceivers is addressed (my published papers used in this chapter: [J2][C5]).
- Chapter 5 goes to a more profoundly physical network design problem. We provide several details of passive filterless networks since these networks are cost-efficient for access and metro-aggregation networks. Next, we design and optimize filterless horseshoe networks supporting P2MP transceivers considering several real network constraints to obtain realistic solutions (my published papers used in this chapter: [J3][C8]).
- Chapter 6 concludes the thesis and suggests paths towards future research.

The main parts of my thesis draws from my original research published in IEEE conferences C1 to C8 and OPTICA journals J1 to J3. I served as the primary author for these papers and made the predominant contributions, including the development of codes and generation of results. However, the collaborative brainstorming with co-authors was pivotal in shaping the ideas, and revising the papers.

Conference papers:

- C1 M. M. Hosseini, J. Pedro, N. Costa, A. Napoli, J. E. Prilepsky and S. K. Turitsyn, "Optimized Design of Metro-Aggregation Networks Exploiting Digital Subcarrier Routing," 2021 Asia Communications and Photonics Conference (ACP), 2021, pp. 1-3.
- C2 M. M. Hosseini, J. Pedro, A. Napoli, N. Costa, J. E. Prilepsky and S. K. Turitsyn, "Design of Survivable Metro-Aggregation Networks based on Digital Subcarrier Routing," 2021 IEEE Global Communications Conference (GLOBECOM), 2021, pp. 1-6, doi: 10.1109/GLOBECOM46510.2021.9685219.
- C3 M. M. Hosseini, J. Pedro, A. Napoli, N. Costa, J. E. Prilepsky and S. K. Turitsyn, "Optimization of Survivable Filterless Optical Networks Exploiting Digital Subcarrier Multiplexing," ICC 2022 - IEEE International Conference on Communications, 2022, pp. 5731-5736, doi: 10.1109/ICC45855.2022.9838887.
- C4 M. M. Hosseini, J. Pedro, N. Costa, A. Napoli, E. P. Jaroslaw and S. K. Turitsyn, "Optimized Physical Design of Metro Aggregation Networks using Point to Multipoint Transceivers," 2022 Optical Fiber Communications Conference and Exhibition (OFC), 2022, pp. 01-03.
- C5 M. M. Hosseini, J. Pedro, A. Napoli, N. Costa, J. E. Prilepsky and S. K. Turitsyn, "Long-Term Cost-Effectiveness of Metro Networks Exploiting Point-to-Multipoint Transceivers," 2022 International Conference on Optical Network Design and Modeling (ONDM), 2022, pp. 1-6, doi: 10.23919/ONDM54585.2022.9782846.
- C6 M. M. Hosseini, J. Pedro, N. Costa, A. Napoli, J. E. Prilepsky and S. K. Turitsyn, "Multi-period Planning in Metro-Aggregation Networks using Point-to-Multipoint Transceivers," GLOBECOM 2022 - 2022 IEEE Global Communications Conference, Rio de Janeiro, Brazil, 2022, pp. 2921-2926, doi: 10.1109/GLOBECOM48099.2022.10001405.
- C7 M. M. Hosseini, J. Pedro, N. Costa, A. Napoli, J. E. Prilepsky and S. K. Turitsyn, "Optimal Design of Filterless Horseshoe Networks Supporting Point-to-Multipoint Transceivers," 2023 Optical Fiber Communications Conference and Exhibition (OFC), San Diego, CA, USA, 2023, pp. 1-3, doi: 10.1364/OFC.2023.W2A.16.
- C8 M. M. Hosseini, J. Pedro, A. Napoli, N. Costa, J. E. Prilepsky and S. K. Turitsyn, "Meta-Heuristic Framework for Designing Filterless Horseshoe Networks with P2MP Transceivers," 2023 Photonics in Switching and Computing (Oral Presentation).

Journal papers:

- J1 M. M. Hosseini, J. Pedro, A. Napoli, N. Costa, J. E. Prilepsky and S. K. Turitsyn, "Optimization of survivable filterless optical networks exploiting digital subcarrier multiplexing," in *Journal of Optical Communications and Networking*, vol. 14, no. 7, pp. 586-594, July 2022, doi: 10.1364/JOCN.451182.
- J2 M. M. Hosseini, J. Pedro, A. Napoli, N. Costa, J. E. Prilepsky and S. K. Turitsyn, "Multi-period planning in metro-aggregation networks exploiting point-to-multipoint coherent transceivers," in *Journal of Optical Communications and Networking*, vol. 15, no. 3, pp. 155-162, March 2023, doi: 10.1364/JOCN.475902.
- J3 M. M. Hosseini, J. Pedro, A. Napoli, N. Costa, J. E. Prilepsky and S. K. Turitsyn, "Optimized design of filterless horseshoe networks exploiting point-to-multipoint coherent transceivers," in *Journal of Optical Communications and Networking*, vol. 15, no. 9, pp. 569-578, September 2023, doi: 10.1364/JOCN.494342.

Chapter 2

Network Resource Allocation and Optimization Methods

2.1 Introduction

The current network infrastructure is facing significant challenges as a result of the rapidly growing demand for bandwidth across all international networks and the emergence of new services and applications. To meet these high bandwidth requirements, metro and core networks have been designed with the capability to handle large amounts of data. When planning networks, it is essential to use optical fibers and optical bandwidth resources wisely, as they are the primary means for transmitting large amounts of data. Additionally, power consumption is one of the biggest expenses in network operations.

In this chapter, we start by examining the Routing and Wavelength Assignment (RWA) problem, which is a central issue in the design of DWDM optical networks. Next, we will discuss more common problems such as Routing and Spectrum Assignment (RSA) and Routing, Modulation Format, and Spectrum Assignment (RMSA), which are encountered in flex-grid optical networks. This section of the chapter will provide an overview of these types of networks. To address these problems, we will provide a firm background on several widely used heuristics and Integer Linear Programming (ILP).

2.2 A Brief History of DWDM Systems and Their Features

During the mid-1990s, network infrastructure providers developed WDM optical networks due to the rising Internet traffic [17], the need for high bandwidth service, and the lower cost of constructing new MPLS or SONET/SDH networks. As seen in fig. 1.1, WDM is

a multiplexing technique that enables numerous optical signals of various wavelengths to be multiplexed into a single optical fiber. Hence, fewer fiber links can handle a certain amount of traffic. However, switching devices are needed to guide each wavelength from its source to its destination when WDM links connect several nodes. Reconfigurable Add-Drop Multiplexers (ROADM) do wavelength-switching functions. ROADMs help to prevent optical-to-electrical-to-optical (O-E-O) conversions as much as possible by adding or dropping the correct wavelength and guiding the remaining in the best directions. Switching devices add complexity and some cost to the networks but can save CapEx in other aspects. Different ROADMs are categorized based on their capabilities in [18].

DWDM system refers to the multiplexing method within the C-band (1530 nm - 1565 nm) and L-band (1565 nm - 1625 nm) described as per ITU-T G.694.1 which is the denser version of WDM systems [19]. Traditionally, C-band is the first choice as optical fibers have the minimum loss in this band. First, it was sliced into 40 channels of 100 GHz, and then with improvement in underlying technologies, it increased to 80 channels of 50 GHz. Three types of DWDM networks have historically existed [20, 21]:

- The transparent optical network, in which all signals are routed optically,
- The opaque optical network, in which all switching nodes experience O-E-O,
- The translucent optical network is a mixture of the former types.

In both translucent and opaque optical networks, the signal is first received and transformed into the electronic domain in all or some intermediate nodes before being modulated into the optical domain. These O-E-O enabled nodes are referred to as repeaters or regenerators, and a 3R regenerator may perform operations including wavelength conversion, modulation format adaption or re-amplification, reshaping, and re-timing.

The optical spectrum is a rare resource nowadays, unlike in the early days of DWDM systems when it was believed that an optical fiber's bandwidth was endless. As a result, the industry is now looking for ways to increase the total spectrum efficiency. Through the use of coherent detection methods and Nyquist pulse shaping, optical communications may now be sent at speeds of up to 100 Gb/s across as little as 33 GHz channels, reducing the amount of spectrum they occupy. Increasing the single carrier bit rate beyond 100 Gb/s requires using higher order QAM—for example, 16-QAM doubles the bit rate compared to QPSK and hence provides 200 Gb/s capability. However, these higher QAM formats only work over shorter transmission distances. One way to implement higher rate channels, such as 400 Gb/s and 1 Tb/s is by adopting multi-carrier signals with at least the same symbol rate as 100 Gb/s signals. As an instance, a 400 Gb/s channel can be achieved with two 16-QAM-modulated

sub-carriers (200 Gb/s each), each in 37.5 GHz, for a total of 75 GHz bandwidth; and a 1 Tb/s channel can be obtained with four 32-QAM modulated sub-carriers, each within 43.75 GHz, for a total bandwidth of 175 GHz. This implementation's first consequence is the need for larger channel spacing, breaking the standard 50 GHz grid per channel policy [22].

2.3 Optical Transport Network

Optical Transport Network (OTN) is a standard telecommunication protocol outlined in some ITU Recommendations, including G.709 and G.798 [23]. OTN offers an effective method for transporting, switching, and multiplexing various services onto high-capacity wavelengths (DWDM systems) over the optical network. The services like IP, Ethernet, storage, digital video, and SONET/SDH can be carried across an OTN framing structure (Fig. 2.1). Usually, muxponders do this conversion. OTN protocol is the dominant type of data in metro and core networks.

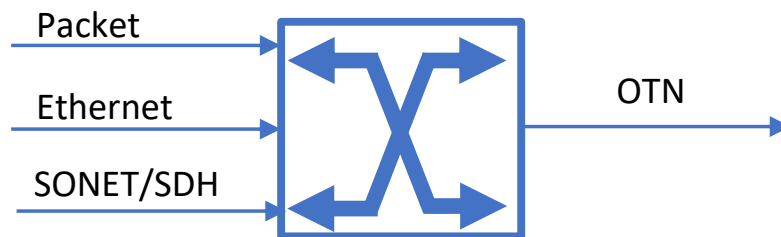


Fig. 2.1 Conversion of different protocols to OTN protocol by a muxponder

2.4 Flex-grid DWDM Systems

In conventional fixed-grid optical networks, it is unlikely that data rates larger than 100 Gb/s fit into the 50 GHz channel [24]. The 100 GHz grid also has its disadvantages. For instance, a large part of the spectrum is wasted when the data rate is low. Flexible and adaptive networks with flexible transceivers and network components that can adjust to actual traffic demands are required to solve these problems effectively. One possible solution

is using 12.5 GHz or 6.75 GHz spacing channels and letting lightpaths use a set of these frequency slots (FS) [19]. Figure. 2.2(a) depicts an illustrative example of a 100 GHz fixed grid DWDM system where a large part of the channel assigned to the blue signal is wasted. The 50 GHz fixed grid network shown in Fig. 2.2(b) cannot support wide spectrum signals, while the 12.5 GHz flex grid system can accommodate both signals with minimum spectrum waste. The flex grid network can create channels of different sizes using Orthogonal Frequency Division Multiplexing (OFDM) technology or exploiting state-of-the-art software-configurable interfaces that support multiple symbol rates (e.g., from around 30 up to 100 Gbaud) [25].

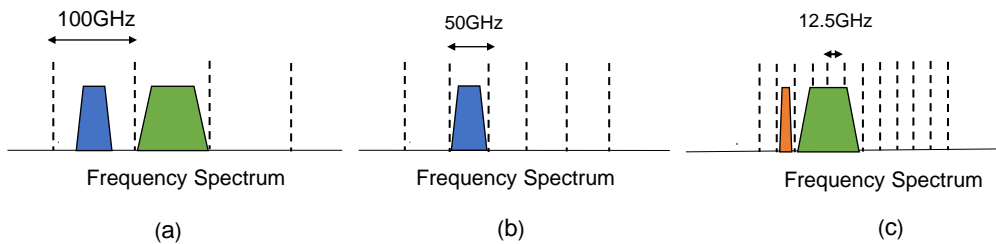


Fig. 2.2 Fixed grid DWDM system with (a) 100 GHz spacing and (b) 50 GHz spacing and (c) flex grid DWDM system with 12.5 GHz spacing.

While Flex grid optical networks have tremendous advantages, they present technology challenges at both network and node levels, such as flexible spectrum allocation, network control and management scheme, high-resolution optical switching, and bandwidth variable transponders [26].

2.5 Combinatorial Optimization

Finding the best solutions from limited but often many possible options is the goal of the branch of mathematics known as combinatorial optimization, where the set of viable options is discrete or may be reduced to a discrete set. An exhaustive search or brute-force approach is often impractical to solve these types of problems due to a large number of solutions. As a result, approximation techniques or specialized algorithms that quickly eliminate significant portions of the search space must be employed. Integer linear programming (ILP), which is the generalized format of linear programming (LP) (or linear optimization), can be used to solve combinatorial problems. Linear programming is a method for the optimization of a linear objective function, subject to linear equality and linear inequality constraints. Its feasible region is a convex polytope that is a space described as the intersection of finitely many half spaces, each specified by a linear inequality. Its objective function is a real-valued

linear function defined on this convex polyhedron. A linear programming algorithm searches for a point in the polytope where this function has the smallest (or largest) value if such a point exists. Typical network problems such as assignment problems, minimum spanning tree (MST), shortest path (SP), minimum-cost flow, and the traveling salesman problem (TSP) are combinatorial problems [27].

Linear programs can be expressed in canonical form as:

Find the vector x that maximizes

$$c^T x \quad (2.1)$$

subject to

$$Ax \leq b \quad (2.2)$$

$$x \geq 0 \quad (2.3)$$

where $b = (b_1, b_2, \dots, b_p)_{p \times 1}$ and $c = (c_1, c_2, \dots, c_n)_{n \times 1}$ are given vectors while A is a given $p \times n$ matrix and $(\cdot)^T$ transposes a matrix. The vector $x = (x_1, x_2, \dots, x_n)_{n \times 1}$ are the variables. The vector x sometimes is a pure integer or a mix of integer and real values that lead to integer linear programming (ILP) and Mixed integer linear programming (MILP), respectively.

2.5.1 Minimum Cost Flow Problem

Network flow problems are multidisciplinary and are shared between mathematics, computer science, engineering, and management. One of the most basic network problems is "Minimum-cost flow" [27]. This problem states how a certain amount of commodity can be transported from suppliers to customers with minimum costs, while each link introduces constraints such as capacity and cost. Take the network depicted in Fig. 2.3 as an example. It is a network of two suppliers and three demand nodes. The goal is to deliver the commodity supplied by nodes 1 and 5 to nodes 2, 3, and 4 with the minimum cost through 7 directed links. In real cases, the commodity can be electricity, gas, or other goods, and links have a limited capacity. Usually, the longer the link, the higher the transportation cost. Although this relation can be linear or nonlinear, we assume it is linear. It means the cost of transporting two units of the commodity is twice the cost of transporting 1 unit using a particular link.

The linear programming formulation for finding flows on each link can be expressed as:

Find f_{ij} that minimizes

$$\sum_{(i,j) \in E} W(i,j) f_{ij} \quad (2.4)$$

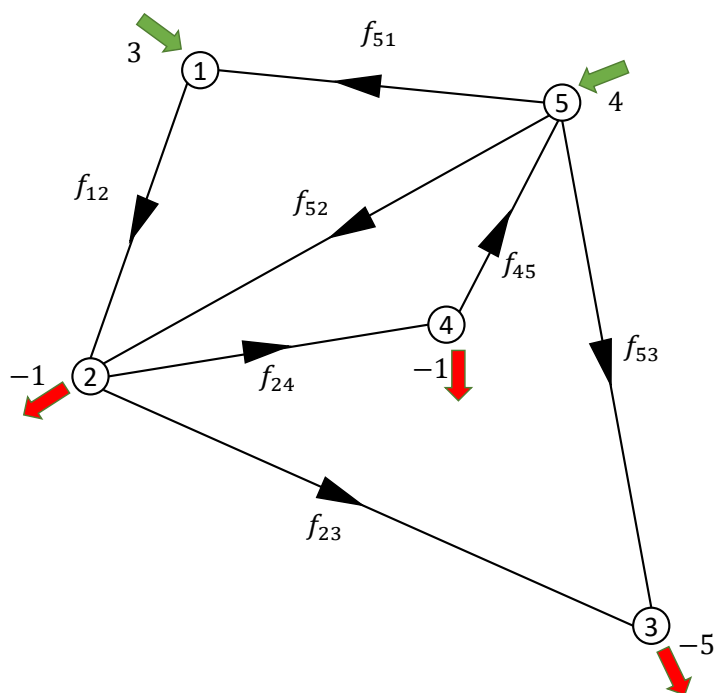


Fig. 2.3 A network of supply and demand nodes connected by a number of links with certain amount of capacity.

subject to

$$\sum_j f_{ij} - \sum_j f_{ji} = S(i) \quad (i, j) \in E \quad (2.5)$$

$$0 \leq f_{ij} \leq c(i, j) \quad (i, j) \in E. \quad (2.6)$$

where E is the set of directed links and i , and j are nodes' indices. $W(i, j)$ is the cost of link (i, j) , f_{ij} is flow on link (i, j) , $S(i)$ is the units of commodity supplied or demanded by node i , and $c(i, j)$ is the capacity of link (i, j) . Constraint (2.5) ensures the conservation of flow at each node, while constraint (2.6) guarantees that the flows do not exceed the capacity of the links. The Simplex algorithm is a well-known approach for solving linear programs.

2.5.2 Simplex Method

In math and computer science, an algorithm is a set of firm and finite steps usually used to solve a set of problems or calculate. A heuristic, on the other hand, is a way to solve problems when there is no well-defined correct or optimized result. The mathematical object

that matches an algorithm is called a Turing Machine. It was invented in 1936 by the British mathematician Alan M. Turing.

Are there well-defined math problems that don't have a solution? Turing showed with brilliant arguments that there are problems that cannot be solved. One of the most common is the so-called "halting problem": Given a description of any program (algorithm) and a finite number of inputs, figure out if the program will end or run forever. Turing showed that no algorithm could solve this problem for all instances [28]. By looking at the program and the input, one can find some heuristic ways to find infinite loop patterns, but there will always be tiny details that need to be figured out. We could run the program and say it worked if we reached the end statement. This strategy is not an algorithm because it does not have a way to stop itself.

During World War II, George Dantzig used a desk calculator to help plan for the US Army Air Force. In 1946, one of his coworkers tried to keep him from getting another job by challenging him to make the planning process more like a machine. Dantzig wrote down the problem as a set of linear inequalities based on Wassily Leontief's work. At the time, he did not include an objective in his writing. He developed a method for solving linear programming problems over the next year known as Simplex [29]. We illustrate how to solve a simple example of a linear programming problem using a graphical method and then discuss the Simplex method. Considering Table. 2.1 the problem is maximizing the amount of alcohol with £10 in a 1L glass using a mixture of beer and wine. If x represents the amount of beer in 1L and y presents the amount of wine in 1L, the linear programming formulation in a standard form can be expressed as:

Find variables x and y that maximizes

$$z = 0.08x + 0.2y, \quad (2.7)$$

subject to

$$x + y \leq 1, \quad (2.8)$$

$$4x + 20y \leq 10, \quad (2.9)$$

$$x, y \geq 0. \quad (2.10)$$

where z is the amount of alcohol, constraint (2.8) is the volume constraint, and constraint (2.9) ensures the cost of drink does not exceed £10.

Since there are only two variables, we can demonstrate the problem graphically in a 2-dimensional Cartesian coordinate system. Figure. 2.4 shows the constraint lines (constraints represent lines in 2-variable problems), which form a region shown in blue. The optimum

Table 2.1 Alcohol percentage and price of two different drinks.

	Beer	Wine
Alcohol (%)	8	20
Price (£/L)	4	20

solution (if it exists) is located somewhere on extreme points where constraint lines meet because the area is convex. As can be seen, the maximum of z happens when the objective meets the extreme point $(x = 0.625, y = 0.375)$ indicated by a green circle. The optimal value of z is 0.125 L or 125 mL. Beyond this point, there will be no feasible solution. When there are thousands of variables and constraints, finding the extreme points is difficult, and checking every single of them to find the optimal one is not practically efficient.

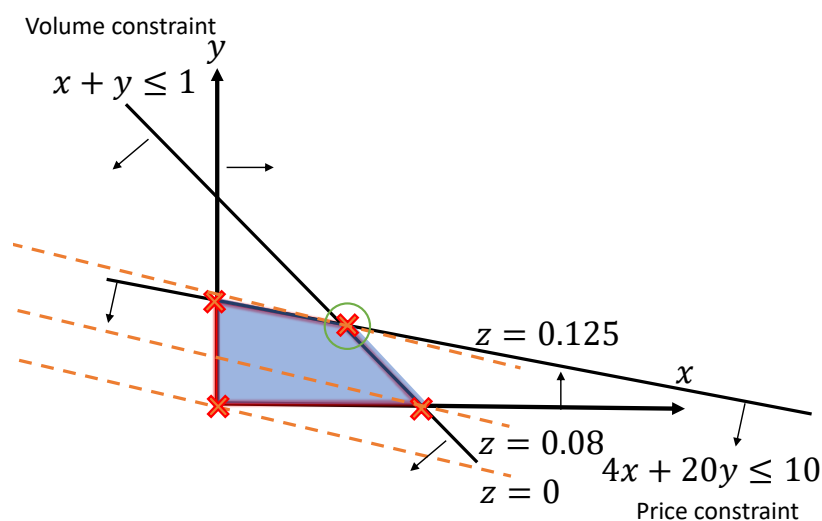


Fig. 2.4 Graphical illustration of the an LP problem.

In the Simplex method, we need to introduce slack variables, which transform inequality constraints into equality equations, and use tableaus and pivot variables to find the optimal solution based on the below algorithm:

To begin, we introduce the slack variables and rewrite the formulation only based on equality equations:

Algorithm 1 Pseudo-code of the Simplex method

Introduce slack variables and create the tableau
while There is at least one negative value in the last row **do**
 Find the pivot variable
 Make the pivot variable 1 by dividing the entire corresponding row by the value of the pivot variable
 Update rows other than the one that includes the pivot variable by proper row operations to make variables in pivot columns 0
end while
Identify basic and non-basic variables and the optimal solution

Find variables x and y that maximizes

$$z - 0.08x - 0.2y = 0, \quad (2.11)$$

subject to

$$x + y + s_1 = 1, \quad (2.12)$$

$$4x + 20y + s_2 = 10, \quad (2.13)$$

$$x, y, s_1, s_2 \geq 0. \quad (2.14)$$

All the coefficients of the variables and constants (right-hand side of equations) in constraints (2.12) and (2.13) and the objective function (2.11) are listed in Table. 2.2.

Table 2.2 The first tableau.

	x	y	s_1	s_2	z	b
R_1	1	1	1	0	0	1
R_2	4	20	0	1	0	10
R_3	-0.08	-0.2	0	0	1	0

Assuming that the solution is not optimal, we pick the smallest negative value in the bottom row, which is -0.2 , in this example. One of the values lying in the column of this value will be the pivot variable. Therefore, 1 from R_1 or 20 from R_2 is the pivot. To find the indicator, we divide the b values of the linear constraints by their corresponding values from the column holding the possible pivot variable. The intersection of the row with the smallest non-negative indicator and the smallest negative value in the bottom row will become the pivot variable. Since $10/20 = 0.5 < 1/1 = 1$, 20 from R_2 is the pivot. Now that the new pivot variable has been determined, the new tableau can be created to optimize the variable and find the new possible optimal solution.

First, we divide all R_2 by the pivot value 20 as shown in Table. 2.3.

Table 2.3 The second tableau.

	x	y	s_1	s_2	z	b
R_1	1	1	1	0	0	1
R_2	0.2	1	0	0.05	0	0.5
R_3	-0.08	-0.2	0	0	1	0

After the pivot becomes the unit value, the other values in the column containing the unit value will become zero. This is because the y in the second constraint is being optimized, which requires y in the other equations (including the objective function, i.e., the last row) to be zero. By operating $\{R_1 - 1 \times R_2\} \rightarrow R_1$ and $\{R_3 + 0.2 \times R_2\} \rightarrow R_3$ we reach Table. 2.4.

Table 2.4 The third tableau.

	x	y	s_1	s_2	z	b
R_1	0.8	0	1	-0.05	0	0.5
R_2	0.2	1	0	0.05	0	0.5
R_3	-0.04	0	0	0.01	1	0.1

Since there is still one negative value in the bottom row, an optimal solution is not found yet. The step of finding the pivot value must repeat. The value 0.8 is a pivot (why?). Then, we do the below steps in order:

- $R_1 \times \frac{10}{8} \rightarrow R_1$
- making value of x in R_2 and R_3 0 by ($\{R_2 - x(R_2) \times R_1\} \rightarrow R_2$ and $\{R_3 - x(R_3) \times R_1\} \rightarrow R_3$)

Table. 2.5 shows the result after ending the process of the second pivot variable. Since all values are greater than or equal to zero in the bottom row, the solution is optimized. A basic variable can be classified to have a single 1 value in its column, and the rest be all zeros. If a variable does not meet this criterion, it is considered non-basic. In this example, x , y , and z are basic variables while s_1 and s_2 are non-basic. Note that if a variable is non-basic, it means the optimal solution of that variable is zero. The final solution shows $x = 0.625$ and $y = 0.375$, and the objective value is 0.125.

Thanks to fast digital computers, it is possible to use the simplex algorithm and its variations on problems with hundreds of thousands of variables and constraints.

Table 2.5 The fourth tableau.

	x	y	s_1	s_2	z	b
R_1	1	0	1.25	-0.0625	0	0.625
R_2	0	1	-0.25	0.0625	0	0.375
R_3	0	0	0.05	0.0975	1	0.125

2.5.3 Simplex Method Time Complexity

For some problems like the "halting problem," there is no algorithm to solve it for all input instances, while for most practical problems, there are algorithms that can solve any instance of the problem. For example, the minimum spanning tree problem can be solved by exhaustively eliminating all spanning trees and selecting the best one among all n^{n-2} possible spanning trees (n in the number of nodes in a connected and undirected graph). However, the time consumed for solving a problem is crucial as there are limited computation power resources. Therefore, the solving time usually determines the performance of an algorithm proposed for a problem.

The number of steps, such as arithmetic operation, comparison, and branching, may represent the time needed for an algorithm to solve the problem. However, the number of operations might be different for all inputs. For example, the Simplex algorithm might solve two instances of an LP problem at very different times. Given this behavior, the worst case of an algorithm is usually analyzed and considered a performance measure. Given the size of a problem, a polynomial-time algorithm is often considered an efficient algorithm. If the size of an instance of a problem is n , a polynomial-time algorithm can solve the problem in $T(n^x)$ for large n [28].

Klee and Minty showed that the Simplex method is not a polynomial-time algorithm by constructing long increasing paths on appropriate convex polytopes [30]. In fact, the simplex method is an exponential-time algorithm in the worst case (polynomial-time algorithms outperform exponential-time algorithms for large instances). However, in practical problems, the simplex is exceptionally efficient, and its run time is linearly proportional to the number of constraints [31].

Over the years, scientists have developed several linear programming algorithms. Most of them did not work very well, and only a few have really been able to compete with the simplex method, which was the first algorithm in history. Nevertheless, at least two methods were inspiring when they were first found. In practice, the first one, the ellipsoid method [32], cannot keep up with the simplex method, but in theory, it was crucial since it is a polynomial-time algorithm. It is the first linear programming algorithm for which it was shown to always run in polynomial time. The second is the interior point method [33]

or the group of algorithms that make up the interior point method. Interior point methods are competitive when it comes to small problems with less than one million constraints and variables, but they are unbeatable for big problems with millions of constraints and variables [34].

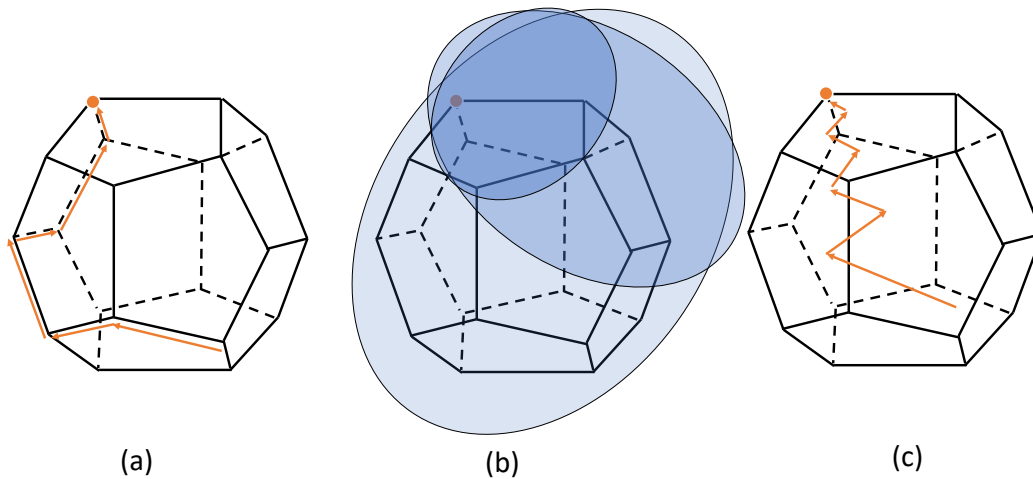


Fig. 2.5 Graphical illustration of (a)Simplex, (b)Ellipsoid and (c)Interior point method for an IL problem.

2.5.4 Integer Linear Programming Solving methods

As discussed earlier, MILP problems are LPs in which variables are constrained to be only integers. It can be proved that ILPs with binary variables are NP-complete problems [35] while they are NP-hard in general [36]. Karp has shown that a group of well-known combinatorial problems, including 0-1 ILPs, are equivalent in that a polynomial-bounded algorithm for any of them would give a polynomial-bounded algorithm for all of them. He also has proved that if these problems have polynomial-bounded algorithms, then so do all the problems in an unexpectedly large class (roughly, the class of problems that can be solved by polynomial-depth backtracking).

Although there are several approximations and heuristics [37, 38] for solving ILP problems, we only briefly describe exact algorithms, including Cutting planes, Branch-and-bound, and Branch-and-cut methods.

The first idea for solving an ILP problem is to relax it to a linear programming problem by allowing variables to be non-integers. If the relaxed problem is infeasible or unbounded,

the original ILP problem will also be infeasible or unbounded [39]. If the relaxed problem is feasible, the ILP problem is also feasible and has an optimal solution in which the relaxed problem solution is a lower bound. Note that if the relaxed linear programming solution is totally integer, then the solution is the optimal solution of ILP as well.

Cutting Plane Method

The cutting plane method for MILP works by solving the linear relaxation of the given ILP. There will always be a linear inequality between the optimal solution and the convex hull of the true feasible set. The separation problem is to find such an inequality (cutting plane). The program can be modified by adding a cut. This is done repeatedly until the best integer solution is found [40]. There are many strategies for creating cutting planes leading to different cutting plane methods.

Branch and Bound Method

Branch-and-bound algorithms for mixed-integer programming use a "divide and conquer" technique to find all possible mixed-integer solutions. These algorithms make a search tree, where each node is a subproblem defined over a part of the feasible region [41]. Branch and bound methods do not go deep like Depth-first search (DFS); the first direction is lateral movement in the tree, similar to Breadth-first search (BFS).

Branch and Cut method

Branch-and-cut methods, which are algorithms made up of a cutting plane method and a branch-and-bound method, can be used to solve ILP problems [42]. The integer programming problem is simplified by solving a series of linear programming problems. Cutting plane methods make the problem easier to solve so that it is closer to the integer programming problem, and branch-and-bound algorithms solve problems using a sophisticated way to divide and conquer.

2.6 Evolutionary Optimization Algorithms

Evolutionary algorithms (EAs) are algorithms with the ability to evolve that carry out learning or optimization tasks. They primarily exhibit three features [43]:

- Population-oriented: EAs keep track of a population of solutions in order to optimize or learn the problem simultaneously. An essential element of the evolutionary process is the population.
- Fitness-based: every member of a population is referred to as an individual. Each individual has a representation of their genes called its code, and an assessment of their performance called a fitness value. The basis for algorithm optimization and convergence is that EAs favor fitter individuals.
- Variation-driven: to seek the solution space, individuals will go through a variety of procedures that imitate genetic changes.

2.6.1 Genetic Algorithms

The earliest, most well-known, and most often applied evolutionary optimization algorithms (EAs) are genetic algorithms (GAs). GAs are natural selection models capable of resolving optimization issues [44]. We build an individual population of candidate solutions for an optimization problem. Some solutions work well, while others do not. While the chances of reproduction are somewhat low for the poor, they are very high for the decent ones. After having children, parents leave the population to create room for their offspring. The population gets fitter as generations come and go. There are instances when one or more individuals grow into highly fit, which can offer solutions that are close to optimal for our optimization problem. The first iteration of a GA is shown in Fig. 2.6. It starts with building an initial population, followed by parent selection, and ends with mutation operations. The cross-over operation is the process of mixing the genes of two individuals while mutation toggles the bits in genes with a specific probability. Roulette-wheel selection, also known as the fitness-proportional selection, is one popular method of choosing parents. The individuals that are better fit and lead to more optimal solutions have a proportionally higher chance of being selected as parents. Therefore, some individuals might be selected as parents several times while others might not be selected at all. There are different ways of cross-over, but the most common one is single-point cross-over, in which a part of genes is exchanged between two parents.

The number of generations needed to reach the most fitted (optimal) solution depends on the type of problem. However, in practice, we are interested in meeting some criteria. Hence, as soon as the requirements are met, the GA can stop continuing and return back the best solution. In some cases, the GA needs to meet a pre-defined criteria such as convergence even with many generations. It is helpful to have the upper bound of the number of generations

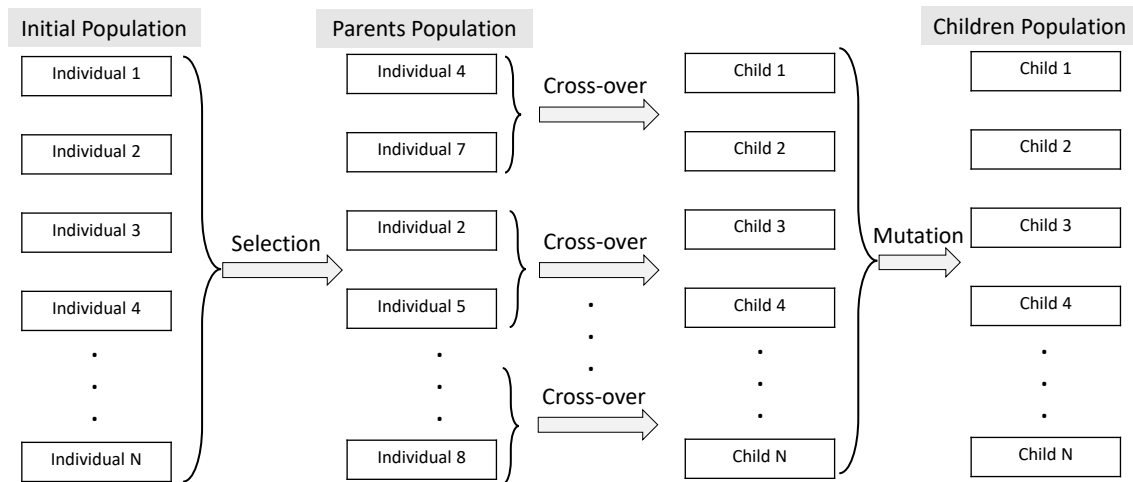


Fig. 2.6 Process of the first iteration of GA optimization starts with creating an initial population, then followed by cross-over, and ends with mutation.

that our computing device can handle inside the algorithm. Algorithm 2 represents a simple form of a GA.

Algorithm 2 Pseudo-code of a simple Genetic Algorithm

```

Parents ← Random population
while termination conditions not met do
  calculate the fitness of each parents
  Children ← ∅
  while size{Children} < size{Parents} do
    Use fitness to probabilistically select a pair of parents
    Mate the parents using cross-over operation and generate children  $c_1$  and  $c_2$ 
    Children ← Children ∪ { $c_1, c_2$ }
  end while
  Randomly mute some of children's gens
  Parents ← Children
end while

```

GA designers must set several factors in order to get satisfactory results. These parameters frequently determine whether an attempt is successful or unsuccessful. Below are some of the parameters:

- Suitable way of encoding problem solutions to genes.
- Proper fitness function.

- Size of population.
- Selection method: in addition to roulette-wheel selection, other types of selection are also possible, including tournament selection.
- Mutation rate: a GA that employs an excessive mutation rate will turn into a random search. However, a GA with a low mutation rate will not be able to scan the search space adequately.
- Cross-over type: in addition to single-point cross-over, other types of cross-over are also possible, including double-point cross-over.
- Fitness scaling: this describes the implementation of the fitness function. If a fitness function is improperly defined, it may result in relatively similar fitness values for all individuals. When fitness levels are clustered together, it is difficult for the selection process to determine which is highly and poorly fit. This discourages the fitter ones from passing on their genes to the following generation. Sometimes, however, the fitness values are too widely diverse, which prevents individuals with low fitness levels from being selected for reproduction.

There are other EAs used in network optimization, such as ant colony optimization (ACO) [45, 46] and particle swarm optimization (PSO) [47, 48].

2.7 Filterless Networks

Filterless Optical Networks (FONs), which replace costly active reconfigurable filters such as ROADMs with splitters and combiners, reduces equipment costs in optical networks and first was introduced by Tremblay et. al [49]. While promising lower power consumption and smaller footprints compared to traditional networks, FONs face challenges like spectrum waste and signal quality issues due to the absence of filters [50]. Since there is no filter, the architecture must be designed without any loops. Otherwise, an optical signal traverse a link more than twice and may cause interference and laser effect.

Moreover, providing link protection is challenging because between a node pair, there must be at least two disjoint path. Using red and blue filters or limited colored filters can help implementing protection but the architecture will not be pure filter-less [51].

2.8 Monte Carlo Simulations

Monte Carlo simulations are a common name for a collection of simulations used for performance analysis [52]. While working on nuclear weapons in the 1940s, John von Neumann, Stanislaw Ulam, and Nicholas Metropolis came up with the name. Numerous experiments were analyzed as part of their study, and there was a clear correlation between the statistical aspects of gambling and the statistical analysis of their studies. The term "Monte Carlo simulations" originated from this link with Ulam's uncle, a legendary gambler at the casinos of Monte Carlo in Monaco. Monte Carlo analysis is a method that uses random sampling and statistical modeling to understand how uncertainty in various factors affects outcomes in complex systems. It involves defining variables, assigning probability distributions to them, generating random samples, running simulations, and analyzing the results to assess risks or predict possible outcomes. It is valuable for decision-making by considering a wide range of scenarios and their likelihoods.

2.9 Routing and Wavelength Assignment Analysis

To build a connection in the optical layer that is analogous to the link in a circuit-switched network [53] in order to transfer data from one node to another. This may be accomplished by choosing a network path between the two nodes and assigning a free wavelength to each connection along the path. A lightpath comprises one DWDM channel per connection and may span several fiber links without requiring any intermediary electronic processing. The lightpath must occupy the same wavelength on every fiber link it utilizes without wavelength conversion. In other words, the wavelength continuity condition must be observed. Since lightpaths are the fundamental unit of this network design, they must be effectively established. In order to optimize a certain performance measure, it is crucial to find the best routes for the lightpath requests and to allocate the proper wavelength to each connection from among the available options. The problem is known as routing, and wavelength assignment (RWA) [54].

If we consider an RWA solver as a black box, its inputs are a graph and a set of traffic requests, and its output is a set of lightpaths. However, this is the case when traffic loads are fixed and known, which is called static traffic loads. In contrast, in dynamic traffic, requests for lightpaths come one by one, and they are terminated randomly. In [8], it is demonstrated that the optimal static lightpath establishment problem without wavelength converters is equivalent to the graph-coloring problem and is thus NP-complete [55]. RWA problem with static traffic is NP-complete as well and can be solved for fixed-grid optical networks design.

However, it has to be generalized to the routing and spectrum assignment (RSA) problem in flex-grid optical systems.

The ILP objective formulation, which has to be maximized for the RWA problem, can be expressed as [56]:

$$z = \sum m, \quad (2.15)$$

subject to

$$C^T B \leq I \quad (2.16)$$

$$m \leq C^T \times I \times A \quad (2.17)$$

$$m \leq q \quad (2.18)$$

where $m_{N_{sd}} \times 1$ is a vector containing integer variables for the number of channels established for each (s, d) pair. $C_{N_{sd} \times w}$ is a matrix comprising binary variables indicating the usage of wavelengths by paths and w is the number available wavelengths. The incident of paths and links is determined by matrix $B_{N_{sd} \times l}$. $I_{w \times l}$ is all-ones matrix, while $A_{l \times l}$ is a unity (identity) matrix where l is the number of links. q is a $N_{sd} \times 1$ vector containing the number of optical channels required for each (s, d) pair. Constraint (2.16) ensures each path uses a unique wavelength while constraint (2.17) and (2.18) guarantee that the number of established channels does not exceed the predefined traffic loads.

2.9.1 Results and Discussions I

We consider the NSFNET network depicted in Fig. 2.7 in this section for RWA analysis [57]. It has 14 nodes ($N = 14$) and 21 bidirectional links ($L = 21$). Hence, there are $N_{sd} = N(N - 1)$ possible source-destination (s, d) pairs.

The shortest path is calculated using the Dijkstra algorithm [58] for each (s, d) pair ($N_p = N_{sd}$). We assume that the number of optical channels is 20 ($W = 20$).

Having limited spectrum resources, we expect that when the required number of lightpaths increases, some of them cannot be established because there is no available light path (i.e., there is no path connecting two nodes while having specific wavelengths free on all links on the path). We assume that each (s, d) pair requires no more than one wavelength and randomly generates demands. Figure 2.8 gives information about blocking ratio, which is the ratio of blocked wavelengths over total required wavelengths. The blue curve is the

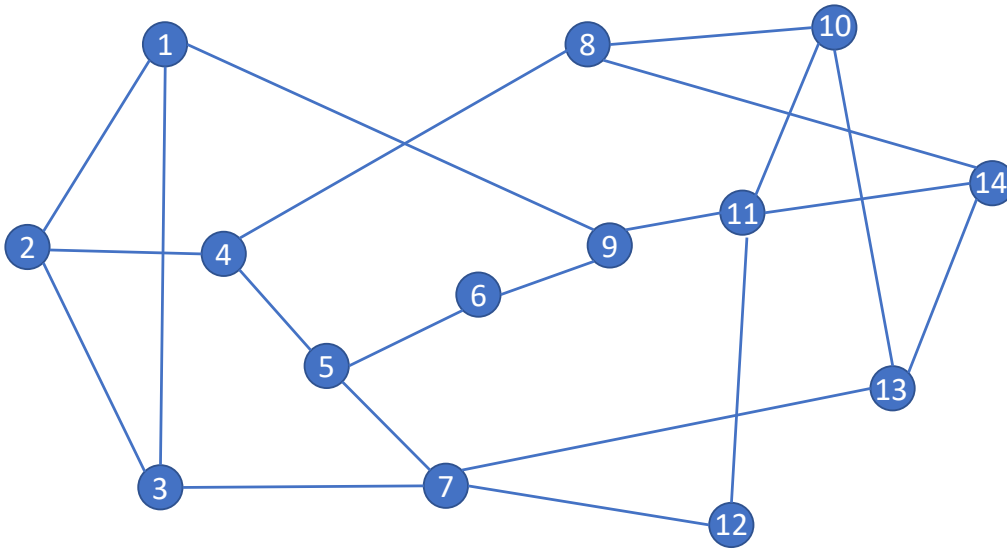


Fig. 2.7 NSFNET network

average of 10 independent simulations, and highlighted regions indicate the 90% confidence intervals. As it can be seen, when the number of wavelengths is fewer than 90, no wavelength is blocked. However, when the number of wavelengths increases, the blocking ratio also increases on average. When trying to establish all 182 lightpaths ($14 \times (14 - 1) = 182$), almost 14% of wavelengths are not established. The confidence intervals are about zero when the blocking ratio is 0 and when all lightpaths are set to be established. These are because at low load demands, blocking ratios are zero independent of the definition of loads, and when all lightpaths are considered, there is no randomness.

Although ILPs give exact solutions, they might not be appropriate methods for large scale networks. When the size of networks increases, the size of the input to the ILP may increase polynomially, and the hardness of ILP itself rises exponentially versus the number of inputs. Therefore, it is crucial to have alternatives for such situations, even at the expense of losing accuracy. Heuristics are approaches for solving large-scale problems. Although they do not guarantee optimum solutions or even being faster, they may provide practical results in a reasonable time.

A common heuristic approach to RWA problems is breaking them down into sub-problems and solving them separately (usually sequentially). A heuristic solver chooses which demand should be established first. It finds a route and then selects an appropriate available wavelength. Different heuristic strategies are born based on how to order requests, how to find

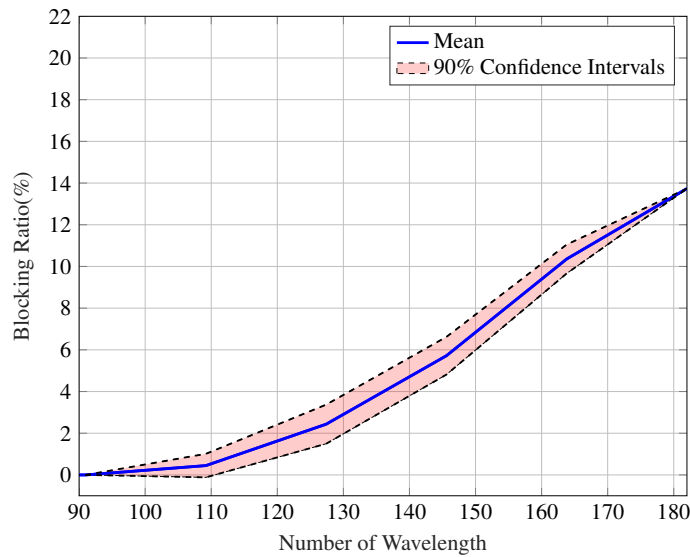


Fig. 2.8 Blocking ratio of NSFNET network using ILP versus number of needed wavelength.

routes, and how to assign wavelength. Table. 2.6 shows some methods for each sub-problem. There are 8 possible combinations using these approaches. For example, random ordering, shortest path routing, and random wavelength assignment. See [56, 59] for more approaches and more detailed information.

Table 2.6 Different heuristic approaches regarding request order, routing, and wavelength assignment for solving RWA problems.

Requests order	Routing	Wavelength assignment
Random	Shortest path	Random Fit
Longest path first	Adaptive routing	First fit

Figure. 2.9 shows the results of the blocking ratio when the random approach is used for ordering requests, the shortest path scheme is employed for routing, and random fit and first fit are used for wavelength assignment. In random fit, a wavelength is selected randomly from the available wavelength for accommodating a request. In contrast, in the first fit method, the spectrum's first available wavelength is used to establish the lightpath. The random fit approach results in higher blockage for all simulated ranges of traffic loads compared to the first fit. Moreover, the first fit heuristic leads to a higher blocking ratio ranging from 0 to 6% more blockage than the ILP method results.

For a larger network (more links and nodes) like European Optical Network (EON) [60], the ILP approach struggles to solve the RWA problem using ordinary personal computers. It comprises 28 nodes and 41 bidirectional links. Figure. 2.10(a) shows the average and

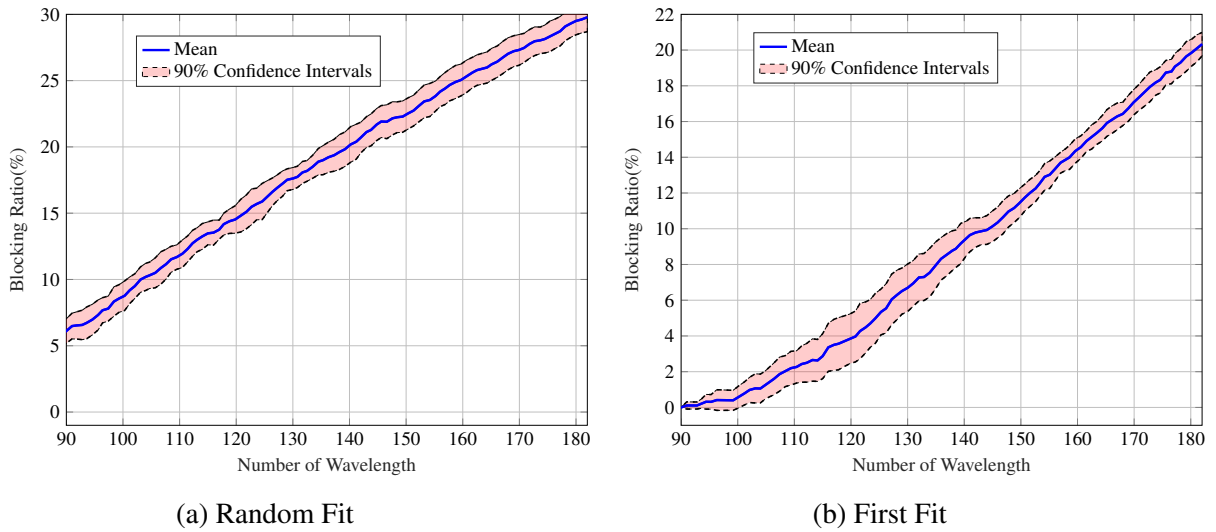


Fig. 2.9 Blocking Ratio of RWA problem using shortest path and (a) First Fit and (b) Random Fit in NSFnet network.

90% confidence intervals for blocking ratio with 100 simulations in logarithmic scale for the EON-28 network using random ordering, shortest path and first fit heuristic against the number of needed optical wavelengths. It is assumed that C-band is partitioned into 80 channels. Note that when the number of simulations increases, the confidence intervals decrease. The congestion of the network's link is depicted in Fig. 2.10(b). The links located at the center of the network usually experience more congestion since they might host more lightpath connecting (s, d) pairs.

2.10 Routing and Spectrum Assignment

When constructing a flex grid optical network, the routing and spectrum assignment (RSA) problem appears. Each lightpath must have a suitable path and a predetermined number of empty, adjacent frequency slots in order to be established. Like RWA, the traffic load can be dynamic or static in RSA. In the case of static traffic, the RSA problem is NP-Complete (see the proof in [61]).

Figure 2.11(a) shows an optical network comprising six links and five nodes. A table of demands is provided in terms of source-destination (s-d) pairs and their needed number of slots (Fig. 2.11(b)). The routes selected accommodating demands are depicted in Fig. 2.11(c). Assuming only five frequency slots exist, the link-spectrum state can be presented by a link-slot table like Fig. 2.11(c). Integer linear programming (ILP) can find the most optimal solution, but evolutionary algorithms might be used for large networks [62, 60]. However,

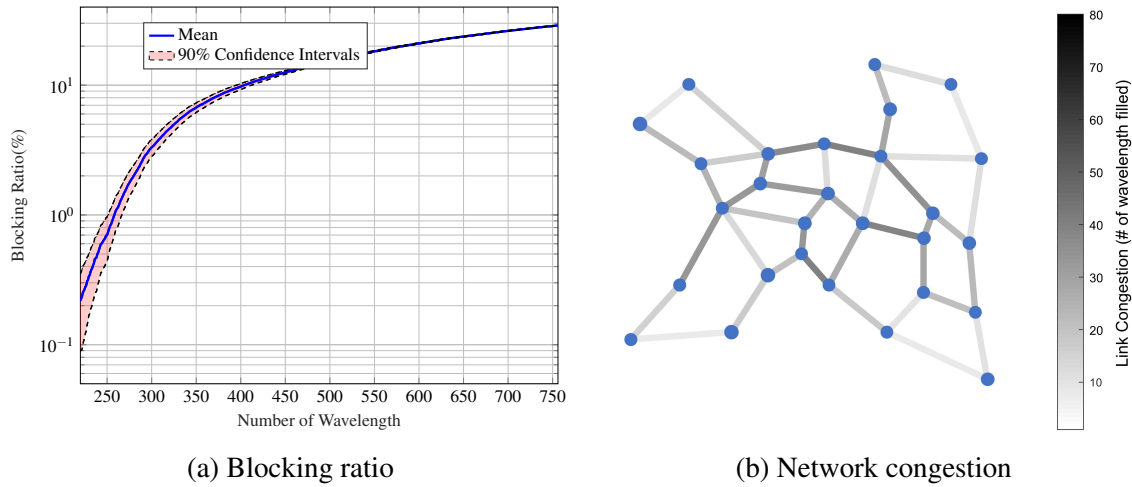


Fig. 2.10 (a) Blocking ratio of EON28 network using random ordering, shortest path, and first fit heuristic versus the number of needed wavelengths and (b) Network congestion in terms of used wavelength when the number requested wavelengths is 756 wavelengths.

the most common way of solving RWA and RSA problems is to use heuristics in which the main problem is broken into sub-problems and solved sequentially [63, 64]. Note that the objective function may vary from one problem to the other one. For instance, minimization of blocking probability or spectrum usage might be employed.

2.11 Routing Modulation Format and Spectrum Assignment

Let us say the traffic is expressed in terms of bit rates. Then, given specific physical distances and the necessary bandwidth, a routing, modulation format, and spectrum assignment (RMSA) problem must be solved further by determining the optimum modulation format [65].

RMSA problem is NP-hard [66], which means it could not be solved in polynomial time. A possible alternative to solve this complex problem is utilizing a Genetic Algorithm (GA), which belongs to the class of evolutionary algorithms. In addition, a GA approach has been employed in [62] to solve ordering and path selection at the same time. A combination of GA and heuristics has been reported in [67] as an efficient way to solve the RSA problem. In this section, we propose a two-step GA for the static RMSA problem to solve ordering and path selection separately using other heuristics considering bandwidth and hop for traffic load definition.

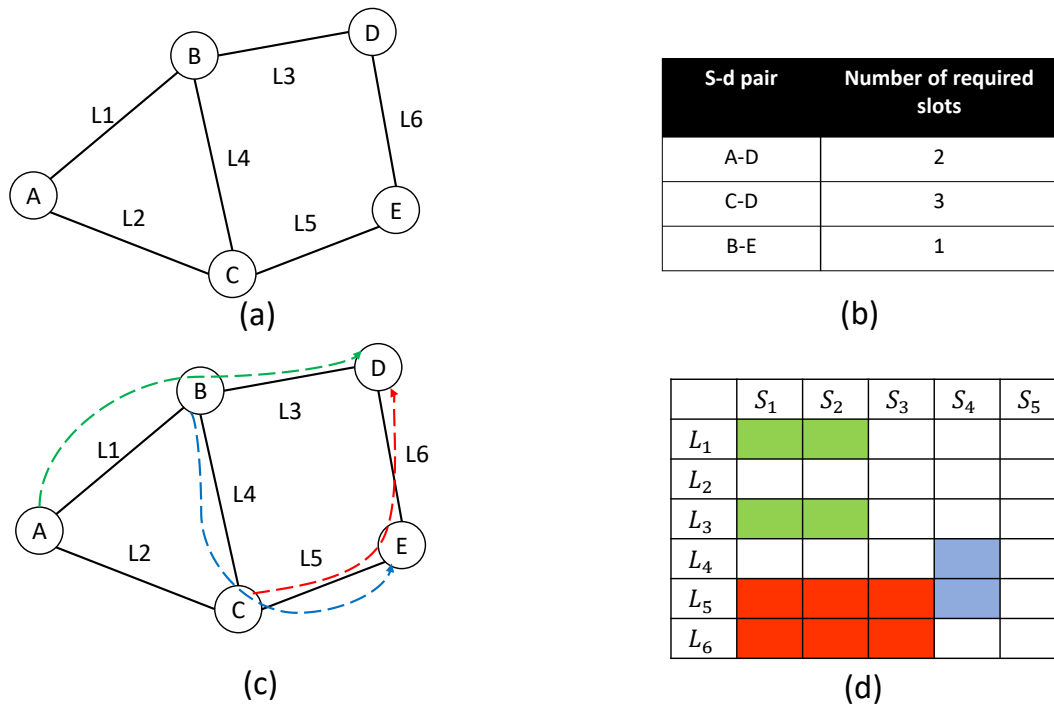


Fig. 2.11 Illustrative example of RSA in a 5-node network with 3 traffic demands.

2.11.1 Network Scenario and Genetic Algorithm Formulation

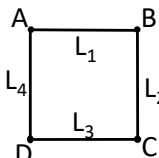
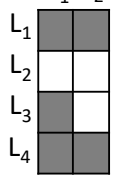
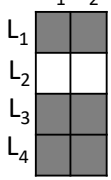
The Spanish network[68] with 30 nodes and 56 links is considered. We assume that each link comprises a single bidirectional fiber pair. The bandwidth for each fiber is 4 THz, which is partitioned into 320 slots, 12.5 GHz each. We also use the data reported in [69] for modulation format selection. The traffic for each node pair is randomly selected from the 40, 100, 200, 400 Gb/s.

The total data rate (e.g., in Tb/s) or the number of requests have been used to characterize the static traffic load in most studies [70]. However, the absolute traffic load does not give information about the size of traffic loads relative to the networks' size. For example, 10 Tb/s may be a significantly large traffic load to support on a given network, while it may be relatively small for another. Consequently, we use a traffic load characterization inspired by the fact that a request with larger bandwidth and a longer path uses more network resources, such as spectrum. A similar metric is used in [71] for designing resilient core networks. We describe the traffic load as the sum of the requested bandwidth (THz) multiplied by the number of hops they travel and use THz·Hop as the unit of this metric. This type of characterization is aware of both length and bandwidth. We use the blocking ratio for this unit and call it the bandwidth-hop blocking ratio (BHBR). Optimizing the bandwidth blocking

ratio (BBR) may give a higher chance of meeting requests with larger bandwidth and fewer hops to be established. Table 2.7(a) shows traffic loads definition for four node pairs in terms of frequency slots and slots×hops in a simple network. Table 2.7(b) compares BBR and BHBR for two different demands ordering. We assume each link has two slots capacity. In the first case, only the A-C request is blocked, while the A-D and D-C requests are blocked in the second one. In contrast to the bandwidth blocking ratio, the bandwidth-hop blocking ratio shows that the second ordering performs better. The link-spectrum usage, depicted in Table 2.7(b), confirms this result as it shows a more effective usage of spectrum resources.

We use the k-shortest path for routing and the first fit approach for spectrum assignment. Each request's modulation format is selected to minimize the number of slots while satisfying the reach requirement. A single slot is left empty as a needed gap between adjacent lightpaths. The requests are ordered in 3 different ways: random, Most Spectrum First (MSF), and Longest Path First (LPF) [56]. The intuition behind these methods is that the larger demands or longer lightpaths are harder to establish at the end and it might better to accommodate them at the beginning when a lot of resources are available and there is less fragmentation. The RMSA starts to establish lightpaths sequentially. This approach leads to a higher probability of blockage for the last requests as the network gradually becomes congested. We employ a GA approach to find an optimal order in this massive search space.

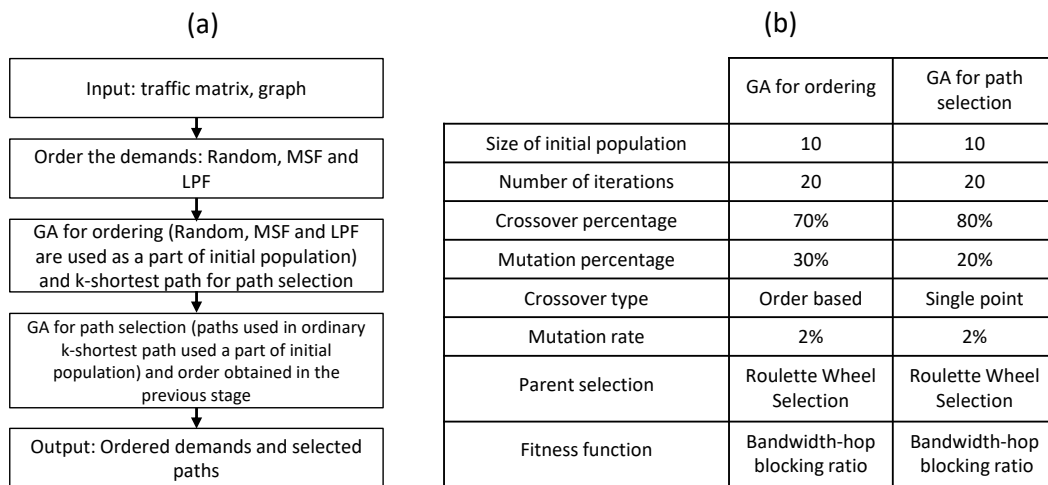
Table 2.7 (a) Demand characterization for a simple 4-node network, and (b) BBR and BHBR for two different demands ordering instances.

(a)				(b)		
Node Pair	Demand (slots)	hops	slots × hops	Order of meeting demands	1-2-3-4	1-3-2-4
A-B	2	1	2	$BBR = \frac{\sum \text{blocked bandwidth}}{\text{total bandwidth}}$	$\frac{2}{7}$	$\frac{3}{7}$
A-D	2	1	2			
A-C	2	2	4	$BHBR = \frac{\sum \text{blocked bandwidth} \times \text{hops}}{\text{total (bandwidth} \times \text{hops)}}$	$\frac{4}{9}$	$\frac{3}{9}$
D-C	1	1	1			
	7	5	9	Link-Spectrum Usage 		

We use the order obtained by the heuristic algorithms as individuals in the initial population of the GA. Therefore, we set the GA to start searching for a more optimal solution around the chosen heuristic solution. Next, we run the second GA to optimize the path

selection process. Similarly, we use the result of the previous GA's path selection as input for the second GA's initial population. Table 2.8(a) shows the flowchart of the process discussed above. Values for GA parameters used in this study are listed in Fig. 2.8(b). The length of chromosomes is equal to the size of the requests. The value of genes is between 1 and the size of requests in the ordering GA, and between 1 and k , in which k is the number of candidate shortest paths, in the path selection GA.

Table 2.8 (a) Overview of the GA approach and (b) value of different GA parameters.



2.11.2 Results and Discussion II

The RMSA problem is solved for six different traffic loads and considering two values for k . Fig. 2.12 depicts the bandwidth-hop blocking ratio obtained from employing six different methods. Interestingly, random ordering outperforms MSF in most loads for both $k = 2$ and $k = 3$. This is because the bandwidth blocking ratio is aware of only the amount of bandwidth established and does not consider the total length of lightpaths.

From Fig. 2.12, it can be observed that LPF outperforms random and MSF methods almost in all considered loads. GA for ordering (enhanced by heuristics) decreases blocking compared to LPF. Moreover, further performance improvement is possible when employing the path selection GA. Note that the path selection GA may prefer a longer route for a request even if the shorter one is available because it results in a lower blockage ratio at the end. The amount of blocking reduction for smaller traffic loads is more significant. To explain this, firstly, the search space is smaller for traffic with fewer requests, while the number of iterations and population size for GAs are fixed. Secondly, the network's resources become

congested when more lightpaths are established, and different optimization methods cannot help considerably.

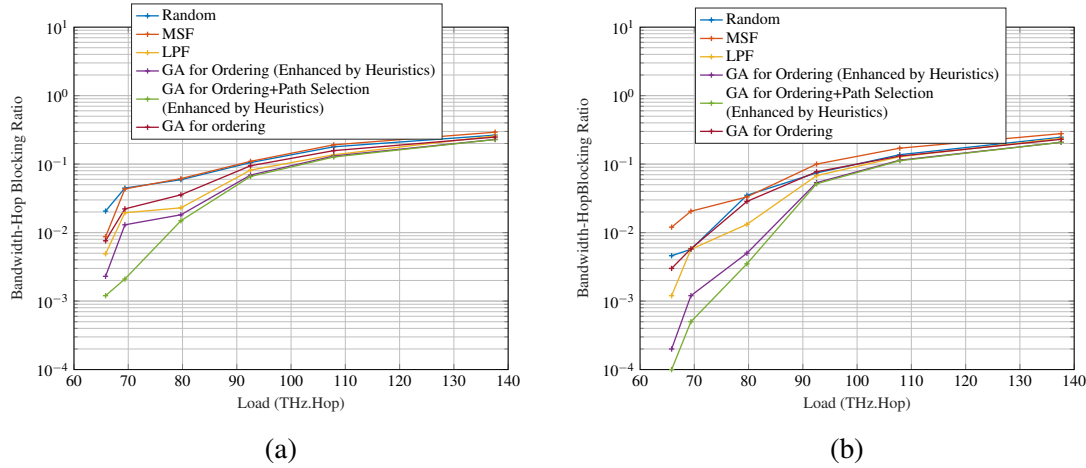


Fig. 2.12 Bandwidth-hop blocking ratio for three different heuristics, two-step GA and GA for ordering with and without using heuristics (a) $k = 2$, (b) $k = 3$.

The results also highlight the importance of enhancing the GA for ordering with heuristics since the results are considerably worse when they are not exploited (see Fig. 2.12). This is due to the fact that the search space is massive, and the GA needs many generations to reach the performance of heuristics. Besides, using heuristics in GA guarantees that, in the worst case, the GA's solution will be as good as that obtained by heuristics.

2.12 Power Consumption of the Internet

Concerns about the internet's power consumption have been started since 2003 by a paper titled "Greening of the Internet" [72]. The exponential rise in network traffic is closely tied to the "green" problem. The market is extremely competitive, especially in developed nations, and despite yearly increases in traffic demands, declines in average revenue per user (ARPU) due to operators' rising OPEX investments, such as the rising cost of electricity, have been reported [73]. There are three major motivations for managing power consumption of the internet and specifically telecommunication networks:

- Reducing energy cost (reducing OPEX)
- Reducing heat dissipation in components
- Reducing carbon footprint

However, modeling the power consumption of ICT is not straightforward because telecommunication networks are complex, and equipment made by different producers may have different features that change over time. Several researchers attempted to model power consumption in some areas of ICT. In an IP-over-WDM network, it is explored if static optical bypass over non-bypassed architecture may save power [74]. This power consumption model considers the IP router ports, transponders, and optical amplifiers. A power consumption per customer model has been presented for optical networks in [75], taking into account all major subnetworks like access, metro, and core. The power efficiency of a typical core router is used to calculate the power consumption in the core nodes. The link power consumption distinguishes between terrestrial and submarine lines using a channel efficiency value based on a typical WDM interface and inline amplifiers. In [76], reference power consumption values for Internet protocol/multiprotocol label switching, Ethernet, optical transport networking, and WDM equipment have been proposed.

Based on a report from Huawei [77], 1700 TWh out of 22000 TWh global electricity usage (7.7% of global electricity consumption) is consumed by ICT. Note that the power consumption of consumer devices like monitors, TVs, and laptops is included in these figures. Also, the report predicts the ICT power consumption will reach 2788 TWh (about 10% of global electricity consumption) by 2025 in the best case, while it can rise to 5860 (about 22% of global electricity consumption) in a realistic case.

To combat power increase, the energy efficiency of equipment has to increase, allowing more traffic transmission with little increase in power consumption or even a decrease in power consumption. Besides, power-efficient network planning and management can improve power efficiency by preventing spectrum waste and underutilization of network components.

2.12.1 Network Power Consumption

Access Networks

As discussed in section 1.1, optical networks are different in size, architecture, and applications. This makes optical networks' power consumption modeling difficult. Researchers have proposed many models and solutions for different scenarios [78]. Fixed access networks still rely on a combination of transmission media, such as copper, coaxial cable, and fiber. In passive optical networks (PONs), the optical network unit (ONU) is responsible for the majority of the network's power usage (about 60% of total power consumption [79]). Even though PONs are more energy-efficient than their predecessors (such as coaxial cables and twisted pairs), the amount of energy consumed is still considerable. ITU-T began researching

PON power savings in 2006 and issued ITU-T Series-G Supplement 45 titled "G-PON power conservation" in 2009. It discusses four fundamental power-saving strategies for reducing PON ONU energy demands: power shedding, dozing, deep sleep, and cyclic sleep [80]. The core idea of all these strategies is not to use power when traffic is not transmitting. The authors of [81] provide analytical models for evaluating the power-saving potentials of appropriate PON dimensioning and sleep modes.

Metro Networks

Today's metropolitan area networks are based on diverse architecture and technologies. Circuit-switched synchronous optical network/synchronous digital hierarchy (SONET/SDH) architectures were initially designed to transport constant-rate voice traffic. These architectures are not the best fit for increasing bursty data traffic demands. Ethernet-based architectures can replace legacy SONET/SDH architectures. They are more flexible, cost-effective, and scalable [82]. Despite these benefits, optical signals must still be translated to the electronic domain at each intermediate network node, making the Ethernet-based metro network an opaque solution. Operating optical fiber networks comes at a significant expense due to optical-electronic-optical conversion [83].

Nowadays, most of the traffic in metro networks is carried by WDM-based network architectures. The technology most likely to be deployed in the metro area is coarse wavelength division multiplexing (CWDM). However, they only can support a limited number of wavelengths. Sharing the capacity of individual wavelengths amongst multiple nodes is a way to get around this restriction. The hub node comprises the chassis, the physical and mechanical assembly, the switching matrix, the cooling system, the power supplies, and the control and management software. Access nodes are equipped with transceivers and add-drop elements. Switches, routers' cards, and transceivers are the primary power consumers in these architectures. WDM-based metro networks are more power efficient than SONET/SDH [84].

Core Networks

Core networks are the backbone of the Internet connecting metro networks. They often have mesh topology and work at the highest available data rates. The power consumption of core networks is usually made up of the consumption of the IP and optical layers [76]. The main power consumers are routers, amplifiers, transponders, optical cross-connects (OXC), and ROADMs. Recent energy-efficiency studies show that optical devices at the optical layer use substantially less energy than electronic equipment in the IP layer, especially routers [78].

According to recent data, wired and wireless access networks dominate in terms of how much energy the Internet uses. However, the backbone network's power consumption is based on traffic volume, while access networks' power consumption is proportional to the number of users. In [75], it is reported that if the access rate per household exceeds 100 Mbps, the backbone network will consume 34.5% of total network power, assuming an energy efficiency increase of 10% per year.

In [85], physical topology design for IP-over-WDM networks has been investigated. Router bypass approaches have extensively been studied for reducing power consumption of IP layer [86, 21]. Powering equipment off when possible can help reduce electricity usage. Optical networks usually are designed to handle peak traffic. Therefore, when the traffic load is lower than peak traffic, some part of the power is wasted [87]. In [88], optimal link on/off scheduling has been studied for minimizing network energy consumption. By turning off idle line cards and router chassis depending on variations in network traffic throughout different times of the day, Zhang et.al. [89] proposed a novel method for saving energy in IP-over-WDM networks. It is worth noting that there is a trade-off between power-saving strategies and the amount of CAPEX needed [90].

2.12.2 Power consumption modelling

Individual components' power consumption directly affects a network's power usage. Therefore, it is crucial to have comprehensive models for devices such as routers, transponders, and amplifiers for research purposes. However, there might exist several technologies and producers. On the other hand, research like [91], which has brought much technical information, may need to be updated quickly. Routers used to be significantly power-hungry. With the advancement in efficient silicon technologies, they have been becoming more and more efficient. We collect data from datasheets provided by three leading router producers, namely Cisco, Huawei, and Juniper, to assess the power consumption of routers in 2021. Figure. 2.13 shows the power usage of different routers and the polynomial regression of degree 2 to the data. As can be seen, the increase in power consumption is not proportional to the router's capacity. The router's power consumption is 0.25 W/Gbps on average for routers with a capacity smaller than 10 Tbps . However, high-capacity routers are more power efficient and consume a figure between 0.13 W/Gbps and 0.18 w/Gbps .

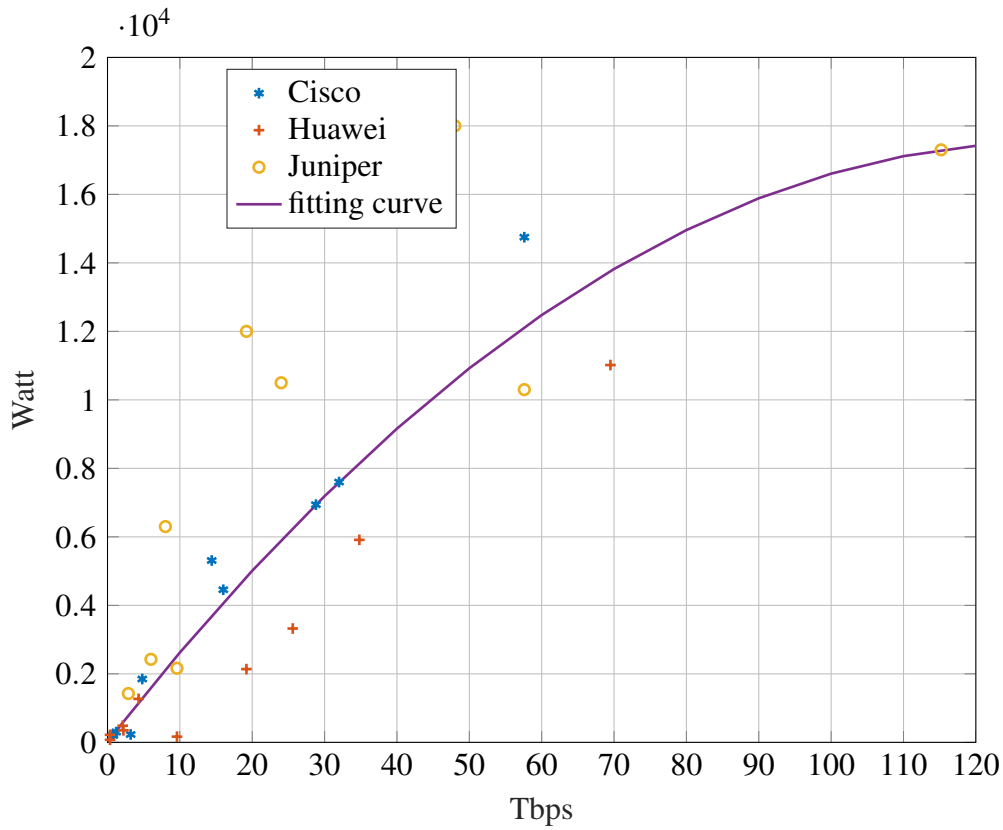


Fig. 2.13 Routers power consumption in different capacities from three major producers.

2.13 Conclusion

DWDM fixed and flex grid networks have been discussed, and the primary problems of lightpath assignment have been solved using different approaches. Linear programming as the backbone of integer linear programming was specifically discussed, and the most famous method of solving such a problem i.e., the Simplex method explained. In addition, the power consumption of different network segments was briefly studied. The router's power consumption as the most power-hungry component in Ip-over-DWDM networks has been modeled using data obtained from major router producers.

Chapter 3

Point to Multipoint Communication

3.1 Introduction

Point to Point (P2P) communication technologies are used to connect two devices or two computers. For instance, two antennas can communicate using a microwave link. However, P2P links are not always the best option. In a network of devices, computers, routers, and switches, implementing P2P links for all possible node pairs might be challenging. It is worth noting that the number of links needed for connecting N nodes is $N \times (N - 1)$, which represents a full-meshed network. On the other hand, point-to-multipoint (P2MP) communication is able to connect a single point to several points. The dominant form of communication is P2MP, when the number of nodes is significant since the number of links is linearly proportional to the number of nodes. For example, a single antenna communicates with tens of mobile devices simultaneously. Figure 3.1(a) shows a tree with four links that connect five nodes. A spanning tree connects all nodes with the minimum number of links $N - 1$ where N is the number of nodes. The logical links that connect nodes 1 to 4 and nodes 3 to 5 are highlighted. As can be seen, they are sharing the link (1,2).

In contrast, in a fully meshed network depicted in Fig. 3.1(b), there are $\frac{N(N-1)}{2}$ links, and each node pair can be directly connected. The principal logic is to share resources as much as possible (without losing the quality of service). Resources are optical links, power, space, and all network equipment (e.g., router cards and transceivers).

Some forms of communication are inherently P2MP. Take a TV satellite as an example; it broadcasts data through the air, and TV sets on earth catch the signal, which might comprise data from different TV channels. The challenge is that the signal experiences massive loss in its journey, but it can be recovered thanks to low noise amplifiers in receivers.

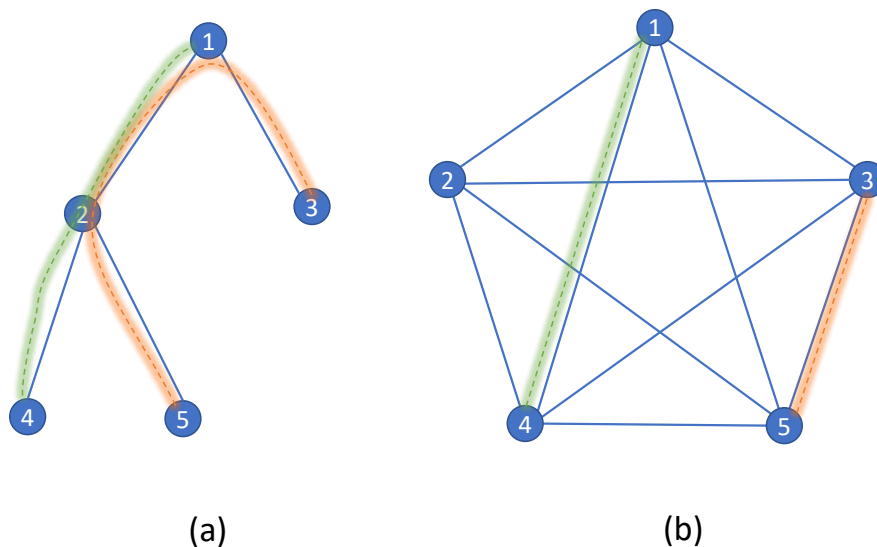


Fig. 3.1 (a) A tree Vs (b) a full meshed network connecting 5 nodes

Generally, P2MP links are more cost-efficient and more scalable, resulting in simpler architectures in large networks. PONs are the most recognized example of P2MP technology in optical network communication. They aggregate and distribute data close to the end users.

Although P2MP communication needs different technologies and infrastructure, this thesis focuses on P2MP optical transceivers, which can be used to transmit over optical fibers. In the following, we first review the evolution of transceivers from the literature. Next, we discuss the digital subcarrier multiplexing (DCSM) P2MP transceiver function and its architecture. Finally, we consider several scenarios for network planning using these transceivers and provide the result of simulations. This chapter is based on publications [J1] and [C2].

3.2 Optical Transceiver Modules Evolution

Optical transceivers are devices for sending and receiving data using optical signals. Data is encoded in 0's and 1's and prepared for transmission using a modulation process. On the receiver's side, the incoming light is demodulated and 0's and 1's extracted. Note that analog modulation is mostly used in voice applications such as radio transmission. Traditionally, light intensity is used for modulation and demodulation, called intensity modulation with direct detection (IM-DD) method. This leads to a simplified architecture and allows data transmission at a low cost. However, the IM-DD systems are not well scalable, and their spectral efficiency (SE) is significantly limited. Second-order nonlinearity is one of the

main obstacles in the typical IM-DD system. This results from square law photodetection, which significantly restricts system capacity [92]. Since the optical intensity modulates the information, chromatic dispersion (CD)– a phenomenon that causes optical frequency components arrives at the destination at different times because of difference in speeds– diminishes the transmission distance [93].

Alternatively, a coherent detection method can track the phase of an optical transmitter to extract any phase and frequency information carried by a transmitted signal which can be exploited for high data rate transmission at the expense of more complexities [94]. Although coherent detection is a concept derived from wireless communication systems, it has been widely used in optical fiber communications since 2011, bringing significant benefits to long-reach optical networks. The main advantages of coherent detection over direct detection are supporting the digital compensation of fiber linear impairments and benefiting from light polarization for increasing spectral efficiency (SE) [92]. The need for additional optical components and DSP in the coherent detection system leads to a higher cost and electricity consumption. Coherent transceivers are currently the dominant type in Metro and core networks [95].

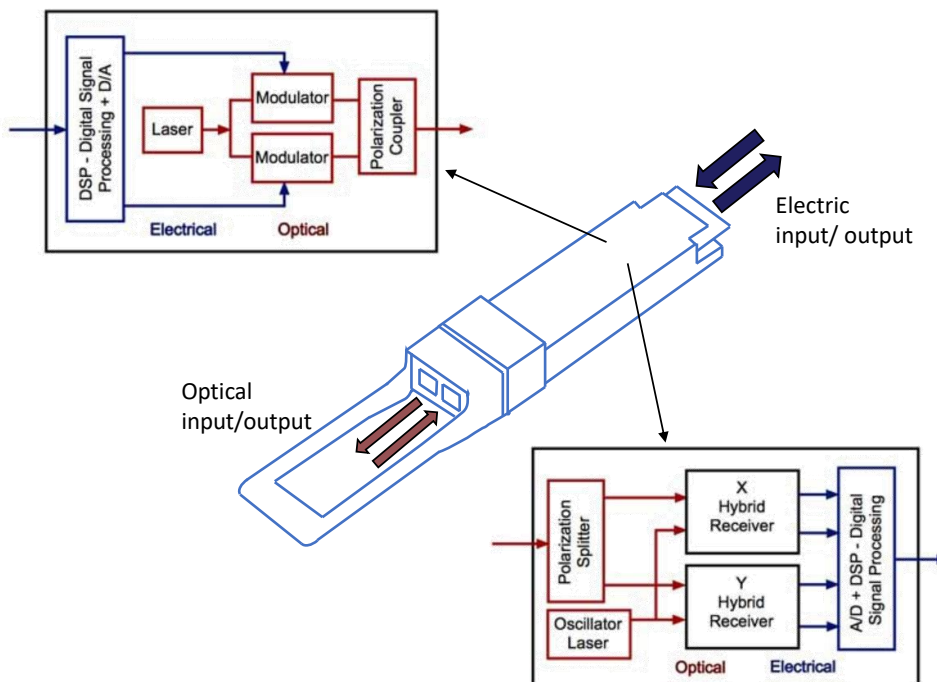


Fig. 3.2 A typical transceivers module with its sub-systems [1]

Many types of transceivers have been provided for different data rates and reach requirements. However, limited enhancement can be expected in transceiver performance due to

Shannon's limit. In recent years, considerable efforts have been made to introduce coherent transceivers for access networks [96, 97] to benefit their advantages. However, it requires essential simplifications to become economically practicable for access networks [98]. A transmitter is usually characterized by the form factor (a factor that determines the physical dimensions of the transceiver), rate, maximum transmission distance, physical layer standard, and working wavelength. Figure. 3.2 illustrates the layout of a typical transceiver as well as block diagrams of receiving and transmitting sub-systems.

3.3 Optical Transponder

When deployed in wavelength-routed optical networks, an optical transponder converts a client signal into an optical signal at the appropriate wavelength for transit. The term "transponder," which is a combination of the words "transmitter" and "responder," is used to describe an optical-electrical-optical (OEO) wavelength converter or a WDM transponder. Without changing the data or signal content, the transponder can automatically receive, amplify, and retransmit a signal on a different wavelength. Muxponders, like transponders, transmit and receive optical signals, but they also have the ability to multiplex several lower-rate client interfaces onto a higher-rate line interface.

3.4 Sliceable Bandwidth Variable Transponder

Shifting from the currently dominant fixed optical networks to spectrally efficient elastic optical networks (EONs) with flexible bandwidth and adaptive channel spacing (see section 2.4) is a new trend in optical networking. A bandwidth variable transponder (BVT) can be deployed in such networks and does the function of the traditional transponder used in fixed-grid networks. Note that other equipment, such as switches, must also be bandwidth flexible to take full advantage of flexibility in optical networks [99, 100]. One of the technologies that can be used for implementing BVTs is coherent optical orthogonal frequency-division multiplexing (CO-OFDM) [101]. CO-OFDM is based on transmitting multiple orthogonal subcarriers, which different formats can independently modulate. The orthogonal subcarriers are overlapped in the frequency domain, providing high spectral efficiency. Its flexible functionalities, unique subwavelength granularity, adaptive modulation, bit and power loading schemes, and subcarrier selection/suppression are the key enablers of BVTs [102]. Additionally, time-frequency packing (TFP) and Nyquist wavelength-division multiplexing (NWDM) can be employed for realizing flex subcarrier modules [103–105]. As depicted in Fig. 3.3, the optimal spectral form for each sub-channel in the Nyquist signal

is rectangular, with channel spacing equal to the baud rate of R_s . Consequently, there is no inter-channel interference (ICI). Due to the rectangular spectrum, however, the pulse within each channel is a *sinc* form in the time domain with zero-crossing points at integer periods of symbol period T_s , achieving zero inter-symbol interference (ISI). In contrast, each carrier in the OFDM system is *sinc*-shaped in the frequency domain and rectangular-shaped in the time domain. Therefore, both systems can theoretically attain ICI and ISI freedom simultaneously [2].

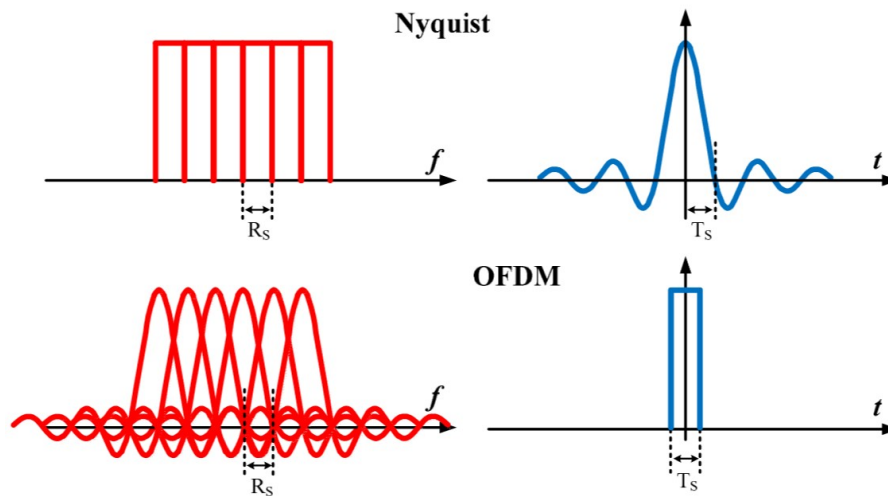


Fig. 3.3 Nyquist Vs OFDM in time and frequency domains [2]

Moving toward multi-flow transponders, in which the client signal is received at a single client-side interface and converted into a number of optical flows with different wavelengths, is a logical next step [3]. This type of transponder is called sliceable bandwidth variable transponder (S-BVT) in the literature. Figure. 3.4 shows the evolution of optical transponder functions in which Fig. 3.4(d) illustrates the multi-flow transponder function. N Client signals are mapped to M adaptive optical flows at the line side and vice versa. The line side flows can be individually routed using ROADMs to reach their destinations.

López et al. showed [106] that the target expenditure of 400 Gb/s and 1 Tb/s sliceable bandwidth variable transponders (S-BVTs) is half the non-sliceable transponders cost in a core network scenario for two different topologies. Utilizing software-defined networking (SDN) (SDN is a type of network architecture that lets software applications be used to "program" or control the network in an intelligent and centralized way), the rate/distance adaptive multi-flow generation and routing/switching, slice-ability, flexibility, and adaptability for the mitigation of spectrum fragmentation, and a smooth migration toward the flex-grid paradigm, have been experimentally studied in [107].

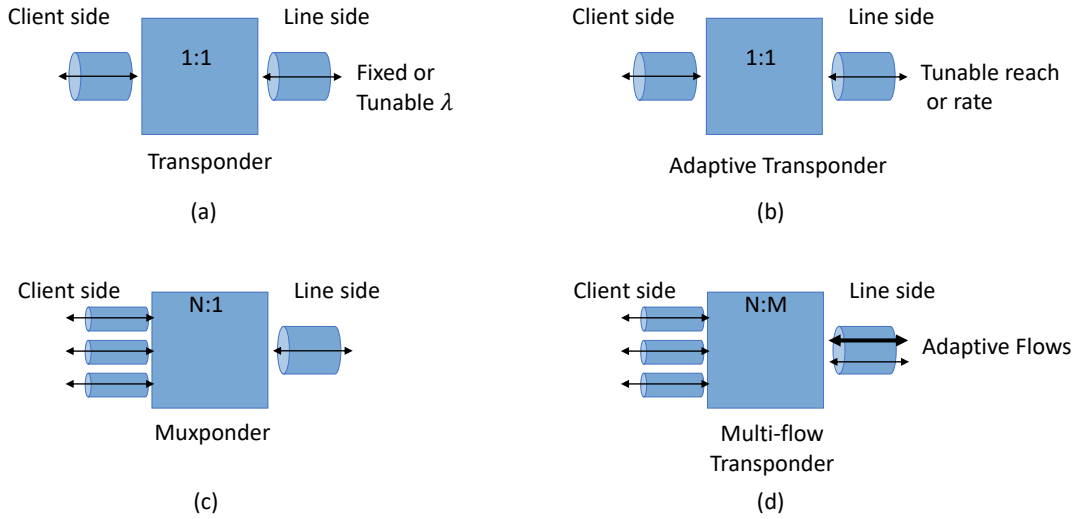


Fig. 3.4 Optical transponder function evolution. [3]

3.5 Digital Subcarrier Multiplexing Point to Multipoint Transceivers

In a typical optical system, a single laser sends a signal that fills the entire channel spectrum called the optical carrier. Since the spectral width of the signal is proportional to the baud rate, a high-baud-rate signal has a more significant gap between its lowest and highest frequency components and thus experiences more significant variation in the speed of its frequencies through the fiber and more “spreading” in the time domain. Moreover, more symbols per second mean a shorter time interval between symbols, meaning symbols can more easily overlap. These two factors combine to make a squared relationship between baud rate and chromatic dispersion [108]. In a coherent implementation with transmitter-based processing (the processing unit is usually only located at the receiver end), it is possible to mathematically shape the single-carrier signal to occupy the least amount of optical spectrum, known as Nyquist pulse shaping. Given that, subcarrier multiplexing reduces the complexity of dispersion compensation compared to the single carrier approach [109]. Additionally, since the subcarriers’ spectra are not overlapped in digital subcarrier multiplexing (DSCM) signals, unlike in OFDM, the subcarriers of the Nyquist DSCM signal can be isolated and processed independently [110].

These remarkable characteristics of DSCM have made it possible to design a new form of P2MP transceiver [111, 112], known as a DSCM-based coherent P2MP transceiver. A high-capacity transceiver divides the optical channel’s spectrum into small chunks and allocates them to many subcarriers. Then, it broadcasts these subcarriers from an aggregation point

(hub node) toward some leaf nodes so that they can receive them. Then, each leaf node equipped with a low data rate transceiver is capable of processing the correct subcarriers in the digital domain. Leaf node transceivers can simultaneously broadcast the same or different optical subcarriers upstream to the hub transceiver(s). Fewer interfaces in switches and routers are one of the key advantages of P2MP transceivers, leading to reduced complexity and expense.

3.5.1 Transceiver Architecture

The number of subcarriers can be arbitrary in DSCM P2MP transceivers, but the most efficient numbers are in the power of 2 because application-specific integrated circuits (ASICs) can be scaled easier [4]. Figure. 3.5 shows the architecture of a transmitter system in P2MP transceivers. The symbols of each SC are mapped to an appropriate modulation format, e.g., 16-QAM. Next, finite impulse response (FIR) filters shape the Nyquist pulses (roll-off $\rho \approx 0.05$). A digital multiplexer is used in front of the $4\times$ digital to analog converter (DAC). Finally, the signal goes through the driver and the dual polarization IQ Mach-Zehnder Modulator (IQ-MZM).

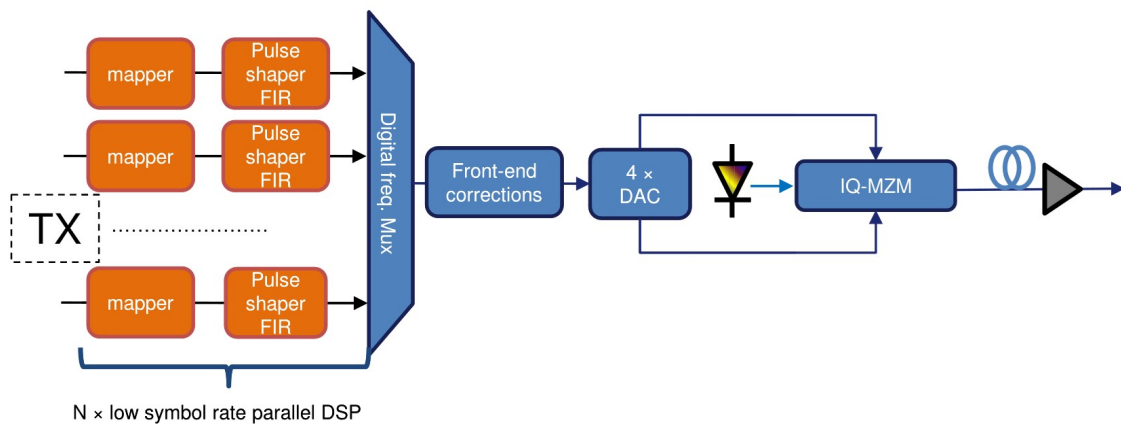


Fig. 3.5 DSCM P2MP transmitter architecture [4].

In the receiver side, as shown in Fig. 3.6, the light is detected by the coherent front end and converted into the digital domain by a $4\times$ ADC (analog to digital converter). Next, the front-end correction block compensates for I/Q skew, roll-off, power imbalance, and frequency ripple. In the following, a digital frequency demultiplexer separates the SCs. Then, Chromatic Dispersion (CD) filters compensate the dispersion accumulated by the channel along the link. Note that the complexity of these filters combined is less than a single-channel implementation with the same total baud rate. A Multiple Input Multiple Output

(MIMO) equalizer then divides the two polarizations and corrects for residual dispersion and Polarization Mode Dispersion (PMD). These two parts maintain the same structure for both single-wavelength and subcarrier (SC) (see [113] for more about digital filters). Notably, frequency and clock synchronization are among the reasons why DSCM was chosen over OFDM. According to [114], the computational complexity of OFDM and DSCM is comparable only in the case of P2P transceivers. As soon as we shift to a P2MP scenario, frequency and phase instability make OFDM considerably more complicated.

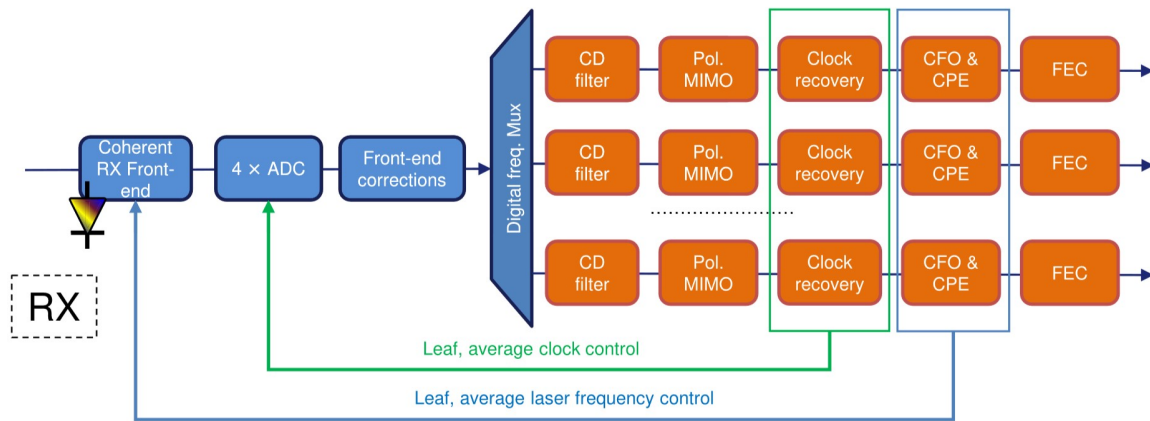


Fig. 3.6 DSCM P2MP receiver architecture (note that Digital freq. Mux refers to Digital freq. DeMux). [4]

3.6 Network Application Scenarios

Although it is expected that transceivers with a greater capacity will have a lower cost per transmitted bit [115], it is only advantageous if the operators can utilize the transceiver capacity efficiently. In contrast to traditional mesh voice traffic, the traffic pattern has been shifted to the hub-and-spoke pattern in access and metro aggregation networks. The reason is that most of the individual nodes send/receive data to/from destinations/sources outside the regions that networks cover. Therefore, hub-and-spoke network architectures such as ring, horseshoe, and tree are better fit for such traffic patterns. However, the traffic load at individual sites is low, and it is difficult to fully take advantage of the cheaper per bit cost of high data rate coherent transceivers.

One way is provisioning high data rate transceivers if they are expected to be fully utilized in the future. However, this wastes capital at the beginning and increases investment risk. P2MP transceivers (in the following of this thesis, we refer to DSCM-based P2MP transceivers as P2MP transceivers) can solve a part of this problem. Instead of several

low-capacity transceivers at the hub node, only one (or few) can communicate with low-data rate transceivers at leaf nodes. This improvement leads to fewer router ports at the hub node and can reduce power consumption and footprint. In addition, the electrical aggregation can be replaced by optical splitters and combiners [4]. Recent works have experimentally demonstrated the feasibility of this technology [116] and highlighted that the cumulative CAPEX savings could reach 76% over five years compared to the traditional P2P solution [117].

Early works exploiting DSCM-based P2MP transceivers have assumed star, chain, and ring network topologies, as exemplified in Fig. 3.7(b). Applying the concept to meshed metro-aggregation topologies is also possible where the traffic might be mainly still in a hub-and-spoke pattern (see Fig. 3.7(c)) but requires a more complex design methodology. Various scenarios, such as protection, multi-hub, and ROADM-based or filterless architectures, can be considered.

3.7 P2MP Transceivers Deployment in ROADM-based Meshed Networks

We assume ROADMs can guide an SC or a group of SCs in optical networks from hub node(s) to leaf nodes and vice versa. To enable this, ROADMs have to support low channel spacing.

3.7.1 Survivable Network Scenarios

Metro-aggregation networks are a vital part of the overall transport infrastructure, collecting, aggregating, and handing traffic over to other network segments that have varying degrees of priority and can be, as a result, subject to strict service level agreements (SLAs). Ensuring survivability to the most likely failure scenarios (e.g., fiber cut) is required in some of these network deployments. In this work, we consider the support of protection mechanisms against two main types of failures: fiber cuts and failures impacting the hub node. Fiber cuts, e.g., due to construction works, can occur relatively often [118]. Protection against link failures consists of provisioning a disjoint connection and sending traffic via both working and protection paths.

Since hub nodes in metro-aggregation networks can represent a single point of failure, i.e., a malfunction or failure event in the hub node can disrupt all traffic in the network, hub node redundancy can be adopted. In this case, at least two hub nodes are present in

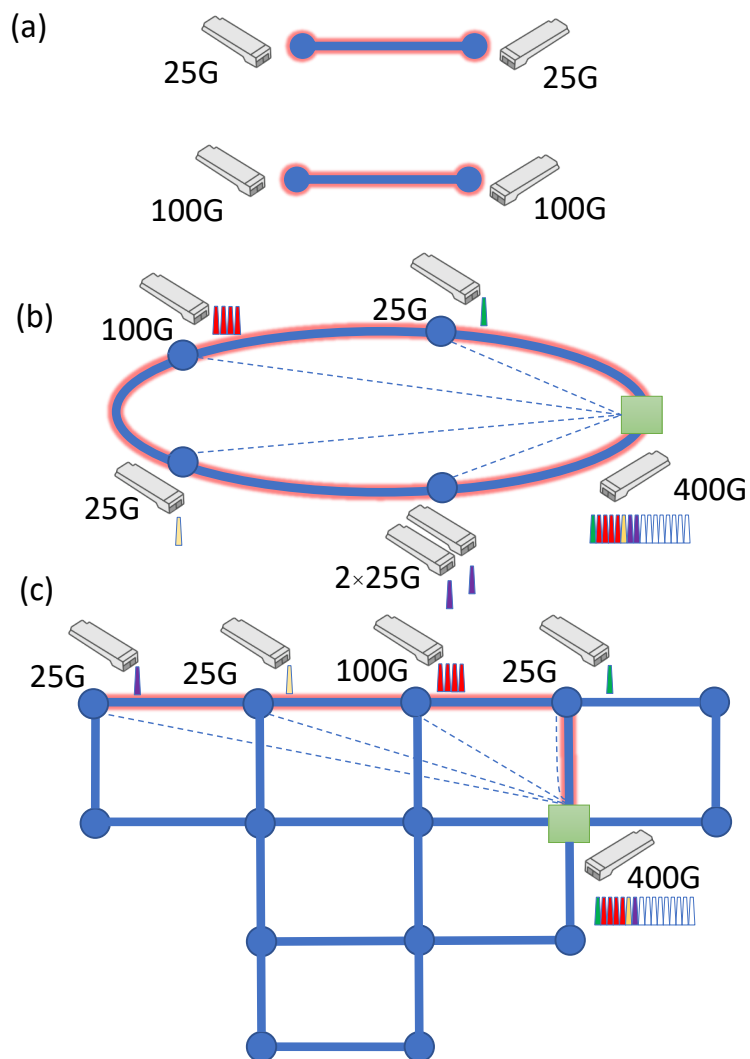


Fig. 3.7 Implementation of communication links with (a) identical P2P transceivers, (b) P2MP transceivers deployment in a ring network, and (c) in a meshed network (dashed lines show logical connections while highlighted paths show optical paths) ([C2] © 2021 IEEE).

the network, and leaf nodes communicate with both of them. The following five different network scenarios are considered in this work:

- Single hub without any protection (SH);
- Single hub with link protection (SH-LP);
- Multi-hub without any protection (MH);
- Multi-hub with link protection (MH-LP);
- Multi-hub with link and hub protection (MH-LHP).

Figure 3.8 shows potential implementations of these five scenarios over a reference mesh topology representative of a region in Spain. This network was defined by Telefónica in the scope of the FP7 IDEALIST project, as detailed in [119], and is utilized to carry out the analysis reported in section 3.7.4. Particularly, potential paths interconnecting leaf nodes A and B and hub node H1 (as well as hub node H2 in the multi-hub scenario) are represented. In the SH scenario (Fig. 3.8(a)), all leaf nodes communicate with a single hub via a single path, whereas in the SH-LP case (Fig. 3.8(b)), each leaf node is connected to the hub with two disjoint paths. Using disjoint paths guarantees that a single fiber link failure in the network will not interrupt services. Fig. 3.8(b) also shows that both backup paths of A and B converge to a common link before reaching H1, which means that their traffic could start/terminate at the same P2MP interface located in H1. As can be seen from Fig. 3.8(c), the MH scenario provides another degree of freedom to route traffic since any of the two hub nodes can be used by the leaf nodes. The MH-LP case provides protection against link failures by setting up two disjoint paths between each leaf and a hub node (Fig. 3.8(d)). Note that, in this scenario, each leaf node communicates only with one hub. The last scenario is MH-LHP (illustrated in Fig. 3.8(e)), and it grants protection against both hub and link failures by enforcing that each leaf node communicates with two different hubs through two disjoint paths.

3.7.2 Optimization Framework

The P2MP optimization problem aims to find the best deployment of P2MP transceivers (in terms of cost) for a given traffic distribution and a specific metro-aggregation network topology. For this purpose, we developed and implemented an ILP model whose input parameters and decision variables are shown in Table 3.1 and Table 3.2, respectively.

We assume that the P2MP transceivers can transmit DP-16QAM (25GHz/SC) and DP-QPSK (12.5GHz/SC) modulation formats, with the use of DP-16QAM limited to links

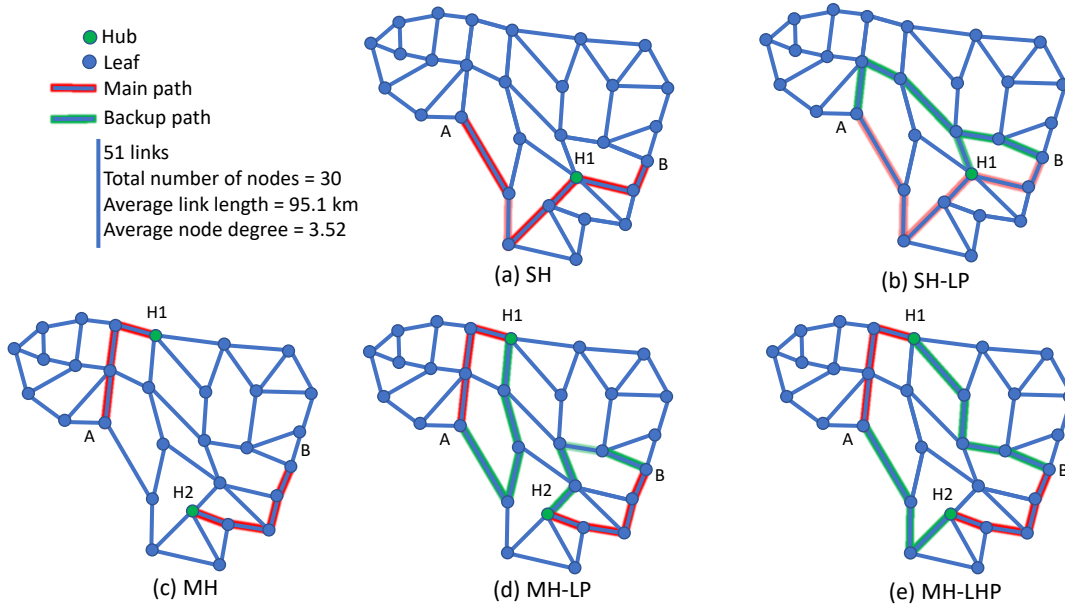


Fig. 3.8 Illustration of the five network scenarios considered in this work over a reference mesh network: (a) single hub (SH), (b) single hub with link protection (SH-LP), (c) multi-hub (MH), (d) multi-hub with link protection (MH-LP), and (e) multi-hub with the link and hub protection (MH-LHP) ([C2] © 2021 IEEE).

Table 3.1 Input parameters of the ILP model

Parameter	Description
$G(V, E)$	Network graph with nodes $n \in V$ and links $l \in E$.
V	Set of all nodes.
I	A subset of V containing the leaf nodes ($N = V - 1$).
H	A subset of V containing the hub nodes.
F	The set of possible channels in paths.
J	Set of k paths from leaf nodes to hub node(s).
sub_h	Subset of paths connecting leaf nodes to the hub h .
$P(i, j) \in [0, 1]$	Leaf-path incident matrix.
$B(l, j) \in [0, 1]$	Link-path incident matrix.
$T(i)$	Maximum of upstream and downstream traffic, expressed by number of 25G SCs for leaf node i .
M_j	Modulation factor for path j .
O_h	Transceiver types of hub nodes.
O_l	Transceiver types of leaf nodes.
C_o	Cost of transceiver type o .
G_o	Capacity of transceiver type o in form of number of SCs.

shorter than 500 km. We have introduced this constraint into the ILP model by defining M_j as follows:

$$M_j = \begin{cases} 1 & \text{if length path } j \leq 500 \text{ km} \\ 0.5 & \text{if } 500 \text{ km} \leq \text{length path } j \leq 1500 \text{ km} \end{cases} \quad (3.1)$$

We calculate a set of k shortest paths from each leaf node to each hub for a given network with a predetermined set of hub nodes H and leaf nodes I and store it in the set J . Then, the matrices $B(l, j)$ and $P(i, j)$ are calculated.

Table 3.2 Decision variables of the ILP model

Variable	Description
$\lambda_{ij} \in [0, 1]$	Binary variable equals 1 if leaf node i communicates with a hub through path j .
$\Delta_{jo} \in N^0$	Number of transceivers of type o which uses path j , and deployed at the hub nodes.
$\delta_{ijo} \in N^0$	Number of transceivers of type o which uses path j , and is deployed at the leaf node i .
$\gamma_{jf} \in [0, 1]$	Binary variable equals 1 if channel f is occupied by path j .

The ILP objective function is given by:

$$z = \sum_j \sum_{o \in O_h} C_o \Delta_{jo} + \sum_i \sum_j \sum_{o \in O_l} C_o \delta_{ijo} \quad (3.2)$$

subject to:

$$\sum_{j \in \text{sub}_h} \lambda_{ij} \leq s_1 \quad \forall i \in I, h \in H \quad (3.3)$$

$$\sum_j \lambda_{ij} = s_2 \quad \forall i \in I \quad (3.4)$$

$$\lambda_{ij} \leq P(i, j) \quad \forall i \in I, j \in J \quad (3.5)$$

$$\sum_i T(i) \lambda_{ij} \leq \sum_{o \in O_h} G_o M_j \Delta_{jo} \quad \forall j \in J \quad (3.6)$$

$$T(i) \lambda_{ij} \leq \sum_{o \in O_l} G_o M_j \delta_{ijo} \quad \forall i \in I, j \in J \quad (3.7)$$

$$\sum_f \gamma_{jf} = \sum_{o \in O_h} \Delta_{jo} \quad \forall j \in J \quad (3.8)$$

$$\sum_j B(l, j) \gamma_{jf} \leq 1 \quad \forall f \in F, l \in E \quad (3.9)$$

$$\sum_j \lambda_{ij} B(l, j) \leq 1 \quad \forall i \in I, l \in E \quad (3.10)$$

By taking into account the cost of each interface and by minimizing Eq. (3.2), solving the ILP model leads to globally optimizing (i.e., minimizing the cost of) the P2MP solution that guarantees that all traffic demands are supported, and the target protection scheme is enforced. Constraint (3.3) ensures that each leaf node communicates with each hub a maximum s_1 times. Constraint (3.4) states that the total number of paths established between each leaf node and all hubs must be equal to s_2 . Based on the value of s_1 and s_2 , the formulation enables modeling different network scenarios defined in section 3.7.1 as shown in Table 3.3. When the number of hubs is higher than one, $s_1 = 1$ and $s_2 = 1$ give the MH scenario, while $s_1 = 2$ and $s_2 = 2$ represent the MH-LP case. The MH-LHP scenario can be modeled by setting $s_1 = 1$ and $s_2 = 2$. When there is a single hub, by simply removing constraint (3.3) from the formulation, the network scenarios SH ($s_2 = 1$) and SH-LP ($s_2 = 1$) are modeled. Constraint (3.5) guarantees that only leaf nodes sharing a common path can communicate with a single P2MP transceiver at one of the hub nodes. Constraint (3.6) and (3.7) calculate the number of different transceivers at the hub nodes and leaf nodes, respectively. Channel allocation is imposed by constraint (3.8), whereas constraint (3.9) sets a limit on individual link capacity. Finally, constraint (3.10) is utilized to enforce that the working and backup paths are disjoint when supporting link protection (i.e., in the SH-LP, MH-LP, and MH-LHP scenarios).

Noteworthy, by setting to 0 all 1 values of each column of $P(i, j)$, except the one showing the path to the furthest leaf node, the ILP model can simulate the P2P scenario.

Scenario	s_1	s_2
Multi Hub	1	1
Multi Hub Links Protection	2	2
Multi Hub Links and Hubs Protection	1	2

Table 3.3 Scenarios based on auxiliary variables s_1 and s_2 values.

3.7.3 Transceivers Cost Model

As stated above, a key motivation for deploying P2MP transceivers is the possibility of using fewer high-capacity devices at the hub node. It is well known that when the transceiver data rate increases (e.g., between consecutive transceiver generations), the cost increases but not directly proportional to the capacity increase [120, 4]. This means that the cost per bit/s reduces when opting for a higher-capacity transceiver. Therefore, it is usually more cost-effective to deploy a smaller number of high-capacity transceivers for the same total aggregate capacity. Figure 3.9 qualitatively illustrates the relation between transceiver cost and data rate. The red dashed line shows the cost if there were no per bit cost savings when scaling capacity, and possible relative cost figures for three transceivers whose data rate is $4\times$ that of the previous one are also represented. We can model the cost of the transceiver supporting s number of 25G subcarriers with $Cost = As^B$, where A is a normalization factor for setting the 400G transceiver cost to 1, and B is a positive constant smaller than one, determining the cost profile. This can be feasible as technology costs tend to decrease exponentially over generations [121]. If B is greater than one, high-capacity transceivers have a more expensive per-bit capacity, whereas if B is one, the cost of transceivers is precisely proportional to the capacity they offer.

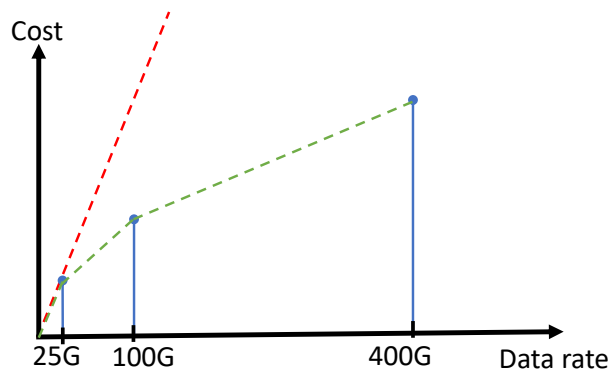


Fig. 3.9 Visual representation of cost profile versus data rate and possible cost decrease compared to linear cost scale.

3.7.4 Results and Discussion I

This section presents a detailed analysis of the effectiveness of deploying DSCM-based P2MP transceivers in the reference mesh network described in section 3.7.1. A set of eight shortest paths are calculated for each leaf-hub node pair. To have a more realistic study, we assume the use of transceivers capable of generating 400G, 100G, and 25G signals. We

consider 400G and 100G transceivers can be deployed at hub nodes. A total of 40 wavelength channels is assumed to be available at each link ($|F| = 40$, 100GHz fixed-grid channels). 100G and 25G transceivers can be deployed at the leaf nodes.

Additionally, we use a non-uniform traffic pattern in which the number of 25G SCs is randomly chosen from the set of $[x, x + 4]$ where x varies from 1 to 6. For simplicity, we use the average number of required SCs, i.e., $x + 2$, when presenting the results. A Monte-Carlo simulation with five iterations is considered and the results presented represent the average value over the five independent runs. Note that the maximum of 90% confidence intervals for different scenarios and different traffic loads is 7%. The GAMS software and its CPLEX solver are used for modeling and solving the proposed ILP models [122]. Some guidance on implementing ILP formulations using GAMS is provided in Appendix A.

The first set of results investigates the impact of the number of candidate routing paths on the solution cost. Considering the SH scenario illustrated in Fig. 3.8(a), the model was solved for a number of candidate paths per node pair that varies between 1 and 8. Figure 3.10 shows the normalized interface cost as a function of the average offered traffic load per leaf node (in number of SCs). As can be seen, when the number of candidate shortest paths k increases, the solution cost is reduced as a consequence of better exploiting the routing solution space to aggregate SCs from different leaf nodes into fewer interfaces at the hub nodes. However, as expected, there are diminishing improvements for k large enough. The remaining analysis assumes that the eight shortest paths are available to the ILP model.

The second set of results considers a single hub node is used (see Fig. 3.8 (a) and (b)). Hence, Figure 3.11(a) shows the normalized interface cost for the SH and SH-LP scenarios in the reference metro-aggregation network and considers the DSCM-based P2MP solution, as well as a typical P2P solution. When the average traffic increases from three to eight 25G the cost of P2MP transceivers without protection rises from an average of 20 to about 48. Implementing link protection further increases these costs by 116% to 135%, which is in line with the common observation that links protection demands at least double the amount of resources provisioned. Notably, the P2MP approach is consistently more cost-effective than the P2P one. Indeed, the results show that using 100G P2P transceivers results in a cost increase of between 30% and 50% compared to the proposed P2MP solution.

The third set of results assumes that two hubs are available (see Fig. 3.8 (c), (d), and (e)). As can be seen in Fig. 3.11(b), evolving from SH to MH leads to only a minor increase in interface cost (around 5%). Noteworthy, for the same scenario, the cost savings of the P2MP approach, when compared to P2P, are similar to those observed in Fig. 3.11(a) for the SH scenario. For instance, in comparison to the P2MP deployment strategy, supporting all traffic demands with P2P transceivers with both link and hub protection increases the average cost

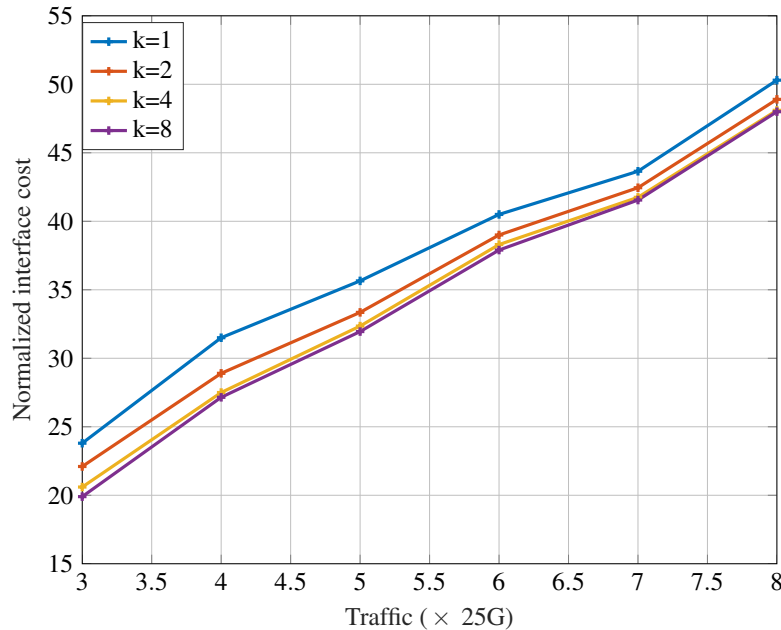


Fig. 3.10 Normalized interface cost calculated for SH scenario when the number of shortest paths increases from 1 to 8 ([C2] © 2021 IEEE).

by approximately 30%. Another interesting observation is that link protection is 5% to 15% cheaper when there are two hubs in the network. This is because shorter paths between leaf and hub nodes can be exploited when two hubs are available, mitigating the need to use DP-QPSK (which halves the capacity of each SC) to provide connectivity to the farthest leaf nodes.

The key advantage of P2MP comes from replacing multiple lower-rate interfaces at the hub node with a single higher-rate interface. In order to observe this effect, Figures 3.12(a) and (b) depict the number of interfaces deployed at the hub node(s) for the scenarios considered in this work. The results show that the number of P2MP transceivers deployed at the hub node(s) is always much smaller than that required with the P2P approach. The number of deployed P2MP interfaces more than doubles when considering link protection.

This result can be a consequence of the greater difficulty in optimizing traffic aggregation in the presence of the path disjointness constraint. Moreover, in the case of SH-LP, it can also be the result of using DP-QPSK in the longer protection paths. The number of interfaces in SH-LP is almost constant when traffic rises from 3 to 8 of 25G capacity demand. The reason is that when traffic increases, the number of 400G transceivers increases, while the number of 100G transceivers decreases. Finally, the number of interfaces in MH-LHP is

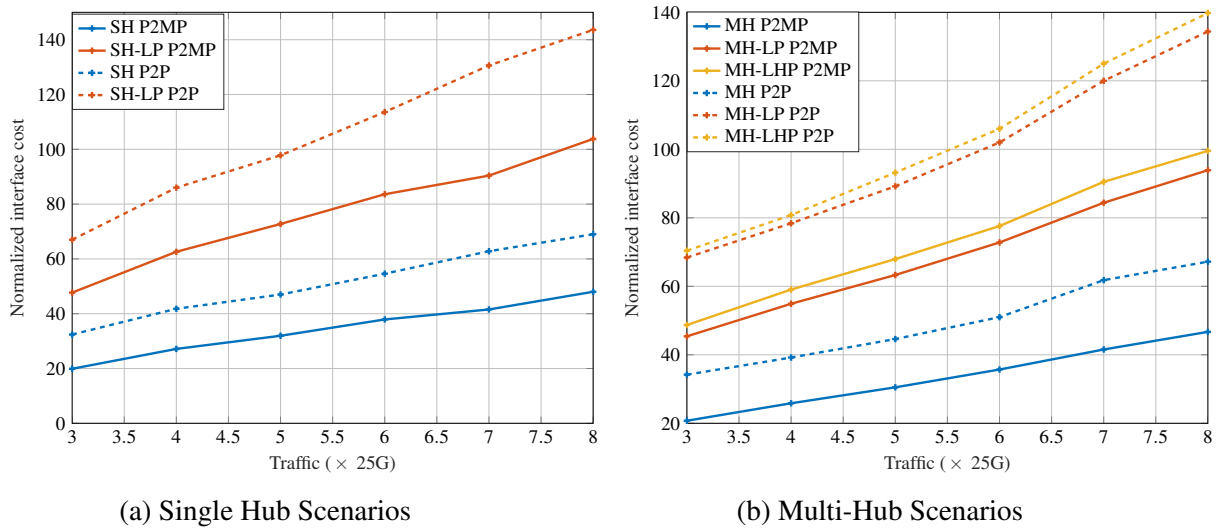


Fig. 3.11 Normalized interface cost ([C2] © 2021 IEEE).

slightly higher than in MH-LP, highlighting that hub protection can be attained with only a small interface cost penalty.

In order to gain further insight into the solutions obtained, Table 3.4 provides the total number of interfaces for an average traffic load of $4 \times 25G$ /s and their related costs for all different scenarios discussed in this paper.

Table 3.4 Total number of interfaces for a traffic load with an average of $4 \times 25G$ /s and their total costs for different scenarios ([C2] © 2021 IEEE).

	P2P		P2MP			
	100G	Total cost	400G	100G	25G	Total cost
SH	83.6	41.8	7.6	34.8	8.6	27.15
SH-LP	172	86	18.2	81.6	14.4	62.6
MH	78.4	39.2	7.6	33.6	6.2	25.95
MH-LP	156.6	78.3	14.2	74.4	14.4	55
MH-LHP	161.6	80.8	16.4	77.6	15	58.95

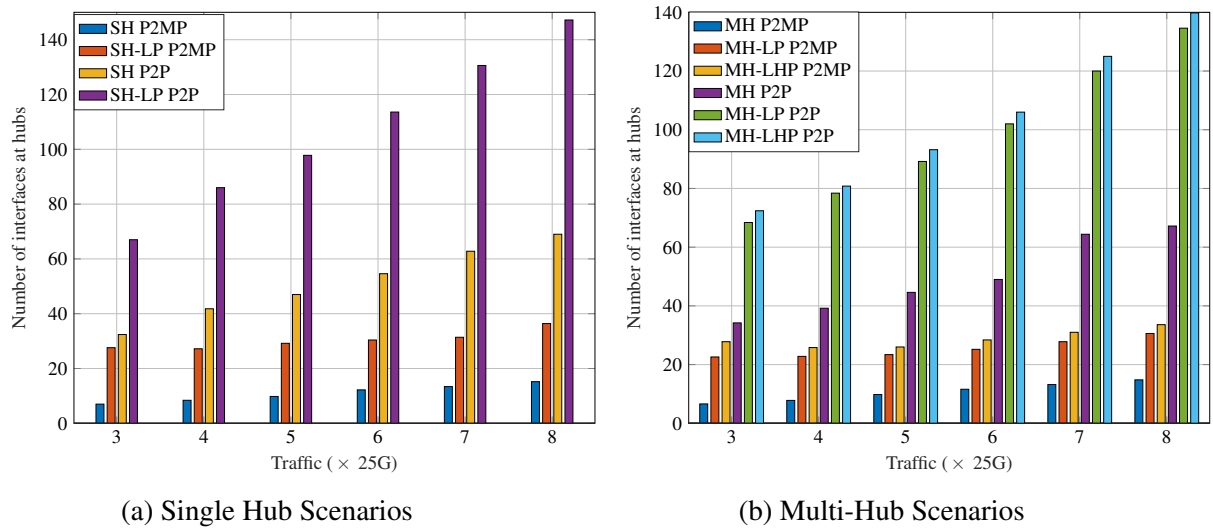


Fig. 3.12 Number of interfaces at the hub node(s) ([C2] © 2021 IEEE).

3.8 Optimized Deployment of P2MP Transceivers in Filterless Networks

Passive optical components are less expensive and less prone to failure than active optical ones. Combiners/splitters, as primary passive components, are blind to frequency channels and cannot distinguish wavelengths. Numerous ways of designing networks using passive optical components have been explored. The concept of a light trail has been proposed in [123, 124]. It comprises an architecture and a protocol that enables each source and destination node pair to dynamically establish a lightpath or trail for a specified duration. Optical combiners/splitters perform the add/drop function. A critical aspect when dimensioning filterless networks is that closed loops must be avoided to prevent the same optical signal from traversing the same link twice. Bearing this in mind, the authors of [49] examined the usage of passive components in wide area networks (WANs), which generally can have a mesh physical topology, and how to establish a set of physical optical connections between all nodes without generating closed loops.

Several path protection strategies using wavelength blockers, colored passive filters, and inter-tree transceivers have been investigated in [51]. It has been shown that the use of wavelength blockers and colored passive filters leads to a better cost-saving, while the deployment of inter-tree transceivers is slightly more spectrum-efficient. Moreover, the work in [125] studied the optimization of optical tree constructions, routing, and wavelength assignment.

Figure 3.13(a) shows an illustrative example of a ROADM-based network when P2P transceivers are deployed. Two leaf nodes with 25G and 100G traffic requirements are considered. Two pairs of 25G and 100G transceivers are needed, and spectrum is allocated only in the required links (i.e., spectrum reuse is possible). In the filterless scenario, which is exemplified in Fig. 3.13(b), ROADMs are replaced by simpler passive optical splitters/combiners. This simplifies the network architecture and reduces cost but may involve spectrum waste due to the broadcast nature of optical splitters (e.g., the spectrum used by the 100G connection between the hub node and the leaf node closer to it becomes unavailable in the link between both leaf nodes). Importantly, two factors mitigate the importance of spectrum waste in metro-aggregation networks: (i) the lower capacity required in this network segment (compared to core and metro-core networks) means they are far from being spectrum constrained; (ii) the hub-and-spoke traffic pattern reduces the usefulness of spectrum reuse.

P2MP transceivers can also be deployed in networks with filterless architectures, as illustrated in Fig. 3.13(c). In this case, a 400G transceiver is deployed at the hub node and communicates with the two leaf nodes. In this implementation, it is assumed that this transceiver transmits/receives up to 16 SCs, being able to communicate with up to 16 separate leaf nodes. Lower-capacity (lower cost) transceivers are installed at the leaf nodes. The utilization of splitter/combiner elements means that the number of SCs intended for each leaf node can be easily reconfigured as long as the maximum number of SCs each leaf transceiver can handle is not exceeded.

3.8.1 Survivability in Filterless Networks

Metro-aggregation networks are critical areas of the telecommunications infrastructure. They gather, combine, and route traffic to other network segments with varying degrees of priority, which may be subject to diverse service level agreements (SLAs). Different mechanisms can be used to assure survivability in the face of the most frequent failure scenarios (e.g., fiber cuts) [126]. A widely employed mechanism relies on setting up two disjoint connections between the hub node and each leaf node, designated as the working and the protection connections, and transmitting the same information over both of them. If a failure impacts one of the links, the connection is not out of service because the traffic is still transmitted and received over the non-affected connection. In the case of ROADM-based network implementation, link disjointness of both connections needs to be ensured.

On the contrary, suppose the nodes are based on optical splitters/combiners. In this case, two link-disjoint spanning trees can provide full protection since connections only for hub-leaf (but not for leaf-leaf) node pairs are required. However, the necessary but not sufficient condition for having two link-disjoint spanning trees is that the network must

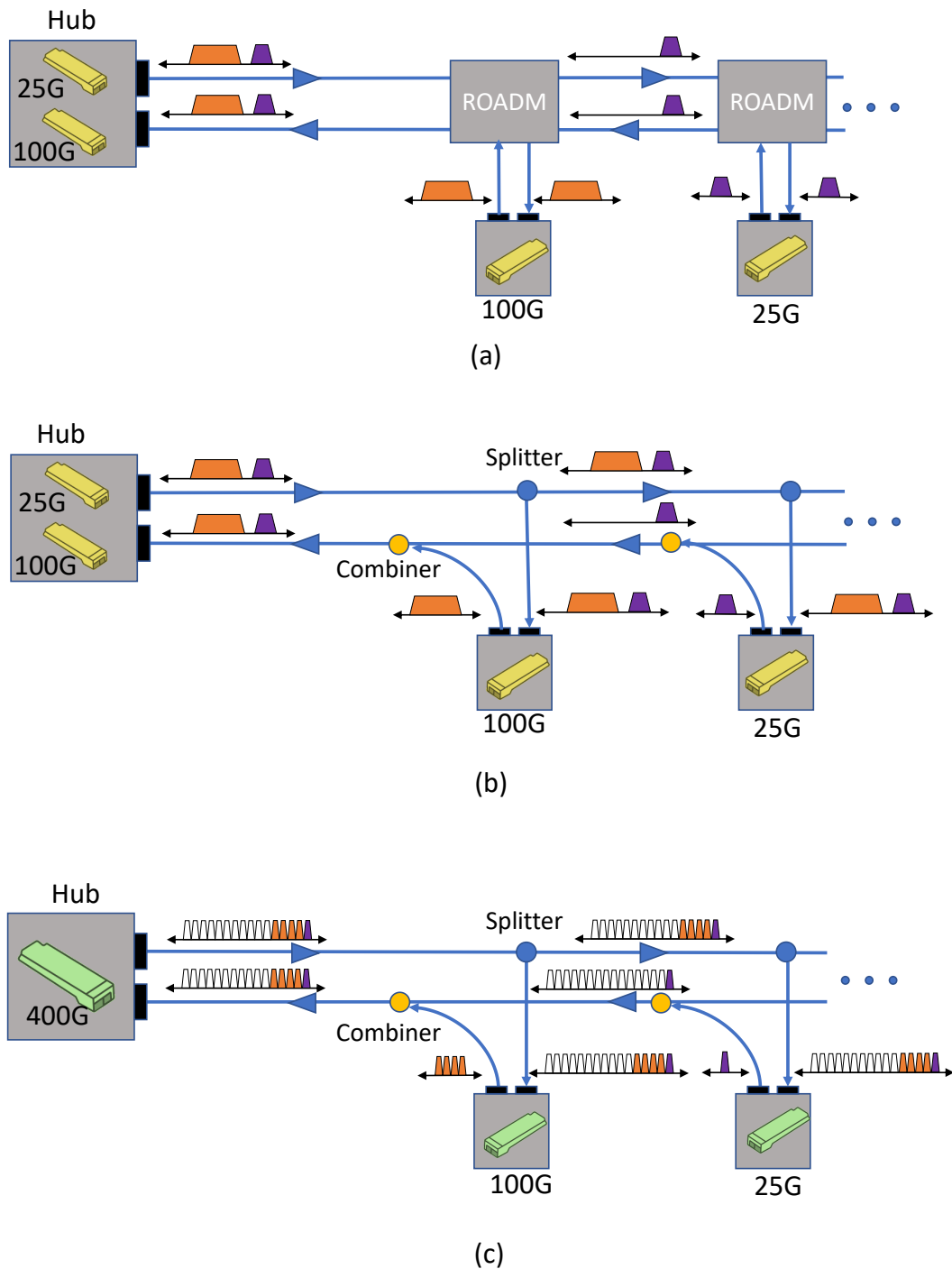


Fig. 3.13 (a) P2P transceivers deployment using active ROADM devices, (b) P2P transceivers deployment using passive optical splitters/combiners, (c) P2MP transceivers deployment using passive optical splitters/combiners (with permission from [J1] ©Optica Publishing Group).

have more than $2 \times (N - 1)$ links, where N is the number of nodes. This is unlikely for most ordinary optical networks. Therefore, one way is constructing two spectrally disjoint optical trees by selectively blocking signal transmission partly or fully between certain nodal degrees. This means that all leaf nodes' working and protection connections have to be considered simultaneously, resulting in a significantly more complex problem to be solved. A multi-tree technique has been proposed in [127] to address the possibility of widespread network failures. The authors suggest a communication protocol based on k rooted spanning trees with the property that the paths between each vertex v and the root are edge-disjoint. The two-tree protocol for edges states:

- Each leaf node transmits data upward to the root (hub) on both trees;
- When the hub receives data from one of its neighbors, the data are routed downward via both trees.

Three stages are involved in locating trees that possess the previously specified attribute. To begin, a depth-first search (DFS) is performed to obtain a DFS numbering, followed by the computation of the $s - t$ numbering (a method of numbering in which all nodes except s (root) and t have adjacent nodes with higher and lower assigned numbers). Then, the main and backup trees are created using the approaches outlined in [127]. It should be noted that although this method can efficiently find a pair of trees with disjoint paths from leaf nodes to the root, using it when designing a metro-aggregation network based on P2MP transceivers can lead to sub-optimal solutions. This is due to the fact that the trees selected can have an impact on the overall quality of the solution (i.e., cost). For example, the paths of a tree may determine which modulation format can be used for SCs transmitted over that tree, impacting the number and type of transceivers required at the hub and leaf nodes. This observation motivated us to jointly solve the problem of setting up trees with disjoint paths and the problem of routing, modulation format, and SC assignment, having – as a final objective – to minimize the transceiver cost.

3.8.2 ILP Optimization Framework

The P2MP optimization framework aims to discover the most cost-effective configuration of P2MP transceivers for a given traffic distribution and metro-aggregation network topology, allowing support of link protection and assuming nodes are based on simple optical splitter/combiner devices. In order to accomplish this goal, we have devised an ILP model. The model's input parameters and decision variables are as follows.

Input Parameters

- $G(V, E)$: network graph with nodes $u, i, j \in V$ and links $l = (i, j) \in E$.
- V^- : a subset of V defining leaf nodes (all nodes minus the hub nodes).
- W_{ij} : length of link $(i, j) \in E$.
- $T(u)$: number of 25 Gb/s SCs required by leaf node u . This is assumed to be the maximum required traffic of downstream and upstream directions.
- L_r : maximum reach with highest modulation format.
- O_h : a set of transceivers used at the hub node.
- O_l : a set of transceivers used at the leaf nodes.
- C_o : cost of transceiver type o .
- D_o : maximum data rate (with the highest modulation format) of transceiver type o .
- B : very large positive number.

Decision Variables

- x_{ij}^t : 1 if edge $(i, j) \in E$ is selected for tree t , 0 otherwise.
- f_{ij}^t : positive integer variable indicating flow from vertex i to j on tree t .
- y_{ij}^{tu} : 1 if edge $(i, j) \in E$ is in the path from leaf u to the hub on tree t , 0 otherwise.
- M_u^t : 1 if path from leaf u to the hub is longer than L_r , 0 otherwise.
- Δ_o^t : number of transceivers of type o used at the hub on tree t .
- δ_{ou}^t : number of transceivers of type o used at leaf node u on tree t .

The objective of the ILP model is to minimize the total transceivers' cost:

$$z = \sum_t \sum_{o \in O_h} \Delta_o^t \times C_o + \sum_t \sum_{u \in V^-} \sum_{o \in O_l} \delta_{ou}^t \times C_o. \quad (3.11)$$

subject to

Constructing tree(s)

$$\sum_{(i,j) \in E} x_{ij}^t = N \quad \forall t, \quad (3.12)$$

$$\sum_j f_{ij}^t - \sum_j f_{ji}^t = \begin{cases} N & \forall t, i = Hub, \\ -1 & \forall t, \forall i \in V^-, \end{cases} \quad (3.13)$$

$$f_{ij}^t \leq Nx_{ij}^t \quad \forall t, \forall (i, j) \in E, \quad (3.14)$$

$$f_{ji}^t \leq Nx_{ij}^t \quad \forall t, \forall (i, j) \in E, \quad (3.15)$$

Guaranteeing disjointedness of trees

$$\sum_j y_{ij}^{tu} - \sum_j y_{ji}^{tu} = \begin{cases} 1 & \forall t, \forall u \in V^-, i = u, \\ 0 & \forall t, \forall u \in V^-, i \neq u, Hub, \\ -1 & \forall t, \forall u \in V^-, i = Hub, \end{cases} \quad (3.16)$$

$$y_{ij}^{tu} \leq x_{ij}^t, \quad \forall t, \forall u \in V^-, \forall (i, j) \in E, \quad (3.17)$$

$$\sum_t y_{ij}^{tu} \leq 1, \quad \forall u \in V^-, \forall (i, j) \in E, \quad (3.18)$$

Counting the number of transceivers

$$BM_u^t \geq \sum_{(i,j) \in E} W_{ij} y_{ij}^{tu} - L_r \quad \forall t, \forall u \in V^-, \quad (3.19)$$

$$\sum_{o \in O_l} \delta_{ou}^t D_o \geq T(u)[M_u^t + 1] \quad \forall u \in V^-, \forall t, \quad (3.20)$$

$$\sum_{O_h} \Delta_o^t D_o \geq \sum_u \sum_{o \in O_l} \delta_{ou}^t D_o \quad \forall t. \quad (3.21)$$

Constraints (3.12) ensures that the size of the trees is equal to the number of leaf nodes (assuming there is no zero traffic load). According to constraints (3.13), N flow units are distributed by the hub node, and all N leaf nodes receive exactly one flow unit. Flows can be only on trees not exceeding the maximum amount of flows by constraints (3.14–3.15). These constraints create spanning trees by fulfilling the tree criteria via a single commodity approach [128]. Paths between each leaf node and the hub on each tree are calculated by the constraints (3.16), where one unit of flow is generated by node u and passes through other nodes; only the hub receives it. Constraints (3.17) confirms that the paths are contained in the trees, whereas constraints (3.18) ensures the disjointedness of paths for each leaf-hub pair.

Constraints (3.19) determines the highest modulation format that can be used. M_u^t takes the value of 1 if the length of any path in tree t is longer than L_r . For simplicity, but without loss of generality, we assume that the highest order modulation format – 16QAM – is feasible for paths shorter than $L_r = 500 \text{ km}$. For paths longer than this value, QPSK is used instead, halving capacity and spectral efficiency. By multiplying $M_u^t + 1$ with $T(u)$, the effective number of SCs needed is doubled when the longest path in the tree forces the utilization of QPSK. Constraints (3.20) and constraints (3.21) count the number of required transceivers per type at the leaf nodes and the hub, respectively.

It is assumed that the 4.8 THz of the C-band provides sufficient bandwidth to meet all demands, and the ILP model does not require link capacity constraints. In a simplistic analysis, the capacity bottleneck in tree architectures is the capacity of a single link multiplied by the number of links connected to the hub, which is usually more than one. However, even a single link can support $64 \times 400\text{G}$ transceiver flows ($64 \times 75 \text{ GHz} = 4.8 \text{ THz}$) which is much larger than the maximum number of 400G transceivers deployed at the hub in this study.

If the physical topology is two-edge-connected, it can be shown that two trees can be constructed, offering one redundant disjoint path for every leaf-hub pair [128]. The ILP model can also model unprotected scenarios by enforcing the number of trees to one.

The ILP model can also be adapted to dimension the network using P2P transceivers. In this case, transceiver pairs (operating at the same data rate) must be installed at the leaf and hub nodes. This scenario can be modeled by removing constraints (3.21) and the first term of objective function (3.11) and by doubling the second term of this function which corresponds to leaf node transceivers cost.

3.8.3 Results and Discussion II

We consider two topologies, namely A and D, and provide a comprehensive examination of the effectiveness of integrating DSCM-based P2MP transceivers with filterless node architecture over these two networks. Topology A has 30 nodes and 51 link pairs, while network D comprises 30 nodes and 53 link pairs, as shown in Fig.3.14.

Transceivers capable of operating at 400G, 100G, and 25G are considered, assuming that the 400G and 100G transceivers can be used at the hub nodes, whereas the 100G and 25G transceivers can be employed at the leaf nodes. For benchmarking purposes, the utilization of a P2P transceiver is also considered. In this case, only 100G interface pairs can be deployed. In terms of spectrum usage, the outcome of all simulations has been verified to confirm the assumption that enough spectrum holds. Regarding the transceiver cost profiles considered, optimistic and conservative choices are examined to account for cost unpredictability. In the

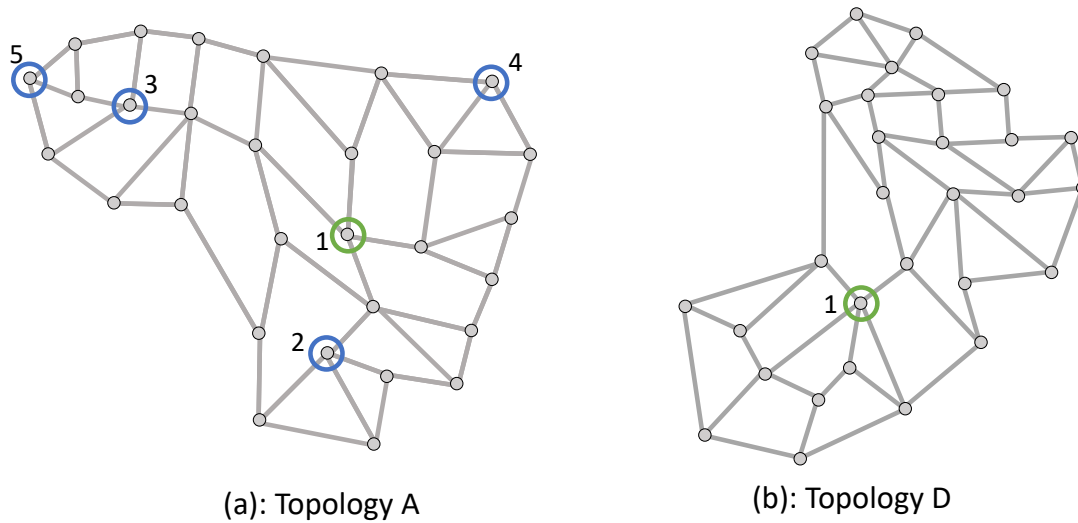


Fig. 3.14 (a) Topology A and (b) topology D defined by Telefónica (with permission from [J1] ©Optica Publishing Group).

optimistic profile, the cost of a 100G and a 25G transceiver is half and one-fourth of the cost of a 400G transceiver ($A = \frac{1}{4}, B = 0.5$, see section. 3.7.3), respectively. On the other hand, in the conservative scenario, these values are instead one-third and one-ninth of the cost of a 400G transceiver ($A = \frac{1}{9}, B \approx 0.79$). The traffic load is defined as that used in section 3.7.4. All the results shown in the remainder of this section are the average values obtained from 10 independent Monte-Carlo runs with 90% confidence intervals falling in about the range of 5% of average.

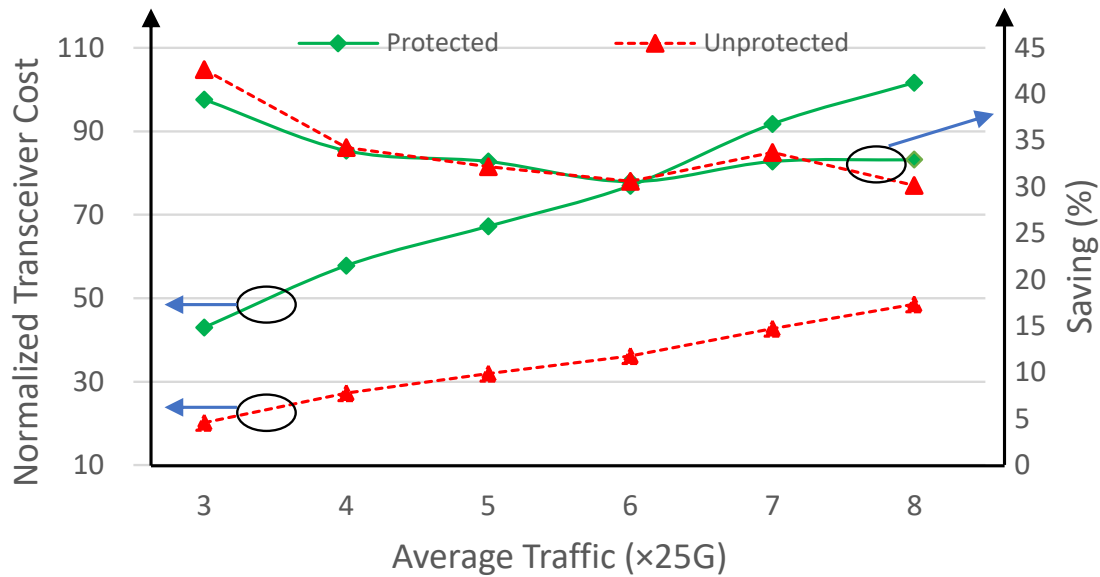
Figure 3.15 shows the results obtained considering the optimistic cost profile. Fig. 3.15(a) presents the normalized cost obtained when P2MP transceivers are deployed in topology A for scenarios with and without protection when node 1 highlighted in Fig. 3.14(a) is the hub node, and the average traffic load varies between 3 SCs and 8 SCs. As expected, the normalized cost is approximately a linear function of the offered traffic in both cases. The cost of interfaces when enforcing protection is slightly higher than twice the cost of the unprotected case. The fraction of cost savings when compared to using P2P transceivers, which are defined as $\frac{Cost_{P2P} - Cost_{P2MP}}{Cost_{P2P}} \times 100$, are also shown in the plot. It can be seen that the amount of saving ranges between 30% and 44% for both protected and unprotected scenarios. Moreover, it can be observed that the amount of savings is higher for traffic load with an average of 3 SCs. This is because when the average traffic is 3 SCs, a significant number of transceivers deployed are under-utilized in P2P scenarios since only 100G transceivers are considered. Hence, for average traffic equal to or below 3 SCs, using 25G transceivers could

reduce the cost in P2P scenarios. However, this would also imply using more transceivers at the hub and leaf nodes, leading to a potentially larger footprint and higher power consumption in the router/switch located at these nodes.

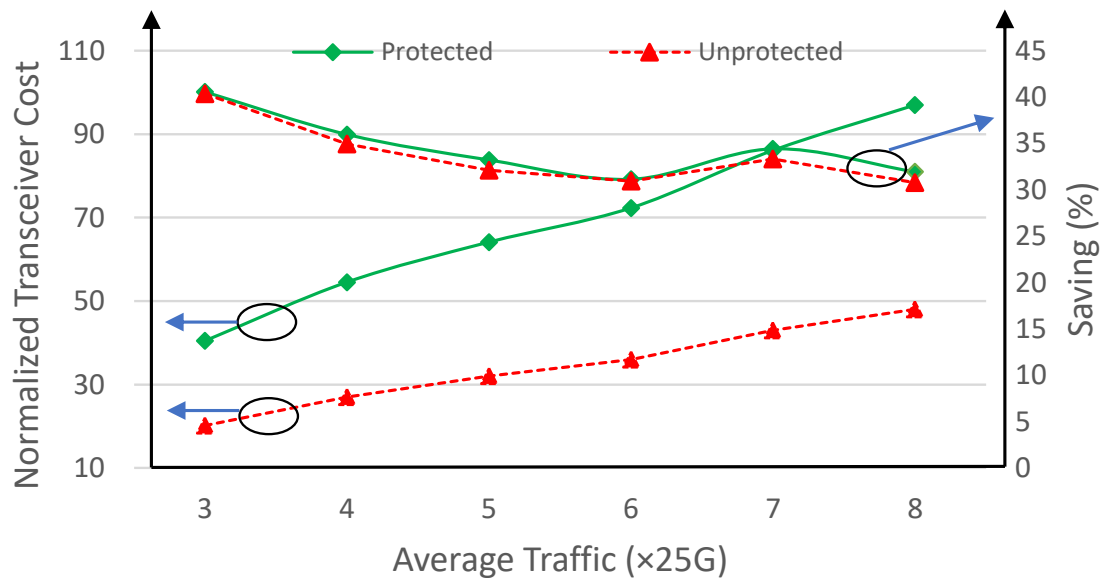
Figure 3.15(b) shows the same set of results but obtained for topology D with node one illustrated in Fig. 3.14(b) as the hub node. Although the number of leaf nodes and the traffic pattern is the same as those in topology A, the normalized P2MP transceiver cost for topology D is slightly lower than that for topology A in the protected scenario, while for the unprotected scenario, it is almost the same. It is important to note that tree construction is more constrained in protected scenarios since the two trees must meet the disjointness conditions. This fact and the fact that the average link length in topology A is longer than that in topology D can lead to higher utilization of the QPSK modulation format in the former topology, increasing cost. Overall, the transceiver CAPEX saved ranges between 30% and 40% in topology D.

In order to gain insight into the tree solutions found by the ILP model, an instance of the working and protection trees computed for topology A is depicted in Fig. 3.16. The black dashed lines indicate two disjoint paths from leaf node X to the hub node. Although the working and protection trees might have shared links, two disjoint paths for each leaf node are guaranteed. In the case of shared links between the two trees, it is assumed that one of the trees uses half of the spectrum, whereas the other half is reserved for the second tree. This strategy can be implemented using red and blue filters, and it is called a semi-filterless solution [129]; however, it maintains the passive feature. In this example, the two trees have 14 shared links, fifteen separate links each, and seven links are unused. When these two trees share a link, a spectrum blocker (or blue and red filters) has to be used to avoid unnecessary light propagation and the formation of loops. As can be seen, one of the optical fibers of link L1, which carries both downstream red and upstream blue signals, is connected physically to one of link L2 fibers (which only carries red light) and one of the L3 fibers (which only carries blue light). Therefore, a blue spectrum blocker has to be used at link L2, and a red spectrum blocker has to be deployed at L3. Note that the drop splitter and add combiner are not shown in the example of node architecture.

For completeness, we also assess the impact of using the conservative cost profile, according to which 400G transceivers are comparatively more expensive than the optimistic cost profile. Figures 3.17(a) and (b) plot the normalized P2MP transceiver cost under the conservative cost profile and the savings when compared to the P2P approach in topology A and topology D, respectively. As observed in both plots, the trends are the same as those reported with the optimistic cost profile. However, as expected, slightly smaller cost savings



(a)



(b)

Fig. 3.15 (a) Normalized P2MP transceiver cost for topology A and corresponding savings compared to P2P approach, and (b) normalized P2MP transceiver cost for topology D and corresponding savings compared to P2P approach for optimistic cost profile (with permission from [J1] ©Optica Publishing Group).

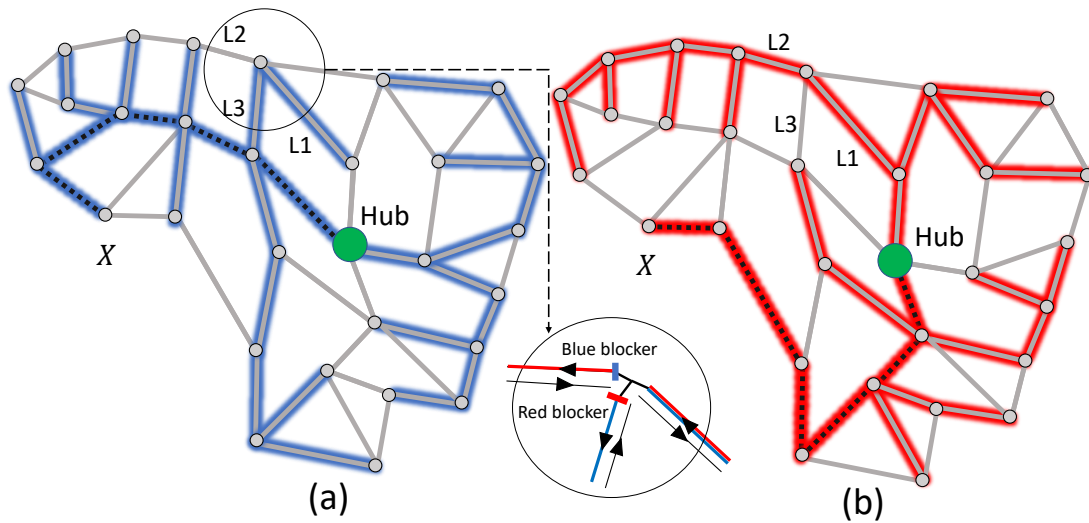


Fig. 3.16 Example of (a) working and (b) protection trees computed for topology A (with permission from [J1] ©Optica Publishing Group).

are obtained. In topology A, cost savings range between 24% and 40%, whereas savings between 23% and 38% are achieved in topology D.

The cost savings enabled by P2MP transceivers are a consequence of two key effects:

- High capacity transceivers have a lower cost per bit/s;
- Aggregation of small traffic flows into a single P2MP transceiver improves utilization.

At low traffic loads, both effects are present, and this explains the larger savings observed in Figures 3.15 and 3.17 for low traffic loads. As the traffic load increases, the second effect has a diminishing impact.

The location of the hub node can affect the total transceiver cost. For instance, having the hub node at a central location, which is the case considered in the previous simulations, should allow reducing the length of the paths used to reach the farthest leaf nodes. Also, it is important that the hub node be well-connected to the rest of the network, for example, higher nodal degree. Additionally, when having more than one hub, it is vital to ensure that the location of the hubs do not include the same risk factors since a single cause can interrupt both hubs at the same time. Nevertheless, the choice of the hub node might be driven by other factors, such as the location of the dominant sources of traffic (e.g., the presence of large data centers) and interfacing with the metro-core network. The impact of different hub node locations is evaluated by considering five possibilities for the hub node in topology A, which are shown in Fig. 3.14(a). Figure 3.18 presents the normalized transceiver cost for all

five cases, considering the two transceiver types (P2MP and P2P) and whether to enforce link protection or not. The results presented were obtained for an average traffic load of 3 SCs. The highest P2MP transceiver cost occurs when node 5 is selected as the hub, whereas the minimum P2MP transceiver cost is obtained when node 1 is chosen. The cost when using P2P transceivers follows the same trend as that observed with P2MP devices; that is, allocating the hub to a node in the network periphery usually results in higher transceiver cost than when the hub is closer to the center. The cost savings from using P2MP transceivers instead of P2P ones are between 29% and 42%. Therefore, these results also provide evidence that the cost advantage of using P2MP transceivers is preserved, regardless of the hub location.

The number of transceivers discriminated per rate for protected P2MP, and P2P scenarios for topology A and optimistic cost profile are shown in Fig. 3.19. In the P2MP scenario, the number of 400G transceivers increases proportionally to the total traffic load. The 100G transceivers also scale with the requirements of leaf nodes, whereas the number of 25G transceivers used is kept at similar levels (only being useful when the usage of 100G transceivers would result in significant capacity under-utilization). With P2P transceivers, there is limited ability to simultaneously address the transceiver under-utilization problem and hub router footprint waste. Particularly, deploying higher data-rate P2P transceivers can aggravate the former, whereas deploying lower data-rate P2P transceivers exacerbates the latter. Conversely, P2MP transceivers enable exploiting low-capacity or medium-capacity transceivers at leaf nodes without an increase in line port usage at the hub node.

3.9 Conclusion

DSCM-based P2MP transceiver architecture and the application of these devices in ROADM-based and filterless networks have been studied. Different protection scenarios also have been studied. The result showed that P2MP transceivers could reduce transceivers' cost in unprotected and protected scenarios as higher capacity transceivers offer cheaper per bit transported and reduce over-provisioning. In addition, using P2MP transceivers offers several benefits, including the simplification of network architecture, a smaller footprint for routers, and reduced power consumption at hub routers.

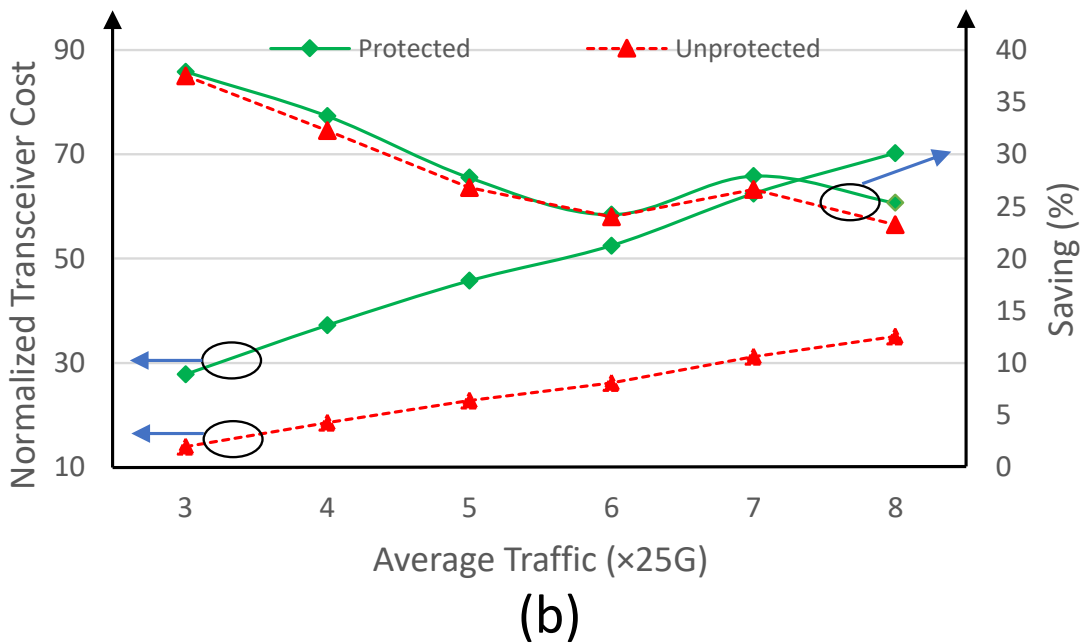
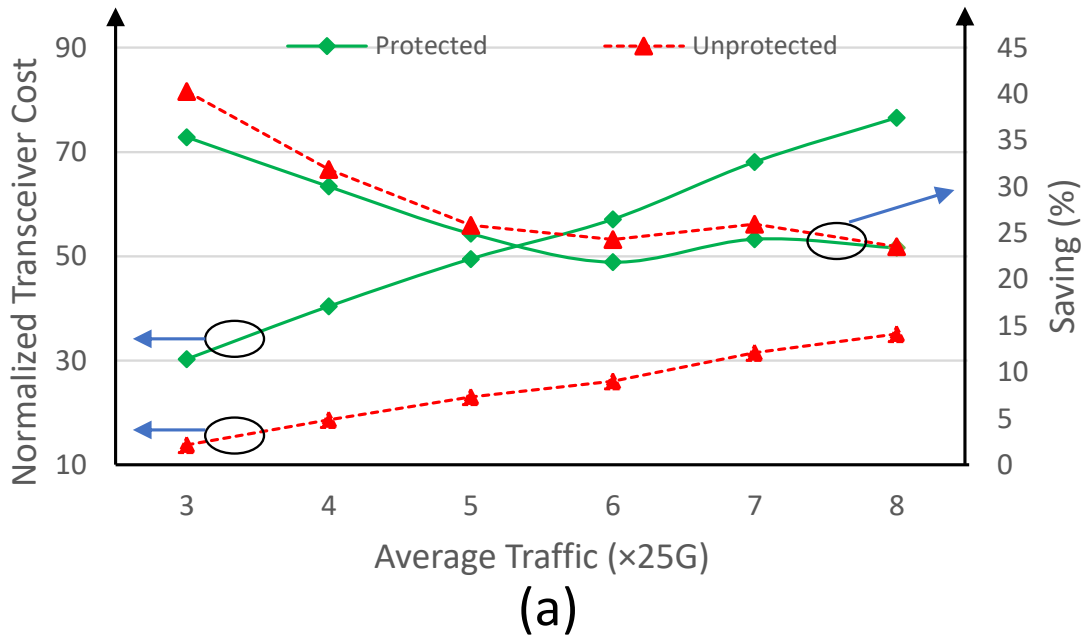


Fig. 3.17 (a) Normalized P2MP transceiver cost for topology A and corresponding savings compared to the P2P approach, and (b) normalized P2MP transceiver cost for topology D and corresponding savings compared to the P2P approach for the conservative cost profile (with permission from [J1] ©Optica Publishing Group).

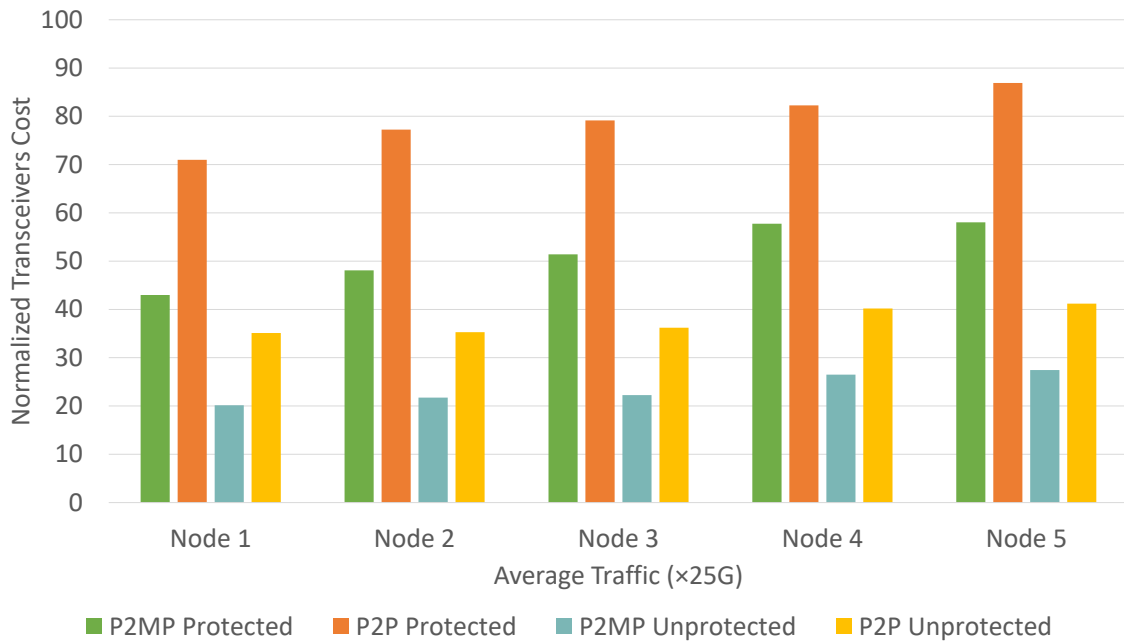


Fig. 3.18 Normalized transceiver costs for different hub locations in topology A (with permission from [J1] ©Optica Publishing Group).

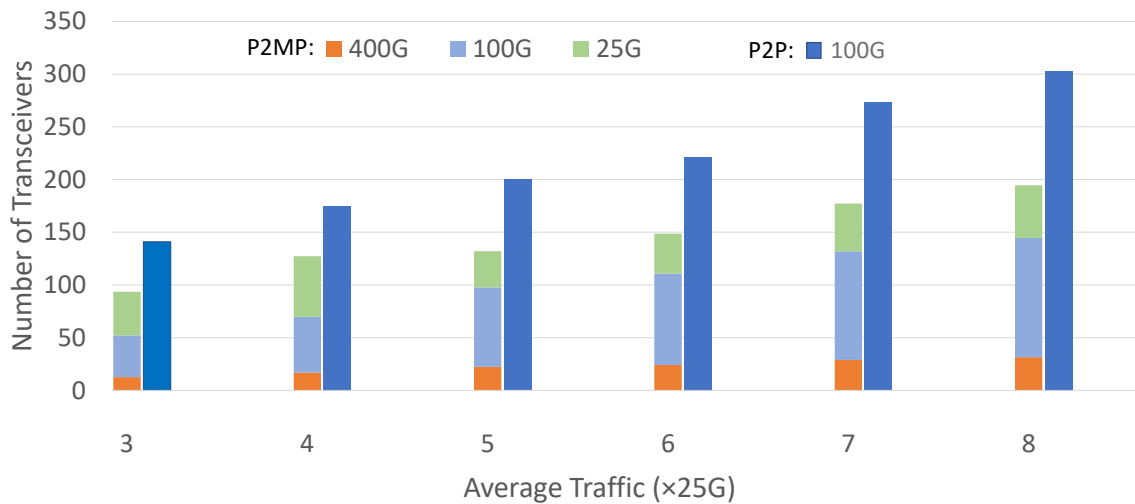


Fig. 3.19 Number of P2P and P2MP transceivers in protected scenario versus traffic loads for topology A and optimistic cost profile (with permission from [J1] ©Optica Publishing Group).

Chapter 4

Multi-period Planning Using Point to MultiPoint Transceivers

4.1 Introduction

Optical networks often change over time due to the evolution of demands and technologies. Therefore, the design and optimization of networks can be constrained to those factors as well as financial limitations. For example, higher data rate transceivers are cheaper considering the cost per transported bit but become available later. Additionally, each generation of transceivers has a finite lifespan, and their deployment is halted after some time as their competitive edge deteriorates. Due to this fact and volume discounts, the price of a particular transceiver generation usually drops steadily during its lifespan. These findings motivate operators to delay capacity upgrades. However, implementing this strategy requires more frequent capacity increases, resulting in higher operating costs and increased risk of degrading service quality.

Greenfield deployment refers to designing, installing, and setting network infrastructure in a location where none previously existed. A brownfield deployment, on the other hand, is an upgrade or expansion of an existing infrastructure employing legacy components.

In this chapter, which is based on my publications [J2] and [C5], we first study crucial components of multiperiod planning. Then, we investigate the long-term cost-effectiveness of point-to-multipoint transceivers as traffic increases per leaf node. Finally, different planning strategies are implemented using the ILP method for P2MP transceivers deployment.

4.2 Technology Evolution

The term evolution of technology means how technology has been evolving. All technologies are born to serve purposes. Since the advent of the internet in the 1970s, we have witnessed massive changes in human civilizations and widely spread applications worldwide thanks to constant technological advances.

Wright established the concept of learning curves (experience curves) (1936). Using actual evidence, he discovered that unit costs for different inputs, when compared to the cumulative output of airplanes, decrease exponentially as cumulative production increases. This heavily connects to so-called growing returns, non-convexities, and the path dependence of technological improvements with the possibility of "lock-in" states. As a result, pure market mechanisms fail to choose new "expensive" technologies that may become "cheap" and environmentally friendly if early investments are appropriately made. The learning curve depicts the investment required to make the new technology competitive with mature, inexpensive technologies but needs to indicate when the break-even point will be reached [130]. It is worth noting that the transition from "old" to "new" infrastructures is not instantaneous most of the time. Different generation infrastructures coexist during the transitional period [131].

The histories of communication technologies, including standard mail, the telegraph, the telephone, and the Internet, have similar patterns. Specifically, the typical story for each service is that quality improves, prices decline, and utilization rises, resulting in increased total revenues [132]. Internet & Television Association (INTA) research reported that the price per megabit per second of cable broadband service has decreased by 98% over the past two decades, falling from a mean of \$28.13 in 2000 to \$0.64 in 2020. In this period, the metal-oxide-semiconductor field-effect (MOSFET) transistor size decreased from around 150nm to 5nm (about 97% decrease). This remarkable improvement is often referred to as Moore's law [133].

4.3 Internet Traffic Characteristics

By 2022, global IP traffic will reach an annual run rate of 4.8 zettabytes per year which shows an 11-fold increase from 2012 and a 3-fold increase from 2017, representing about 30% growth annually [134]. However, the growth rate is different among different network segments. Network capacity is moving closer to the edge, and almost one-third of capacity will bypass the core entirely by 2022, mainly due to storing content at the edges of the ISP networks [135]. End users would retrieve content within the metro network, avoiding

increasing the capacity at the peering points. Edge-to-edge node traffic constitutes less than 1% of the overall traffic flow received by a hub node, according to assessments of Orange’s metropolitan networks[135].

Moreover, the use of internet traffic is not flat over time. Busy internet traffic is predicted to be nearly six times greater than average by 2022 [134].

4.4 Long-term Cost-effectiveness of Point to Multipoint Transceivers

We discussed in chapter. 3 that in metro-aggregation networks, traffic at leaf nodes is small while it is significant at the hub node. We showed that P2MP transceivers could be a cost-effective solution in these networks taking advantage of high data rate coherent transceivers. However, the traffic has been increasing over the years, and the question is whether P2MP transceivers can continue delivering such cost-efficiency.

We assume 800G and 1.2T are next-generation P2MP transceivers. The cost of transceivers, which is obtained using the formula presented in section 3.7.3, and the corresponding number of SCs are tabulated in Table. 4.1.

Table 4.1 Transceiver cost per data rate type (assuming $A = \frac{1}{4}$, $B = \frac{1}{2}$) ([C5] © 2022 IEEE)

Data Rate	1.2T	800G	400G	100G
Number of SCs	48	32	16	4
Cost	1.73	1.41	1	0.5

4.4.1 Optimization Framework

The P2MP optimization framework tries to identify the most cost-effective P2MP transceiver configuration for a particular traffic distribution and metro-aggregation network topology, assuming nodes based on optical splitter/combiner devices and wavelength blockers. In order to achieve this, we developed an integer linear programming (ILP) model. Below are laid out the model’s input parameters and decision variables.

Input Parameters

- $G(V, E)$: network graph with nodes $u, i, j \in V$ and links $l = (i, j) \in E$.
- V^- : a subset of V defining leaf nodes (set of all nodes minus the hub node, $N = |V| - 1$).

- W_{ij} : length of link $(i, j) \in E$.
- $T(u)$: number of 25 Gb/s data rate required by leaf node u . This is assumed to be the maximum required traffic of downstream and upstream directions.
- L_r : maximum reach with highest order modulation format (16QAM).
- O_h : set of transceivers used at the hub node.
- O_l : set of transceivers used at the leaf nodes.
- C_o : cost of transceiver type o .
- D_o : maximum data rate in terms of number of 25G (with the highest modulation format) of transceiver type o .
- B : very large positive number.

Decision Variables

- f_{ij} : positive integer variable indicating flow from node i to j .
- x_{ij} : 1 if link $(i, j) \in E$ is selected for tree, 0 otherwise.
- y_{ij}^u : 1 if edge $(i, j) \in E$ is in the path from leaf u to the hub, 0 otherwise.
- M_{1u} : 1 if path from leaf u to the hub is longer than L_r (QPSK), 0 otherwise.
- M_{2u} : 1 if path from leaf u to the hub is shorter than L_r (16QAM), 0 otherwise.
- Δ_{1o} : number of transceivers of type o used at the hub with QPSK modulation format.
- Δ_{2o} : number of transceivers of type o used at the hub with 16QAM modulation format.
- δ_{ou} : number of transceivers of type o used at leaf node u .

The objective of the ILP model is to minimize the total transceivers' cost:

$$z = \sum_{o \in O_h} \Delta_{1o} \times C_o + \sum_{o \in O_h} \Delta_{2o} \times C_o + \sum_{u \in V^-} \sum_{o \in O_l} \delta_{ou} \times C_o, \quad (4.1)$$

subject to

$$\sum_{(i,j) \in E} x_{ij} = N, \quad (4.2)$$

$$\sum_j f_{ij}^t - \sum_j f_{ji}^t = \begin{cases} N & i = Hub, \\ -1 & \forall i \in V^-, \end{cases} \quad (4.3)$$

$$f_{ij} \leq Nx_{ij} \quad \forall (i, j) \in E, \quad (4.4)$$

$$f_{ji} \leq Nx_{ij} \quad \forall (i, j) \in E, \quad (4.5)$$

$$BM_{1u} \geq \sum_{(i,j) \in E} W_{ij} y_{ij}^u - L_r \quad \forall u \in V^-, \quad (4.6)$$

$$M_{1u} + M_{2u} = 1 \quad \forall u \in V^-, \quad (4.7)$$

$$\sum_{o \in O_l} \delta_{ou} D_o \geq T(u)[M_{1u} + 1] \quad \forall u \in V^-, \quad (4.8)$$

$$\sum_{o \in O_h} \Delta_{1o} D_o \geq \sum_u 2T(u)M_{1u}, \quad (4.9)$$

$$\sum_{o \in O_h} \Delta_{2o} D_o \geq \sum_u T(u)M_{2u}. \quad (4.10)$$

Constraint (4.2) guarantees that the size of the tree is equal to the number of leaf nodes (assuming all leaf nodes have to be connected to the hub). According to constraint (4.3), N flow units are distributed by the hub node, and all N leaf nodes receive precisely one flow unit. Flows can only be on trees not surpassing the total amount of flows by constraints (4.4–4.5). These constraints create spanning trees by fulfilling the tree criteria via a single commodity approach [128]. For the sake of simplicity but without loss of generality, we assume that the QPSK modulation format is feasible for paths longer than $L_r = 500 \text{ km}$; for paths shorter than that, 16QAM can be used. Constraints (4.6) and (4.7) determine if a QPSK or 16QAM

modulation format is used. M_{1u} (M_{2u}) takes the value of 1 if the path to the leaf node requires the QPSK (16QAM) modulation format. Note that it is assumed that all the SCs transmitted/received by a transceiver must use the same modulation format. Constraints (4.8-4.10) count the number of required transceivers per type at the leaf and hub nodes according to the modulation format selected.

Again like the formulations provided in Chapter 3, the ILP model can also be adapted to model the case of P2P transceivers. In this case, transceiver pairs (operating at the same data rate) must be installed at the leaf and hub nodes. This scenario can be modeled by removing constraints (4.9), (4.10) and the first two terms of objective function (4.1) and multiplying the third term, which corresponds to leaf node transceivers cost, by a factor of two.

4.4.2 Results and Discussion I

In this section, we provide a detailed analysis of the performance of DSCM-based P2MP transceivers with varying data rates in a metro-aggregation mesh network. Table 4.2 presents four different scenarios regarding the types of P2MP transceivers that can be utilized at the leaf and hub nodes. It models the possible evolution of consecutive transceiver generations.

Table 4.2 Transceiver data rate scenarios ([C5] © 2022 IEEE).

Scenario	1	2	3	4
Hub	400G	800G	1.2T	1.2T
Leaf	100G	100G	100G	400G, 100G

A non-uniform traffic pattern is assumed: the number of 25G data rates each leaf node requires is randomly selected from the set of $[x, x + 4]$, where x takes the value of $\{1, 2, 3, 4, 5, 6, 7, 8\}$ to cover a broad range of traffic load conditions. In the following, we use the average number of 25G data demands per leaf node to ease the display of results. The results shown in this section are the average value of 10 independent Monte-Carlo simulations. In other words, the process of generating traffic and solving the problem is done ten times, and then the average figure of the costs is reported.

Figure 4.1(a) shows the cost of transceivers deployed at the hub. As expected, when traffic increases from 3 SCs to 10 SCs, the hub node transceivers' cost increases almost linearly. However, Scenario 1 (yellow), which utilizes 400G transceivers at the hub, leads to the highest cost, while the other scenarios benefit from the higher capacity 800G and 1.2T transceivers to reduce the cost at the hub. Particularly at higher traffic loads, Scenarios 3 (blue) and 4 (black) provide the lowest cost by exploiting the decrease in cost per bit enabled by 1.2T transceivers. The cost of transceivers at the leaf nodes is presented in Fig. 4.1(b).

At low to moderate traffic loads, and because only 100G transceivers are used at the leaf nodes, all four scenarios result in a similar cost. Notably, the advantage of also making 400G transceivers available for deployment at these nodes (Scenario 4) becomes evident for traffic loads larger than 6 SCs. According to the model used to generate traffic, an average traffic load above 6 SCs implies that the traffic load will go beyond 8 SCs (i.e., > 200G when using 16QAM) for some leaf nodes. This is a threshold above which a 400G transceiver becomes less costly than using (three or more) 100G transceivers, according to the transceiver cost model employed in this work. In our analysis, the Monte Carlo method indicates that 90% confidence intervals tend to be around 5% of the average.

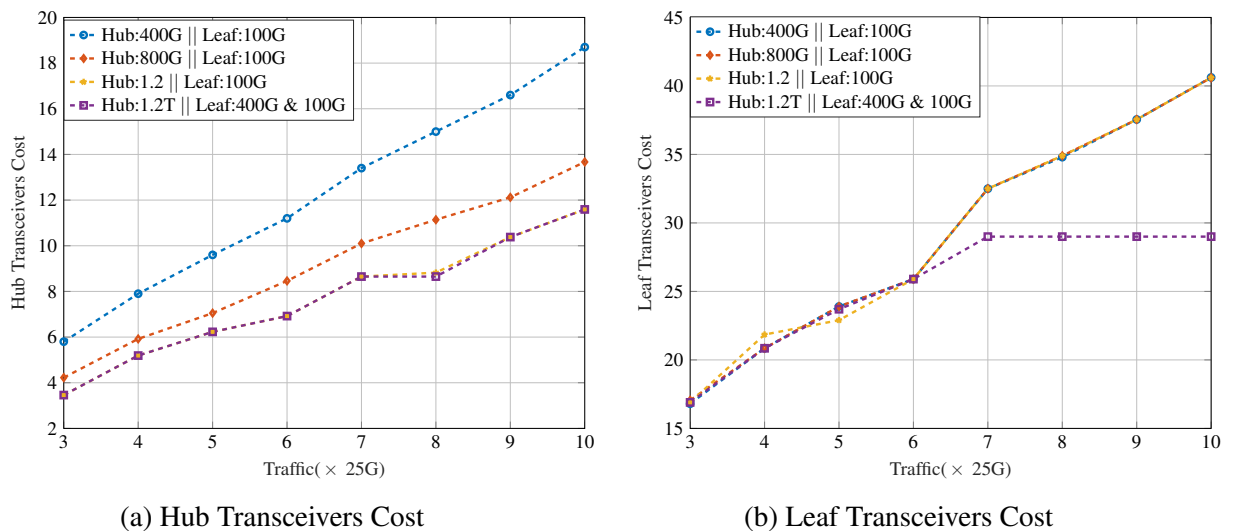


Fig. 4.1 Cost of transceivers deployed at (a) the hub and (b) the leaf nodes versus average traffic loads ([C5] © 2022 IEEE).

The cost savings of using P2MP instead of P2P transceivers is defined as $\frac{Cost(P2P) - Cost(P2MP)}{Cost(P2P)} \times 100$. Figure 4.2(a) illustrates the savings achieved compared to the case where only 100G P2P transceivers are used. Using higher data rate transceivers at the hub generally leads to more impressive savings. Moreover, transceiver savings for Scenarios 1–3 (yellow, magenta, blue) are fairly constant while traffic increases, whereas Scenario 4 (black) savings become more pronounced from 6 to 10 SCs. As discussed above, this is a consequence of being able to exploit 400G transceivers at leaf nodes with very high traffic requirements (larger than 6 SCs). To have a fair comparison with traditional P2P approaches, we present in Fig. 4.2(b) the savings of the P2MP scenarios compared to the P2P case where 400G and 100G transceivers are available simultaneously. These results highlight that if, in both cases (P2MP and P2P), 100G and 400G transceivers can be used at the leaf nodes (Scenario 4), P2MP enables considerable savings (i.e., between 30% and 40%) up to very high traffic

loads. This provides evidence that, in the long term, P2MP transceivers will continue to hold their advantage over traditional P2P transceivers in metro-aggregation networks.

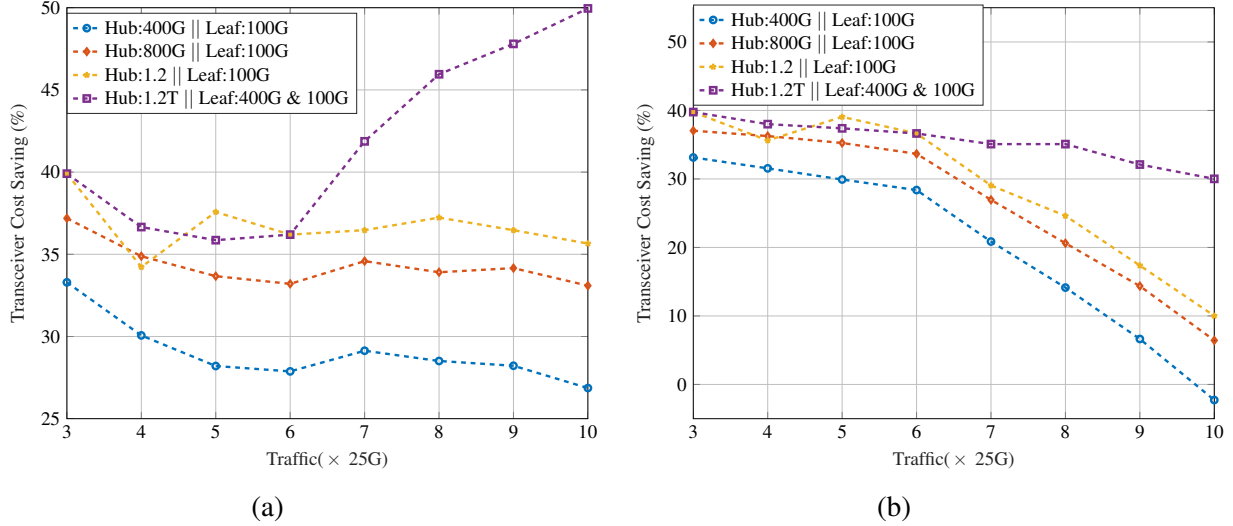


Fig. 4.2 P2MP transceiver savings compared to (a) 100G P2P and (b) the combination of 100G and 400G P2P transceivers versus average traffic loads ([C5] © 2022 IEEE).

4.5 Multiperiod Planning Scenarios

Network operators must consistently plan to deploy resources in response to the growing demand for traffic. However, several factors can affect planning, including uncertainty in traffic prediction, technology shifts, and budget limitations. For instance, higher data rate transceivers become available later but offer a per bit/s cost advantage. Moreover, each transceiver generation has a limited lifespan, discontinued after a number of years because their competitive advantage eroded. This fact, coupled with volume discounts, means that the price of a given transceiver generation gradually decreases during that lifespan. These observations encourage operators to postpone capacity upgrades. However, this approach means more frequent capacity upgrades, increasing operational expenses and affecting the quality of service. We assume a five-year planning scenario in which 800G and 1.2T transceivers only become available in the market after the second and fourth years, respectively.

Three different multi-period planning scenarios are modeled: (i) all-period planning, (ii) incremental or single-period planning, and (iii) extended-period planning. The all-period planning considers the traffic forecast for all periods and is best suited when there is high confidence in that prediction. On the contrary, single-period planning is used when there

is low confidence in traffic predictions and/or near-term investments are to be kept to a minimum. Extended-period planning sits between these extreme cases, assuming traffic predictions are relatively reliable over three years.

There are two ways to manage leaf node transceivers. One way is to keep a transceiver in place for the rest of the planning period once it's been deployed in a leaf node, which is called the unmovable transceiver strategy in this paper. The other way is to move a transceiver to a different leaf node in the future if it enables the reduction of CAPEX (the movable transceiver scenario). Note that each time a leaf node is upgraded, either by removing or deploying a transceiver, it is necessary to visit the leaf site. Therefore, the chosen approach can affect both CAPEX and OPEX (the latter is measured as the number of site visits).

4.5.1 Optimization Framework

This section proposes a novel optimization framework to identify the most cost-effective P2MP transceiver configuration under filterless architecture constraints for a particular planning scenario, network, and traffic load. The main input parameters and decision variables of the ILP model are described below.

Input Parameters

- $G(V, E)$: network graph with nodes $u, i, j \in V$ and links $l = (i, j) \in E$.
- V^- : a subset of V defining leaf nodes.
- W_{ij} : length of the link $(i, j) \in E$.
- S : set of planning periods.
- T_u^s : number of 25 Gb/s data rates required by leaf node u in period s . This is assumed to be the maximum required traffic of downstream and upstream directions.
- L_r : maximum reach with highest-order modulation format (16QAM).
- O_h, O_l : sets of transceivers that can be used at the hub and leaf nodes.
- C_o^s : relative cost of transceiver type o in period s .
- D_o : maximum data rate in terms of the 25G number (with the highest modulation format) of the transceiver type o .
- B : very large positive number.
- $J(s)$: weighting factor of period s determining the importance of each period.
- $Q(s)$: cost decline parameter for period s .

Decision Variables

- f_{ij} : positive integer variable that indicates the flow from node i to j .
- x_{ij} : 1 if the link $(i, j) \in E$ is selected for the tree, 0 otherwise.
- y_{ij}^u : 1 if edge $(i, j) \in E$ is in the path from leaf u to the hub, 0 otherwise.
- M_{1u} : 1 if the path from leaf u to the hub is longer than L_r (uses QPSK), 0 otherwise.
- M_{2u} : 1 if the path from leaf u to the hub is shorter than L_r (uses 16QAM), 0 otherwise.
- Δ_{1o}^s : cumulative number of transceivers of type o used in period s at the hub with QPSK modulation format.
- Δ'_{1o}^s : integer number indicating the number of transceivers of type o added in period s in the hub with the QPSK modulation format.
- Δ_{2o}^s : cumulative number of transceivers of type o used in period s at the hub with 16QAM modulation format.
- Δ'_{2o}^s : integer number indicating the number of transceivers of type o added in period s in the hub with the 16QAM modulation format.
- δ_{ou}^s : cumulative number of transceivers of type o used in period s at leaf node u .
- δ'_{ou}^s : integer number indicates the number of transceivers of type o added in period s in leaf u .

The objective of the ILP model is to minimize the total transceivers' cost:

$$z = \sum_{s \in S} Q(s)J(s) \left[\sum_{o \in O_h} (\Delta'_{1o}^s + \Delta'_{2o}^s) \times C_o^s + \sum_{u \in V^-} \sum_{o \in O_l} \delta'_{ou}^s \times C_o^s \right], \quad (4.11)$$

subject to

$$\sum_{(i,j) \in E} x_{ij} = N, \quad (4.12)$$

$$\sum_j f_{ij}^t - \sum_j f_{ji}^t = \begin{cases} N & i = \text{Hub}, \\ -1 & \forall i \in V^-, \end{cases} \quad (4.13)$$

$$f_{ij} \leq Nx_{ij} \quad \forall (i, j) \in E, \quad (4.14)$$

$$f_{ji} \leq Nx_{ij} \quad \forall (i, j) \in E, \quad (4.15)$$

$$BM_{1u} \geq \sum_{(i,j) \in E} W_{ij} y_{ij}^u - L_r \quad \forall u \in V^-, \quad (4.16)$$

$$M_{1u} + M_{2u} = 1 \quad \forall u \in V^-, \quad (4.17)$$

$$\sum_{o \in O_l} \delta_{ou}^s D_o \geq T_u^s [M_{1u} + 1] \quad \forall u \in V^-, \forall s \in S, \quad (4.18)$$

$$\sum_{o \in O_h} \Delta_{1o}^s D_o \geq \sum_{u \in V^-} 2T_u^s M_{1u} \quad \forall s \in S, \quad (4.19)$$

$$\sum_{o \in O_h} \Delta_{2o}^s D_o \geq \sum_{u \in V^-} T_u^s M_{2u} \quad \forall s \in S, \quad (4.20)$$

$$\delta'_{ou}{}^s = \delta_{ou}^s - \delta_{ou}^{s-1} \quad \forall u \in V^-, \forall o \in O_l, \forall s \in S, \quad (4.21)$$

$$\Delta'_{1o}{}^s = \Delta_{1o}^s - \Delta_{1o}^{s-1} \quad \forall o \in O_h, \forall s \in S, \quad (4.22)$$

$$\Delta'_{2o}{}^s = \Delta_{2o}^s - \Delta_{2o}^{s-1} \quad \forall o \in O_h, \forall s \in S. \quad (4.23)$$

Constraint (4.12) ensures that the size of the tree is equal to the number of leaf nodes N (assuming all leaf nodes have to be connected to the hub). According to constraint (4.13), N units of flow are distributed by the hub node, and all N leaf nodes receive precisely one unit of flow. Flows can only be on trees that do not exceed the total number of flows by constraints (4.14–4.15). These conditions create a spanning tree by fulfilling the criteria of the tree through a single commodity approach [128]. We consider that the quadrature phase-shift keying (QPSK) modulation format is feasible for paths longer than $L_r = 500 \text{ km}$, while for paths shorter than that, 16QAM can be used. Note that using QPSK instead of 16QAM halves the capacity per SC. Constraints (4.16) and (4.17) specify if QPSK or 16QAM modulation format can be used. M_{1u} (M_{2u}) takes the value of 1 if the path to the leaf node requires the QPSK (16QAM) modulation format. Note that it is assumed that all SCs transmitted/received by a transceiver must use the same modulation format. Constraints (4.18–4.19) measure the cumulative number of required transceivers while constraints (4.21–4.22) count the number of transceivers added in period s per type at the leaf and hub nodes according to the modulation format selected.

The scenario of movable transceivers can be implemented by adding Eq. (4.24) to the set of constraints and letting $\delta'_{ou}{}^s$ take both positive and negative integer values, allowing the number of transceivers of a given type to increase or decrease at each leaf node.

$$\sum_{u \in V^-} \delta'_{ou} = \left[\sum_{u \in V^-} (\delta_{ou}^s - \delta_{ou}^{s-1}) \right] \geq 0 \quad \forall o \in O_l, \forall s, \quad (4.24)$$

The ILP model can also be modified to design the network with P2P transceivers. In this case, the leaf and hub nodes must have transceiver pairs that operate at the same data rate. Therefore, we can model it by removing the first term of the objective function (4.1) and doubling the second term of this function.

Table 4.3 presents the baseline cost matrix for all transceivers considered in this study based on the model provided in 3.7.3. A very high value (e.g., 1000) is used in the ILP formulation when a transceiver is not available.

Table 4.3 Relative transceiver cost per data rate by year without considering cost discount (with permission from [J2] © Optica Publishing Group).

	100G	400G	800G	1.2T
Year 1	0.5	1	Unavailable	Unavailable
Year 2	0.5	1	1.41	Unavailable
Year 3	0.5	1	1.41	Unavailable
Year 4	0.5	1	1.41	1.73
Year 5	0.5	1	1.41	1.73

The weighting factor $J(s)$ is introduced in the objective function (Eq. 4.11) to model the relevance of each planning period in the CAPEX optimization. For instance, if $J(s)$ takes a much larger number (100 times larger for instance) for a given year with respect to that for the remaining years (e.g., first year), then the model will give preference to minimizing CAPEX in that particular year. For extended period planning the values of $J(s)$ for the five years can be selected as [100, 100, 100, 1, 1]. With this definition, we ensure that first three years are priority to be optimized and then the next two years.

Given pricing policies such as customer-driven pricing, price skimming, and premium pricing, transceivers' cost usually declines after they reach the market. We considered a 10% reduction per year after they become available in the market by setting the cost decline to $Q(s) = 0.9^{s-1}$ in Eq. (4.11), where s varies from 1 to 5.

4.5.2 Results and Discussion II

This section investigates the performance of DSCM-based P2MP transceivers during a five-year planning span under different scenarios. It compares the outcome with employing traditional P2P transceivers in the metro-aggregation reference network depicted in Fig.3.14(a), and node 1 is the hub node.

A Poisson distribution with a mean value of 100G is used to construct the first traffic pattern. For each leaf node, the annual growth rate is set at a random number between 35% and 45% for different periods. This way of traffic definition, along with the use of Monte Carlo simulations, gives confidence to the results against uncertainty in the traffic load definition, as it covers up to 10% traffic variations in different years and in different leaf nodes. There are other ways to deal with traffic uncertainty, such as analyzing unexpected traffic changes [136] or predicting traffic using machine learning methods [137]. To facilitate the interpretation of the data from the reader, we express the average traffic load per leaf node in terms of multiples of 25G.

Figure 4.3(a) depicts the total cost of transceivers for the three scenarios outlined in Section 4.5 while considering the unmovable strategy. The starting cost is higher with all-period planning, but the cost growth is slower, resulting in the lowest cost in the final periods. This is expected because this method prioritizes minimizing the final CapEx, even if it means settling for a less optimum solution in the early stages due to capacity over-provisioning (i.e., higher capacity transceivers deployed to satisfy low/moderate initial traffic requirements). The costs of extended and single-period planning in the first two years are comparable. However, because of decisions that are not optimal in the long run, single-period planning becomes less cost-effective over time. Interestingly, extended-period planning outperforms all-period planning until the third period, resulting in a greater cumulative cost than all-period planning afterward.

Figure 4.3(b) illustrates the cost reductions achieved using P2MP transceivers against P2P transceivers. It should be noted that the traffic requirements between the hub and a single leaf node only justify adopting 100G and 400G data rates in the P2P scenario. At a glance, the amount of savings is between 20% and 32% in different planning strategies. All-period P2P planning initially deploys a greater number of 400G transceivers, reducing the need to replace the transceivers in subsequent years. This clarifies why the savings are higher at the start and lower at the end of the planning cycle. The amount of CapEx saved with the other two planning options is less dependent on the planning years. It can be seen that P2MP transceivers grant the highest cost savings when adopting single-period planning in the final period. The variation of results among the instances of single-period planning is higher than the other two scenarios, but still the 90% confidence interval is about 6.6% of the average at maximum.

The effects of being able to relocate transceivers across leaf nodes throughout various planning periods are evaluated in the following results. Figure 4.4(a) shows the advantage of the movable P2MP transceiver approach compared to the non-movable one in terms of cost reduction. Additionally, an OpEx-related metric, the number of site visits to deploy/swap

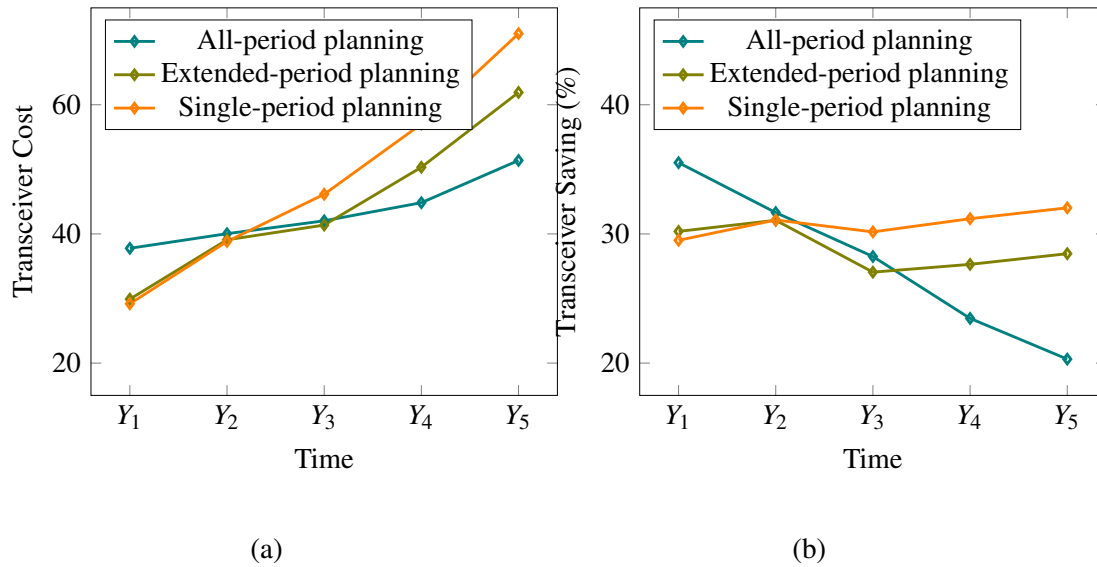


Fig. 4.3 (a) P2MP transceiver cost for all-period, extended-period, and single-period planning, and (b) the amount of savings compared to the corresponding P2P transceiver approaches (with permission from [J2] © Optica Publishing Group).

transceivers – is depicted in Fig. 4.4(b). The possibility of moving transceivers between leaf nodes reduces the cost of all-period planning by roughly 13% at first (reduced over-provisioning compared to the unmovable transceiver strategy), but there are no meaningful benefits for the next four years. However, in order to have this early CapEx decrease, site visits increase from 44 to 78 (77% increase). In the last planning periods, there have been significant improvements in both extended-period and single-period planning methods. Compared to the unmovable transceiver strategy, CapEx is cut by ~12% at the end of the planning cycle, whereas OpEx increases by ~8% for extended-period planning. The single-period planning strategy results in a nearly 14% reduction in CapEx and a marginal reduction in OpEx. Single-period planning always necessitates more site visits, followed by extended-period planning, whereas all-period planning requires fewer visits (benefit from adopting higher data rate transceivers early on).

To gain further insight into how movable and unmovable strategies affect the final solutions, Table 4.4 provides information on the number of transceivers deployed of each type for one of the traffic load sets in the single-period planning strategy. Both unmovable and movable transceivers' strategies deploy the same number of transceivers in the first and second years. Yet, due to rising traffic, the unmovable transceiver approach continues to add additional 100G transceivers in the following years. The movable transceiver strategy, in contrast, moves existing transceivers, particularly 100G transceivers, between leaf nodes (the number of displaced transceivers is specified in parentheses). As a result, even if only traffic

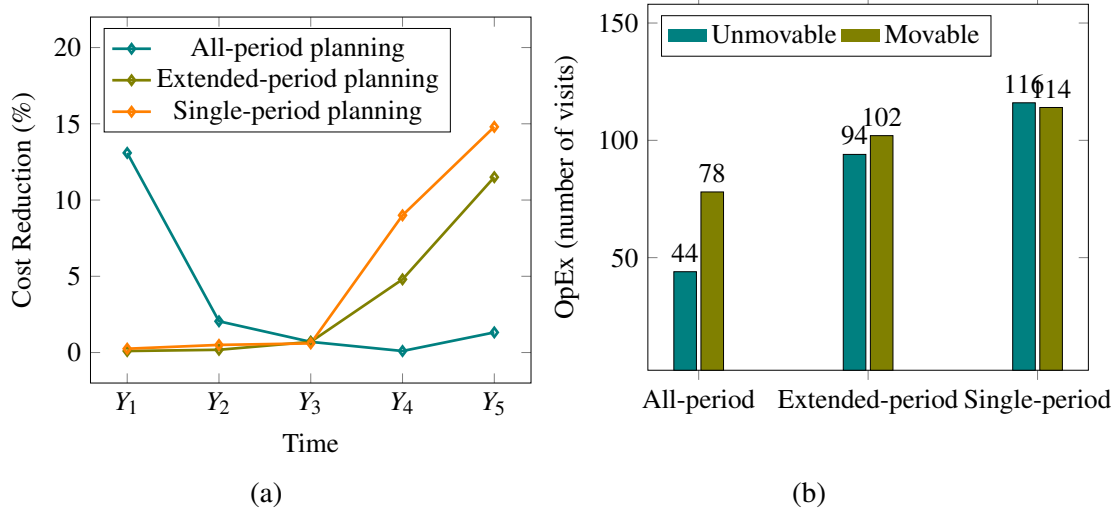


Fig. 4.4 (a) Cost reduction of the movable transceiver approach compared to unmovable transceivers for different planning strategies and (b) their number of visits to the leaf nodes (with permission from [J2] © Optica Publishing Group).

for the next year is planned, the low data rate transceiver count can be reduced by facilitating transceiver reuse. In summary, all-period planning can result in the lowest transceiver cost and the fewest leaf site visits at the end of the five-year planning period in situations where the traffic forecast is available for all five years. On the other hand, the movable transceiver strategy enables a significant reduction in transceiver cost in the event that extended-period or single-period planning is selected based on specific circumstances (e.g., traffic uncertainty and initial budget constraints).

Table 4.4 Number of transceivers added per type at leaf nodes in unmovable and movable transceivers approaches (with permission from [J2] © Optica Publishing Group).

	Year 1	Year 2	Year 3	Year 4	Year 5
Unmovable Transceivers	44×100G	14×100G	13×100G	22×100G	34×100G
Movable Transceivers	44×100G	14×100G	5×400G (8×100G)	5×400G (2×400G+18×100G)	8×400G (5×400G+36×100G)

Sometimes, the cost of visits is considerable, and it is necessary to investigate all aspects of the scenarios carefully. One way is by running a Pareto analysis [138] on different possibilities of the OpEx and the CapEx. Eq. (4.1) in the ILP model can be replaced by Eq. (4.25):

$$z = CapEx + w \times OpEx \quad (4.25)$$

where $CapEx$ is the total CapEx in Eq. (4.1) and $OpEx$ is the number of visits. By varying weight w , different pairs of OpEx-CapEx can be calculated since the importance of OpEx and CapEx is changed in the objective function. Decision-making can then select the most suitable solution based on predefined criteria. Fig. 4.5 shows the OpEx (in terms of the number of visits) against normalized CapEx in all-period planning when the approach of unmovable transceivers is used for four different sets of traffic demands. As can be seen, there is a trade-off between CapEx and OpEx. The results confirm that minimizing CapEx and OpEx can be conflicting. In these cases, the OpEx ranges between 30 and 46 visits, while the CapEx changes from about 50 to 66. Reducing the OpEx (associated to the number of site visits) from 45 to around 33 is possible at the expense of a CapEx (transceiver cost) increase from about 52 to 54 on average.

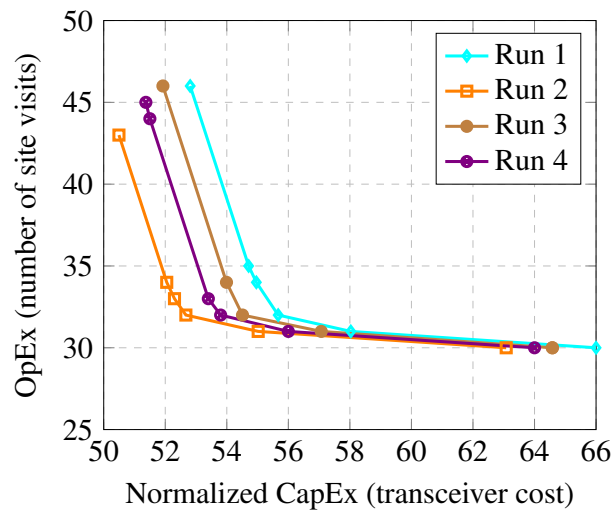


Fig. 4.5 OpEx vs. CapEx relation in unmovable all-period planning for four traffic sets (with permission from [J2] © Optica Publishing Group).

4.6 Conclusion

Network operators are willing to make sure that a solution holds its advantages over a long time. In this chapter, the multi-period planning of the P2MP solution is studied. Short-term, mid-term, and long-term planning (five years) have been analyzed using an ILP framework. Usually, the short-term benefits only sometimes lead to long-term benefits. Constraints on technology evolution and traffic prediction confidence can affect decisions related to CapEx deployment. We showed that moving transceivers from one site to another can help tackle overprovisioning or underutilization, especially in short- and mid-term planning approaches.

Chapter 5

Horseshoe Architecture For Point-to-Multipoint Transceivers Deployment

5.1 Introduction

Passive optical networks (PON), the most deployed filterless networks, are usually in the form of a single-stage tree or multistage tree typologies, which are often created by P2MP infrastructure [139]. Customers can access more bandwidth thanks to P2P technology, but P2MP is less expensive per subscriber and does not require less active equipment. However, metro-aggregation networks usually have ring [140], horseshoe [141, 142] topologies. Filterless optical networks are briefly discussed in Section 3.8, but we discuss it in more detail in this chapter. Horseshoe networks are responsible for aggregating traffic in metropolitan regions. They comprise two hub nodes and several leaf nodes. Traffic from leaf nodes is aggregated at Hub nodes, which are usually connected to the core networks. The existence of two hub nodes can enable link and hub protection.

This chapter is dedicated to filterless horseshoe network design for P2MP transceivers deployment based on our publications [J3] and [C8]. We first study different architectures of horseshoe topologies; then, we discuss the constraints of filterless horseshoe typologies when deploying P2MP transceivers. In light of these, we provide an optimization framework for the physical design of horseshoe typologies using a drop-and-waste (D&W) approach, including unbalanced splitters/combiners selection and amplifier placement that serves the DSCM-based P2MP deployment.

5.2 Horseshoe Topology

The horseshoe topology can be an optimized choice where the traffic pattern is hub-and-spoke. They might have different architectures, but the goal is to connect traffic aggregation nodes to core networks cost-efficiently and reliably.

The design of a Filterless Metropolitan Network (FMN) is described in [5]. The architecture operates in the C and L frequency bands, as shown in Fig. 5.1. Regarding L-band, FMN is filterless, but C-band FMN is filter-based. Two fibers connect the horseshoe's hub nodes to the horseshoe's leaf nodes. In either of these directions, each node's preconfigured fixed channels are already tuned to a specific frequency. Additionally, coherent transponders (Tx and Rx) are incorporated in all nodes offering channels with varying bitrates, modulation schemes, and FEC. As WSS-based ROADMs, leaf nodes have filtering properties, but transit nodes have a Fixed Optical Add/Drop Multiplexer (FOADM) for C-band but no filter for L-band. Therefore, couplers are the only devices that are compatible with both bands. Leaf nodes also include splitters and EDFA amplifiers for signal management at this point. Hub nodes are interfaces to the network's core (backbone) and communicate with leaf nodes via broadcast.

In [143], FMN is protected by a C-band filterless configuration in which leaf nodes lack filters. Instead, FMN uses a single fiber for both upstream and downstream transmission.

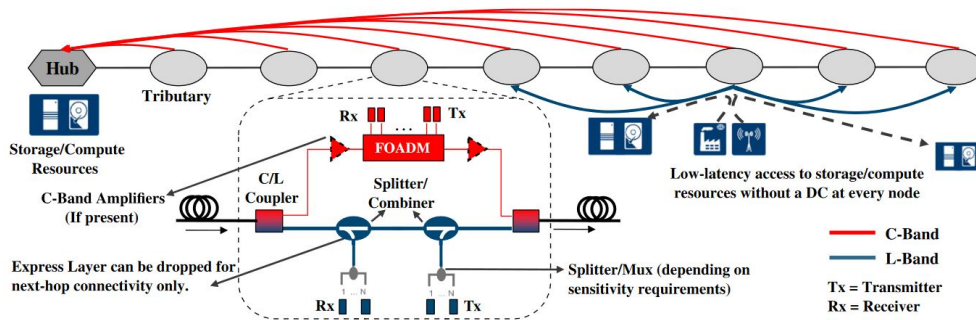


Fig. 5.1 Dual-band MAN with filtered C-band and filterless unamplified L-band [5].

Networks with filterless architectures have their own drawbacks, such as waste of power and spectrum, and filterless horseshoe networks are no exception (these problems are discussed in more detail in the following sections). Usually, these networks are small enough that the loss of power and spectrum are not crucial. Another critical issue related to filterless architectures is that receivers might receive a large amount of power since many channels with different frequencies enter receivers due to the lack of filters in the network. One solution is implementing a simple filtering function inside the receivers to avoid nonlinearity effects in

photodiodes. Cugini et al. have shown that a receiver architecture encompassing a low-cost tunable integrated filter can increase reach by 40% in filterless horseshoe architectures [144]. In [145], a successful experimental demonstration of silicon-on-insulator filters for tackling the excessive power at receivers in these architectures has been presented.

5.3 Filterless Networks

A filterless network is based on the design of a collection of fiber links that optically connect all nodes employing passive optical splitters and combiners added to some nodes. The resulting filterless physical topology and network connectivity are dependent on the configuration of each node's splitter and combiner. A set of interconnected fibers forms a fiber tree. In addition, all fiber trees are optically isolated from one another and can therefore be addressed individually when physical impairments and wavelength assignment are taken into account. The filterless architecture complies with the drop-and-waste principle, whereby unfiltered signals continue propagating on all links in the fiber tree beyond the destination node due to the lack of active switching components.

Fig. 5.2 illustrates an example of a passive filterless network configuration for establishing five traffic demands [6]. As can be seen, two fiber trees are constructed (shown in red and green colors). Nodes 1, 2, 5, and 6 are located on both trees, while nodes 3 and 4 have access to only a single tree. Therefore, no route can be found for any potential demands for source-destination pair 3-4 in case trees are optically isolated.

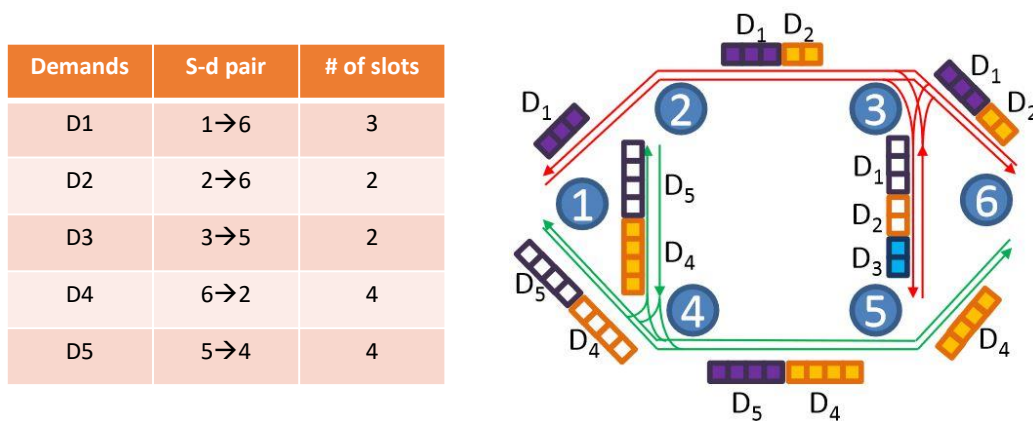


Fig. 5.2 Illustrative example of constructing two trees on top of 6-node topology or accommodating 5 demands [6].

Establishing a lightpath for all possible source-destination pairs in a meshed topology is only possible when all nodes are located on single or more spanning trees. Single-spanning tree solution has two significant drawbacks. Firstly it wastes a huge amount of spectrum as the frequency spectrum of all demands occupies all links across the tree. In addition, some of the optical fibers might be unused. Secondly, the size of the tree is extensive as it is spanned across the network. This may lead to a large amount of loss when optical signals propagate because of more splits into branches. Constructing more than one spanning tree requires large connectivity. A network with N nodes can have $N(N - 1)/2$ links at maximum when it is fully meshed. Considering that each spanning tree comprises $N - 1$ links, the necessary condition for the existence of k spanning trees is as follows:

$$\frac{N(N - 1)}{2} \geq k(N - 1) \Rightarrow N \geq 2k \quad (5.1)$$

The smallest topology that can support two spanning trees ($k = 2$) is a 4-node fully meshed topology that is depicted in Fig. 5.3(a). Trees, which are shown in green and red colors, are totally disjoint. Note that every node is reachable to every other node using each tree. However, the shortest paths might be located on different trees, as shown in the table.

Fig. 5.3 (b) shows two spanning trees for a 5-node topology that comprise eight links overall and their shortest paths in the table embedded. It is worth reminding that using a single tree leads to longer shortest paths and a larger waste of spectrum. In the following, possible solutions to issues related to protection and spectrum and power waste will be discussed.

Rooted trees can be used in the hub-and-spoke traffic pattern in which all traffic goes to and comes from one hub. A tree with one vertex identified as the root is called a rooted tree. In a directed rooted tree, the edges have been given a natural orientation, either away from or towards the root. An arborescence, or out-tree, is a directed-rooted tree oriented away from the root; an anti-arborescence, or in-tree, is oriented toward the root [146].

5.3.1 Protection

The filterless network solutions can be identified by their inherent protection ratio, which is the proportion of all source-destination (s-d) node pairs in the network that are connected by at least two link-disjoint paths. Networks shown in Fig. 5.3 can provide full protection as both have two (disjoint) spanning trees. Since it is not always possible to ensure that two edge-disjoint trees cover all s-d node pairs, the inherent protection ratio of a particular filterless network solution, which is entirely defined by the fiber tree architecture, might be less than 100% [147]. Because of this, some traffic could only have a single route and cannot

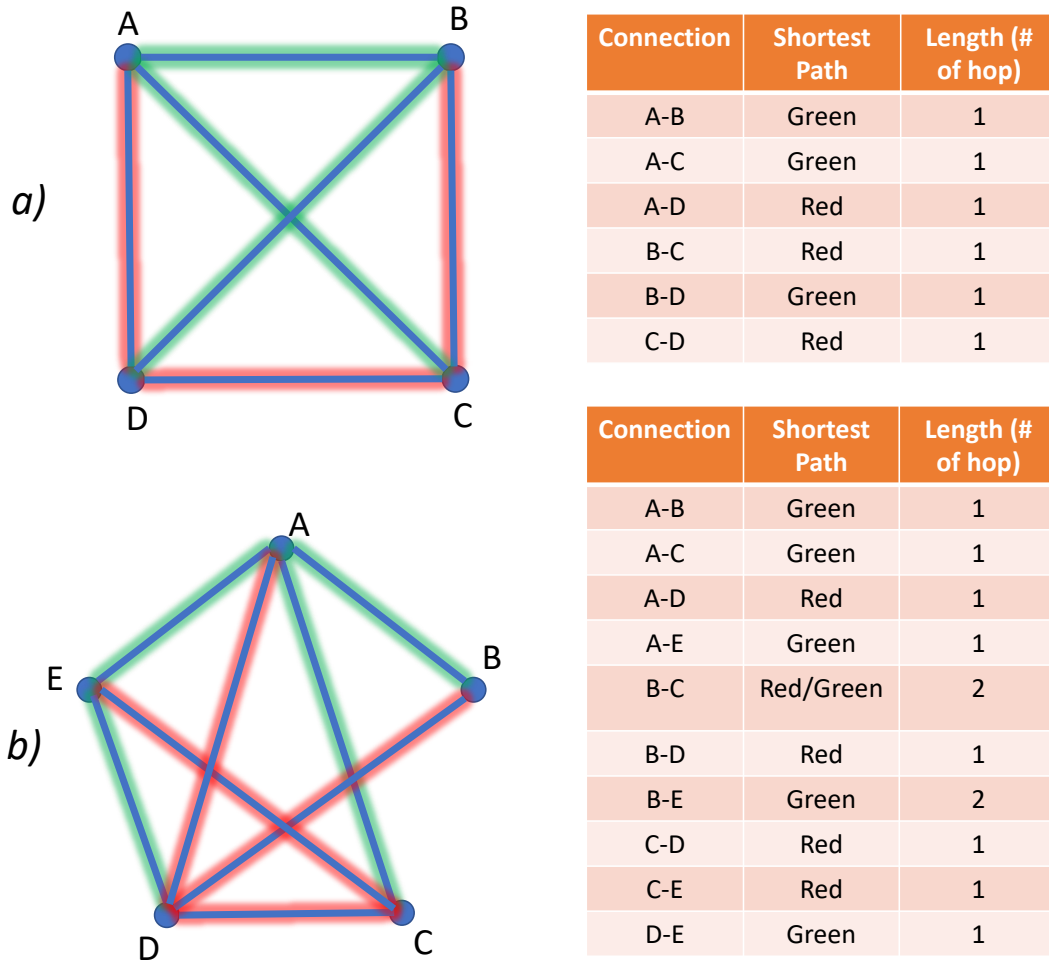


Fig. 5.3 4-node and 5-node topologies with their illustrative examples of two spanning trees.

be protected in the event of a link failure. Therefore, the use of some filtering devices is inevitable.

In [147], protection paths are provided by utilizing wavelength-selective components positioned at selected nodes for interconnecting the fiber trees. Filterless networks require dividing the network topology into non-overlapping fiber trees, and lightpaths cannot transit from one tree to another unless additional devices are installed. In [51], the deployment of three types of devices, namely Inter-Tree Transceivers (ITTs), Wavelength Blockers (WBs), and Colored Passive Filters (CPFs), with the aim of achieving dedicated path protection has been studied.

5.3.2 Semi-Filterless Architectures

To address the spectrum and power waste drawbacks of passive filterless networks, some sort of flexibility must inevitably be employed in node architecture. By adding passive wavelength filters (e.g., Fiber Bragg grating, red/blue filters) to a few chosen nodes, the semi-filterless optical network can increase resource utilization in contrast to the filterless approach [148].

Programmable node architecture is a solution proposed in [149] for elastic optical networks for more flexibility, such as flexible spectrum switching to adaptive architectures that support elastic switching of frequency, time, and spatial resources plus on-demand spectrum defragmentation. The idea is modified for filterless architectures using optical white boxes [6]. Programmable switches that act as optical backplanes are used in programmable filterless white box networks to connect nodes to one another. The express function is achieved inside each node via fiber switching, directly connecting a pair of input and output ports and omitting all node components, or by connecting the relevant ports using passive splitters and couplers. Fig. 5.4 depicts examples of node architectures under ROADM, filterless and programmable filterless designs. Avoiding spectrum waste can also prevent power waste in most cases since the light goes into fewer branches before reaching its destination.

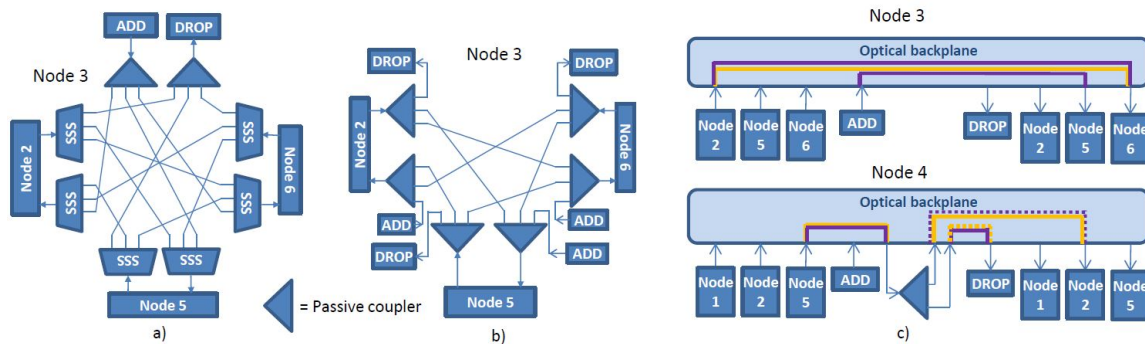


Fig. 5.4 An illustrative example of node 2 architecture in Fig. 5.2: (a) in the conventional ROADM network, (b) in the passive filterless network, and (c) node 3 and node 4 in the white box-based programmable filterless network architecture [6].

Optical splitters and combiners are the backbones of filterless architectures. In the following section, we discuss different technologies behind optical splitters/combiners.

5.4 Optical Splitters/Combiners Technologies

A variety of technologies have been developed to combine or split light signals in silicon with different power, mode, and polarization characteristics. Silicon photonics has attracted increasing attention over the past few decades and is a promising key technology for future everyday applications due to its many advantages, including its ultra-low cost, high integration density due to silicon's high refractive index, and compatibility with the current semiconductor fabrication process [150]. Fiber-to-chip optical interconnections, including data centers and optical transmission systems, are essential in application scenarios. Due to the extremely narrow cross sections of silicon waveguides with less than $1\mu\text{m}$ mode-field diameter (MFD), silicon nanophotonic circuits can display a very high level of functional integration. However, these circuits still need to interact with optical fibers with much greater dimensions, such as those with roughly $10\mu\text{m}$ MFD, in order to be used in data optical transmission networks. To reduce the coupling loss that results from this size mismatch, a coupling structure is needed [151].

Over the past three decades, fused biconical couplers have been employed extensively in optical fiber networks and systems. The majority of research was conducted in the 1990s when fused couplers first became commercially available. With the right design, the fused couplers can work as optical power splitters, polarisation beam splitters, and WDMs (Wavelength Division Multiplexing). The most popular wavelength for today's fiber coupler-based WDM is 1310 nm/1550 nm. The fiber coupler-based WDM is more challenging to manufacture for wavelengths between 1480 nm and 1550 nm or other ranges [152].

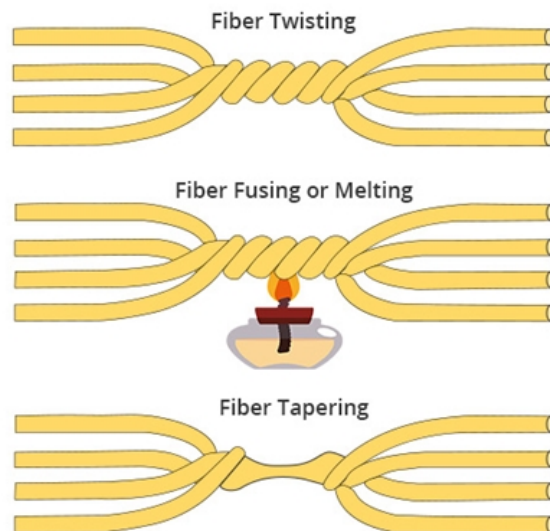


Fig. 5.5 Technologies used for constructing optical couplers [7].

Light going down a single-mode fiber experiences an intensity profile that is essentially Gaussian; that is, the intensity is highest in the core and gradually decreases as the core/cladding interface is approached. The Gaussian profile's tail ends extend only slightly farther away from the core and into the cladding, called evanescent waves. Some light will pass from one fiber into the others if the claddings of two or more fibers are partially removed, and the fibers are put close together over a length. The length of the section where the fibers are close together and the thickness of the remaining cladding can affect the coupling amount. A bunch of fibers with the cladding exposed can be used to create this coupler by applying force and heating the junction. The degree of tension and the duration of heating determines the coupling fraction. During the manufacturing process, light is sent into an input port, and the output power from each output port is carefully monitored. The fully automated production process is terminated when the appropriate coupling ratio is reached. This method can be used to create the T coupler, Tree coupler, and Star coupler. Fig. 5.5 illustrates different technologies used for constructing optical couplers.

The case of the 1x2 fused optical fiber coupler is just a 2x2 coupler with one fiber cut short, terminated (to reduce back reflection from the port), and held inside the housing of the coupler.

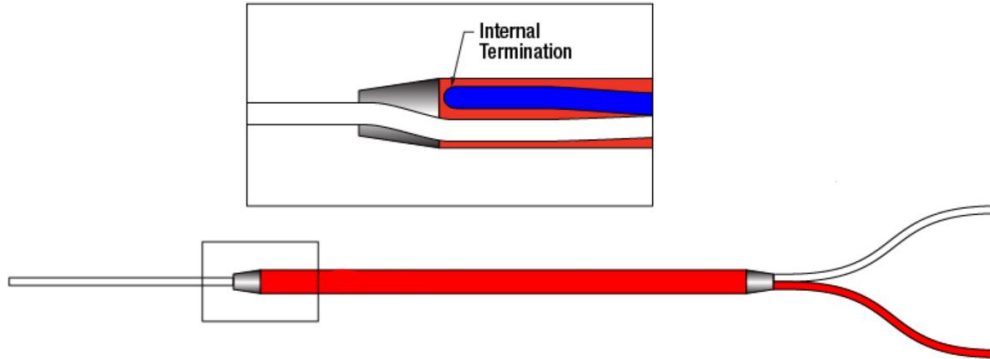


Fig. 5.6 A 1 by 2 coupler made by a 2 by 2 coupler [8].

5.5 Filterless Horseshoe Architecture

Trees, rings, and horseshoe topologies are exceptionally suitable for metro-aggregation networks, which are mostly planned in a filterless architecture. Splitters and combiners guide the whole optical spectrum, and they cannot distinguish optical frequency channels. Note that

filterless architectures enable simplicity and low-cost designing at the expense of spectrum and power waste [153]. Therefore, it is essential to employ such architectures where the optical bandwidth is larger enough than traffic demands and power loss is manageable. The amount of power loss limits the reach. For instance, based on Ethernet PON standards, optical signals can tolerate a 20 km distance and a 1:32 split ratio. Different generations of PON networks, such as G-PON [154] and WDM-PON, have been proposed to provide more capacity and reach. Optimized network topology can reduce the cost of PONs. In [155], the cost of connecting every subscriber to the central offices (COs) has been studied under realistic restrictions, such as possible fiber paths, the splitting ratio of optical splitters, and locations when the locations of COs and subscribers are given. The use of adjusted splitting ratios of asymmetrical splitters in order to fit area characteristics has shown a 6.1 dB gain in power budget in specific areas [156]. However, the cost, bandwidth per user, splitting ratio, and maximum reach are the main factors for commercial success [157].

Figure. 5.7 shows a horseshoe topology comprising two hub nodes, five leaf nodes, and six links. Each link consists of a pair of optical fibers, and passive optical splitters and combiners do the add and drop functions. Every leaf node communicates with both hub nodes bidirectionally using disjoint paths. This protection is obtained at the expense of doubling the number of transceivers and introducing more loss at leaf nodes (optical signals pass two optical combiners/splitters when passing each leaf node). Transceivers are placed in appropriate routers where optical signals are converted to the electrical domain.

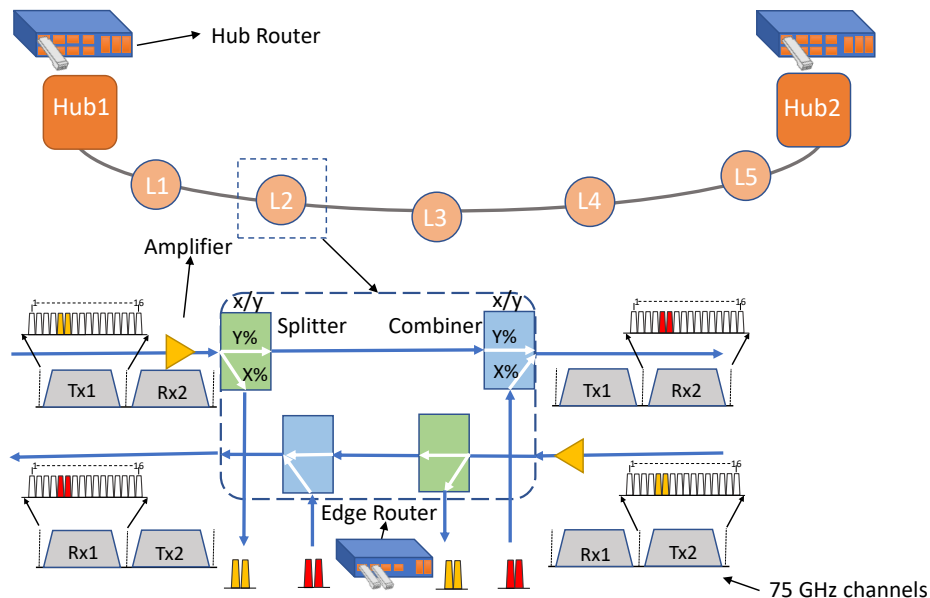


Fig. 5.7 Illustration of DSCM-based P2MP transceiver in horseshoe topology using passive optical splitters/combiners (with permission from [J3] © Optica Publishing Group).

In addition, in upstream directions, optical subcarriers might reach hub nodes with different levels of power and might cause dysfunction. A similar problem exists in PON optical networks, where optical packets travel through different paths; as a result, signal levels vary at the optical line terminal (OLT). This problem can be addressed using an automatic gain control (AGC) approach [158] or optimized semiconductor amplifiers [159]. Deploying splitters/combiners with asymmetrical ratios and placing amplifiers with the appropriate level of gains can help equalize SCs' power.

5.5.1 Link Length Statistical Model

We use the data from the real horseshoe topologies described in [142] to generate new topologies. We fit a log-normal distribution in which the probability density function (pdf) is defined by parameters μ and σ as follows:

$$f(x) = \frac{1}{x\sigma\sqrt{2\pi}} e^{-\frac{(\ln x - \mu)^2}{2\sigma^2}}, \quad \text{for } x > 0. \quad (5.2)$$

Fig 5.8 shows a log-normal distribution fitted to the empirical data with parameter values of $\mu = 2.45$ and $\sigma = 0.41$. The average link length is 13.2 km, while the standard deviation is 5.65 km. We use this distribution to generate horseshoe topologies with different link lengths for statistical confidence in the results.

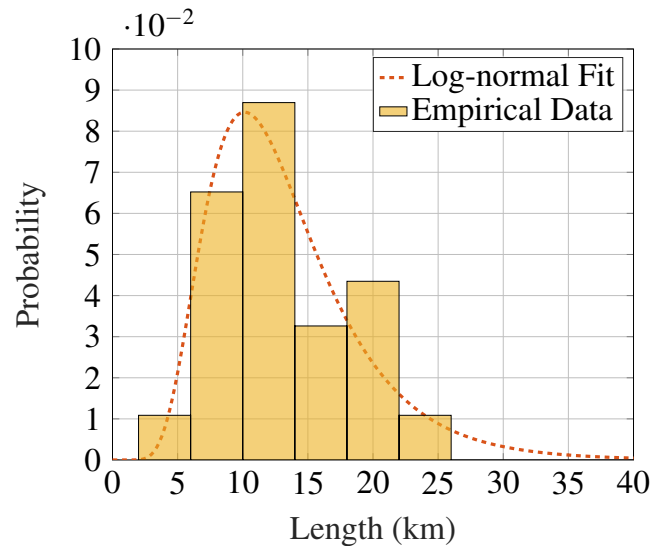


Fig. 5.8 Log-normal distribution fitting the length of optical links from real networks (with permission from [J3] © Optica Publishing Group).

5.5.2 Optimization Framework

This section provides an optimization framework based on integer linear programming to meet the optical reach requirements and subcarrier power equalization in horseshoe topologies. The optimal infrastructure deployment for each fiber is decoupled from the other in the horseshoe topology. Therefore, we only consider the design of fiber that carries light from Hub1 to Hub2. The ILP model's main input parameters and decision variables are as follows:

Input Parameters

- $G(V, E)$: graph with leaf nodes $u, u_p, v \in V$ and links $l \in E$,
- $W(u)$: length of the link entering the leaf node from the left u (W_e will be the link adjacent to the Hub 2),
- α : fiber attenuation (in this study equals to 0.22),
- $G_e(g)$: EDFA gain,
- P_{sc} : power launch per SC in dBm,
- P_n : threshold power per SC for nonlinear effects in dBm,
- P_s : sensitivity power level in dBm,
- P_l : maximum power difference of SCs at Hub receiver,
- $H(s, p)$: list of splitters/combiners containing loss per port.

Decision Variables

- Δ_s^u : binary variable for combiner selection; 1 if combiner s selected for leaf u otherwise 0,
- ∇_s^u : binary variable for splitter selection; 1 if splitter s selected for leaf u otherwise 0,
- γ_p^u : loss of port p of combiner selected for leaf u ,
- δ_p^u : loss of port p of splitter selected for leaf u ,
- μ_g^u : binary variable for amplifier placement; 1 if amplifier located at leaf u has gain g ,
- ϕ_u^1 : Hub 2 receiver (Rx) power per SC coming from leaf u ,

- ϕ_u^2 : leaf u Rx power per SC coming from Hub 1,
- ε_1 : lower bound of ϕ_u^1 ,
- ε_2 : upper bound of ϕ_u^1 .

The goal of the ILP model is to minimize the number of amplifiers and the difference between the highest and lowest SC power levels at the Rx input of the Hub2 (Eq. 5.3). The weight factor w ensures that the highest priority is to minimize the number of amplifiers.

$$z = \sum_u \sum_{G_e(g) \neq 0} \mu_g^u + w[\varepsilon_2 - \varepsilon_1], \quad (5.3)$$

subject to constraints as follows:

$$\sum_s \Delta_s^u = 1 \quad \forall u \in V, \quad (5.4)$$

$$\sum_s \nabla_s^u = 1 \quad \forall u \in V, \quad (5.5)$$

$$\gamma_p^u = \sum_s \Delta_s^u H(s, p) \quad \forall u \in V, \quad (5.6)$$

$$\delta_p^u = \sum_s \nabla_s^u H(s, p) \quad \forall u \in V, \quad (5.7)$$

$$\sum_g \mu_g^u = 1 \quad \forall u \in V, \quad (5.8)$$

$$\begin{aligned} \phi_u^1 &= P_{sc} + \sum_{v>u} G_e(g) \mu_g^u - \alpha \sum_{v>u} W(v) - \alpha W_e - \gamma_{p_1}^u - \\ &\sum_{v>u} (\gamma_{p_2}^v + \delta_{p_2}^v) \quad \forall u \in V, \end{aligned} \quad (5.9)$$

$$\begin{aligned} \phi_u^2 &= P_{sc} + \sum_{v<u} G_e(g) \mu_g^u - \alpha \sum_{v \leq u} W(v) - \delta_{p_1}^u - \\ &\sum_{v<u} (\gamma_{p_2}^v + \delta_{p_2}^v) \quad \forall u \in V, \end{aligned} \quad (5.10)$$

$$\begin{aligned}
& P_{sc} + \sum_{v \leq u} \sum_g G_e(g) \mu_v^g - \sum_{v \leq u} (\gamma_{p_2}^v + \delta_{p_2}^v) \\
& - \alpha \sum_{v \leq u} W(u) - \alpha W_e \leq P_n \quad \forall u \in V,
\end{aligned} \tag{5.11}$$

$$\begin{aligned}
& P_{sc} + \sum_{u_p < v \leq u} \sum_g G_e(g) \mu_v^g - \sum_{u_p < v \leq u} (\gamma_{p_2}^v + \delta_{p_2}^v) \\
& - \alpha \sum_{u_p < v \leq u} W(u) - \gamma_{p_1}^u \leq P_n \quad \forall u, u_p \in V,
\end{aligned} \tag{5.12}$$

$$\epsilon_1 \leq \phi_u^1 \quad \forall u \in V, \tag{5.13}$$

$$\epsilon_2 \geq \phi_u^1 \quad \forall u \in V, \tag{5.14}$$

$$\phi_u^1 \geq P_s \quad \forall u \in V, \tag{5.15}$$

$$\phi_u^2 \geq P_s \quad \forall u \in V, \tag{5.16}$$

$$\epsilon_2 - \epsilon_1 \leq P_l. \tag{5.17}$$

Constraints (5.4) and (5.5) select an index of combiners and splitters while constraints (5.6) and (5.7) assign corresponding loss of combiners and splitters to different ports. Amplifier with gain g located at leaf u through constraint (5.8). Note that if gain 0 is selected, it means there is no need for any amplifier at that node. Amplifiers gain can be in the range of 6 dB to 20 dB with 1 dB granularity. Constraints (5.9) and (5.10) calculate the power received by Hub 2 from leaf nodes and the power received by leaf nodes from Hub 1 per subcarrier, respectively. The terms in these equations are representing the launch power, accumulation of amplifiers gain in the path, the accumulation of links loss, the drop/add loss and the summation of losses occur when passing leaf nodes. Constraint (5.11) and constraint (5.12) ensure that the power per SC does not exceed the non-linearity threshold power on optical fibers in downstream (Hub1 to leaf nodes) and upstream directions (leaf nodes to Hub2), respectively. The lower bound and upper bound of power received by Hub 2 are determined by constraints (5.13) and (5.14). Constraints (5.15) and (5.16) guarantee that received powers meet the transceiver's sensitivity demands. Constraint (5.17) ensures that the difference between the highest and lowest SCs power is smaller than P_l . Note that the leaf nodes are numbered from 1 to $|V|$ when moving from Hub 1 to Hub 2.

In a horseshoe topology, only 1:2 splitters/combiners are needed since the degree of all leaf nodes is two. Table. 5.1 shows a list of balanced and unbalanced splitters/combiners ratios and equivalent losses in dB. In addition to split/combine loss, other types of loss occur inside splitters/combiners. Excess loss is the difference between the sum of the powers entering the output ports in each fundamental mode and the power exiting the device in the input fundamental mode [160]. This study assumes a fixed 0.5 dB excess loss, which is a relatively realistic choice. Note that these splitters/combiners are four-port devices, and one of the ports is unused.

Table 5.1 List of 1:2 splitters/combiners as well as ports insertion losses in dB in ideal and realistic cases (with permission from [J3] © Optica Publishing Group).

Splitting Ratio [%]		Ideal Insertion Loss [dB]		Realistic Insertion Loss [dB]	
port 1	port 2	port 1	port 2	port 1	port 2
50	50	3.01	3.01	3.51	3.51
60	40	2.22	3.98	2.72	4.48
70	30	1.55	5.23	2.05	5.73
80	20	0.97	6.99	1.47	7.49
90	10	0.46	10	0.96	10.5

At each leaf node, a splitter, a combiner and their add/drop port assignment, and an amplifier gain (including gain 0, which means no amplifier) must be selected, resulting in a solution search space of size $(|g| \times 2|s| \times 2|s|)^{|u|}$.

5.5.3 Results and Discussion

In this section, we investigate the optimized design of metro-aggregation horseshoe topologies. We assume that hub node transceivers can communicate using 16-QAM modulation format, which functions with minimum power of -24 dBm per SC at the receiver. Although the launch power can be variable, we consider -12 dBm launch power per SC for both leaf nodes and hub node transceivers for the sake of simplicity. In our design, we assume there is no nonlinearity mitigation mechanism. Hence, we assume the power per SC does not exceed the nonlinearity power threshold at any point along the optical fibers. In the ILP model provided in the previous section, we only need to make sure the start points of optical fibers with the highest levels of power do not exceed this threshold (constraints (5.11) and (5.12)). We assume a nonlinearity power threshold of -10 dBm per SC.

We consider two horseshoe networks comprising 5 and 10 leaf nodes, in which the links are randomly generated based on the log-normal distribution. In the following, all the results

shown were obtained from 100 independent simulation runs. Amplifiers can be placed at the leaf nodes' input (according to the ILP model). Note that placing amplifiers at the output of leaf nodes might be limited due to the nonlinearity effects. The maximum power difference of SCs at Hub receiver P_l is set to 8 dB.

Fig 5.9(a) shows the average maximum power difference between SCs at the input of Hub 2 Rx and the average minimum number of amplifiers placed in horseshoes with 5 leaf nodes when different sets of candidate splitter/combiner types are considered. 95% confidence intervals are also shown as error bars. When all the splitters/combiners listed in Table. 5.1 are considered in the optimization (referred to as scenario "All"), the minimum number of required amplifiers is around 2, increasing to 3.9 when only 50/50 splitters/combiners are considered. Using only 90/10 splitters/combiners leads to fewer amplifiers being deployed, but at the expense of a higher maximum power difference between SCs. Figure. 5.7(b) shows the same analysis and similar trends when the number of leaf nodes is increased to 10. For instance, deploying a set of 70/30 and 90/10 amplifiers leads to an average of 4.2 amplifiers, which is slightly larger than that in the "All" scenario and still almost half of that of using 50/50 splitters/combiners.

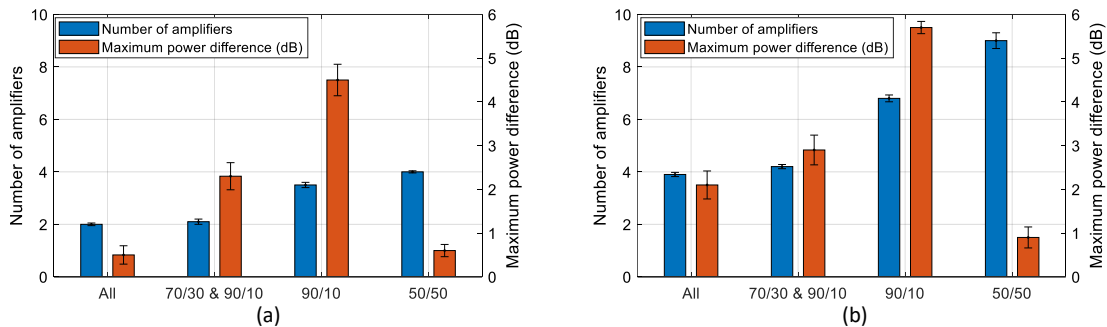


Fig. 5.9 Minimum number of amplifiers and maximum power difference of SCs at Hub 2 Rx versus set of candidate splitter/combiner types used in horseshoe network with (a) 5 leaf nodes and (b) 10 leaf nodes (with permission from [J3] © Optica Publishing Group).

Table. 5.2 shows the probability of usage of different splitters and combiners type in the "All" while considering topologies with 10 leaf nodes. It can be seen that 80/20 splitters and combiners are used more than any other type. However, 50/50 splitters and combiners have the minimum usage. This evidence suggests that too much unbalanced (90/10) or balanced (50/50) ratios might be less helpful compared to splitters/combiners with 80/20 ratio for designing filterless horseshoe networks. Unbalanced splitters/combiners can introduce significant losses, while balanced ones have no degree of freedom to meet design criteria.

Figure 5.10 depicts the loss of links, add/drop loss (excess loss included), and leaf nodes' losses for transit signals in a 10-leaf node network, optimized for both Scenario1 and

Table 5.2 Usage probability of the different splitter/combiner types in 10-leaf horseshoe networks obtained by 100 simulation (with permission from [J3] © Optica Publishing Group).

	90/10	80/20	70/30	60/40	50/50
Combiners	0.30	0.35	0.21	0.10	0.03
Splitters	0.29	0.32	0.22	0.12	0.06

Scenario4. In Scenario1, although the number of amplifiers is lower, their gain values are higher compared to Scenario4. Power calculation is shown for SCs launched by Hub1 to leaf2 and from leaf8 to Hub2. Additionally, most of the leaf nodes employ splitters/combiners with lower ratios for add/drop functions, resulting in reduced leaf loss across the optical link. These findings emphasize the significance of the range of amplifiers' gain. For example, if the maximum amplifiers' gain is limited to 14 dB, then five amplifiers would be required in Scenario1 instead of four.

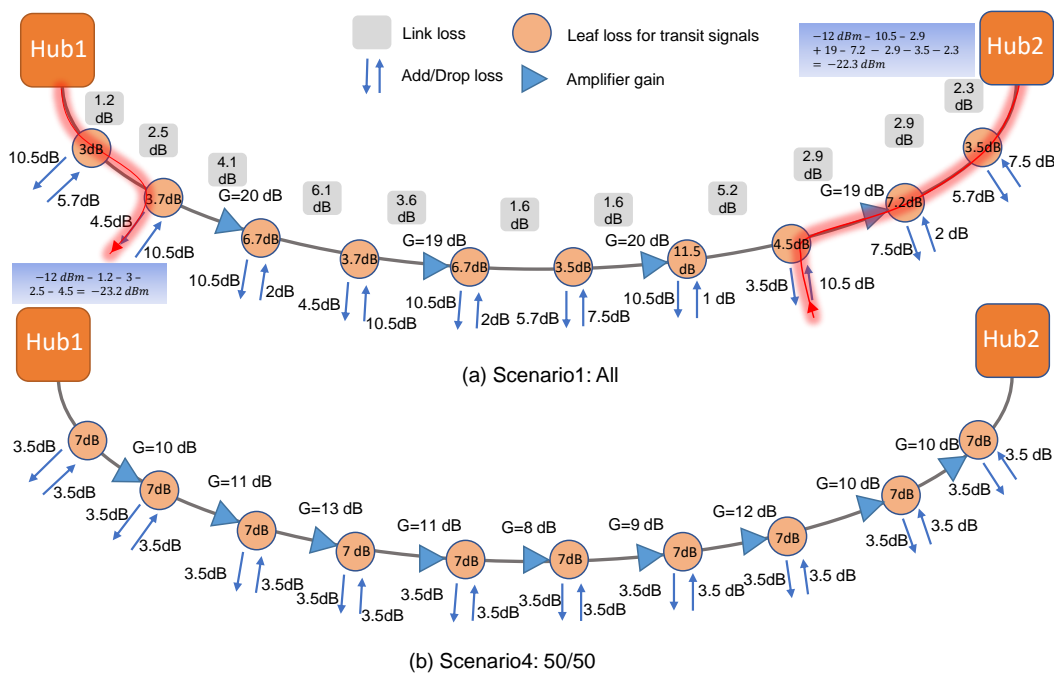


Fig. 5.10 Characterization of losses and gains for an optimized instance of 10-leaf node network (optical fiber link directed from Hub1 to Hub2) for (a) Scenario1 and (b) Scenario4 (with permission from [J3] © Optica Publishing Group).

5.5.4 Optical Signal to Noise Ratio

Optical signal-to-noise ratio (OSNR) is a critical metric as it can directly affect signal recovery. Optical amplifiers add amplified spontaneous emission (ASE) noise to signals and

all noises accumulated in the journey of a signal from its transmitter to a receiver. The ASE noise in an EDFA can be presented as follow:

$$P_{ASE} = mn_{sp}h\nu(G - 1)B_{ref} \quad (5.18)$$

where m represents the number of polarization modes (1 or 2), n_{sp} is the spontaneous emission factor, h is Planck constant, G is amplifier gain, and B_{ref} is usually considered the bandwidth equivalent to 0.1 nm band around 1550 nm with the purpose of referencing. As a result, OSNR at the output of an EDFA is approximated by:

$$OSNR[dB] \approx P_{signal}^{in}[dBm] - NF[dB] + 58 \quad (5.19)$$

where P_{signal}^{in} is the power of the optical signal at the input of the amplifier, and NF is the amplifier's noise figure. The total OSNR, however, depends on how many times a signal is amplified. It can be formulated as Eq.5.20:

$$\frac{1}{OSNR_t} = \frac{1}{OSNR_1} + \frac{1}{OSNR_2} + \dots + \frac{1}{OSNR_n} \quad (5.20)$$

in which $OSNR_t$ is the total OSNR, and $OSNR_n$ is n_{th} amplifier. Obviously, the total OSNR is smaller than the smallest individual OSNRs. Total OSNR is a nonlinear function of individual OSNRs as expressed in Eq. 5.20. For simplicity and to avoid nonlinearity in the model, we analyze OSNR via post-processing. We assume the required OSNR for 16-QAM modulation format per SC on 0.1 nm spectrum around 1550 nm is 12 dB. Also, we assume that the noise figure of each amplifier is 5 dB, independent of the amplifiers' gain.

Figure. 5.11(a) shows the average total OSNR of downstream SCs at leaf nodes' receivers in different splitter/combiner scenarios. In the presented horseshoe architecture, downstream SCs, i.e., SCs going from Hub 1 to leaf nodes, travel together towards leaf nodes. They are amplified together and also dropped together at leaf nodes. Therefore, $OSNR_i$ is always larger than $OSNR_{i+1}$, and the total OSNR declines when a leaf node is further from Hub 1. The minimum average OSNR is for leaf 10 in the 50/50 scenario, and it is about 18 dB which is higher than the 12 dB OSNR sensitivity target. The value of total OSNR depends on the number of amplifiers and their individual OSNR (Eq. 5.20). On the other hand, individual OSNR values depend on the power of a particular SC at the amplifiers' input as shown in Eq. 5.19 (link length and selection of splitters/combiners affect the amount of loss and consequently the input's power). Scenario 50/50 leads to the lowest average total OSNR since the number of amplifiers is around 9 (see Fig. 5.9). Scenario 90/10 results in the highest average total OSNR for all leaf nodes despite leading to more amplifiers compared to "All" and 70/30 & 90/10 scenarios. To justify this, 10% ports of combiners and splitters are often

employed as add and drop while ports with a 90% ratio are deployed as express. As a result, the in-line loss is smaller, which leads to higher amplifiers' input power and higher individual OSNRs.

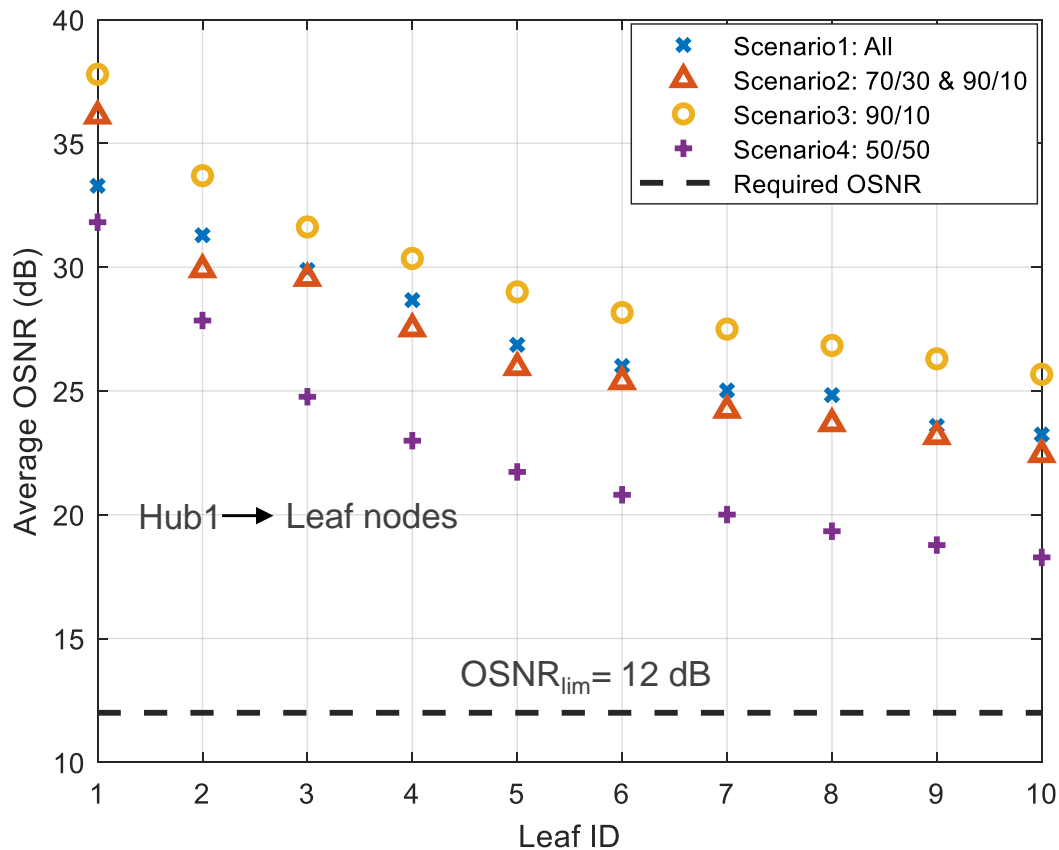


Fig. 5.11 Average OSNR of signals from Hub 1 to leaf nodes and in 10-leaf horseshoe networks in different scenarios (with permission from [J3] © Optica Publishing Group).

When an EDFA is placed in the horseshoe, a broadband unfiltered ASE noise is also introduced. Since we are considering a filterless transmission network scenario, this ASE noise is never blocked and always reaches the hub node in the upstream direction (from leaf nodes to hub). Consequently, at the receiver located in Hub2, the ASE noise level remains constant across the complete transmission bandwidth. Therefore, the OSNR variation between the different SCs is equal to the power difference between SCs only, independently of their point of origin (leaf node). Through extensive simulation, we found that the OSNR always exceeded 20 dB across all transmission scenarios and network instances for the SC originating in the first leaf node. Since the SCs power difference must be smaller than 8 dB,

as imposed by the ILP model, it can be asserted that the OSNR for all other leaf nodes is always greater than 12 dB threshold. It is noteworthy that, for both downstream and upstream transmission, the analysis shows that the required OSNR of a DSCM-based P2MP transceiver (assumed to have similar performance to that specified by 400G OpenZR+ MSA [161]) can be met. However, this might not always be the case and if OSNR values fall below the threshold, the design would not have been valid and alternative ways would have to be employed.

Table 5.3 shows the average solving time and the standard deviation of 100 runs of the ILP model when considering Scenario1, which has more variables than the other scenarios, and networks with different numbers of leaf nodes using a typical laptop with 16GB RAM and a Core i7 @1.8 GHz CPU. As can be seen, the solving time rapidly increases with the increase of the network size and consequently the number of variables and constraints. In networks with 15 leaf nodes, there are some problem instances that take a longer time to solve, reflected in the significantly higher standard deviation value. Note that ILP is classified as an NP-hard problem [?], which means that finding an optimal solution can be extremely difficult and time-consuming for large-scale problems. In addition, non-linear constraints can be modeled with ILP methods and, as previously mentioned, other approaches, such as heuristics, would have to be employed.

Table 5.3 Average and standard deviation of the ILP model solving time for the Scenario1 and networks with 5, 10, and 15 leaf nodes (with permission from [J3] ©Optica Publishing Group).

Network Size (# of leaf nodes)	5	10	15
Number of Variables	215	430	645
Number of Constraints	81	186	316
Average Solving Time (second)	4.03	9.32	52.44
Std of Solving Time (second)	0.92	1.23	105.23

5.5.5 Constrained-Optimization Framework

The proposed ILP model can only integrate linear constraints and, thus, excludes relevant constraints that cannot be expressed in linear terms, which is the case for those needed to meet the required OSNR at the receiver side. In addition, the ILP model may prove to be too slow when solving very large problem instances. To address both limitations, we propose a new meta-heuristic framework tailored for solving the previous constrained-optimization problem.

The framework developed to solve the described problem uses the genetic algorithm (GA) meta-heuristic. GA is a type of optimization algorithm that is inspired by the principles of natural selection and genetics [162] and has been exploited to solve optimization problems that are difficult or impossible to solve with traditional methods. GA operates on a population of potential solutions and uses genetic operators such as mutation, crossover, and selection to evolve the population over a series of generations toward an optimal or near-optimal solution. The algorithm starts with an initial population of candidate solutions, and through successive iterations, the fittest individuals are selected to produce offspring that inherit the characteristics of their parents. Over time, the population converges towards a set of improved solutions.

5.5.6 Genetic Algorithms for Constrained-Optimization

Adapting a GA for solving constrained optimization problems involves incorporating constraints into the fitness function or modifying the genetic operators to maximize the likelihood that the solutions generated are kept in the feasible region. A gradient descent-based GA has been proposed in [163] to tackle a constraint optimization problem with continuous variables. Another approach is to add a penalty term to the fitness function that penalizes solutions that violate constraints. The penalty term could be a function of the degree of violation, fixed penalty value (the penalty for a certain number of constraint violations is fixed regardless of the number of violations), and the death penalty, which discards unfeasible individuals by penalizing them with a large value [164]. The penalty term ensures that the algorithm can converge to the optimal solution from all directions, even if the path passes through an infeasible region. Note that maintaining feasibility is difficult for many problems. Even with two feasible parents, crossover can lead to unfeasible children. This happens especially in combinatorial problems, where the encoding is based on integer numbers. Other approaches can generally be classified into different categories [165] such as methods based on a search for feasible solutions and methods based on the preservation of the feasibility of solutions.

Generally, a constrained optimization problem is expressed as a nonlinear optimization problem. GAs encode the design variables of the search space in structures called chromosomes (or individuals). Each chromosome represents a possible solution (either feasible or infeasible) of the optimization problem modeled and is coded by a vector of components or variables which are analogous to genes.

Problem Formulation and GA Customization

A horseshoe architecture with l leaf nodes needs l splitters, l combiners and l possible amplifiers. Therefore, it requires $3l$ variables, which can be used to describe a combination of splitters, combiners, and amplifiers, to form a solution. The length of the chromosomes is also $3l$ and the value of each gene represents the index of the ratios for splitters/combiners and the amplifiers' gain.

The primary optimization objective is to minimize the number of amplifiers, followed by a secondary objective to minimize the largest difference between the power levels of the DSCs at the input of the hub's receiver (Rx), if possible. The latter is used to optimize transceiver performance at the hub, since a constraint is also enforced to ensure a threshold on this difference. Overall, the objective function can be expressed as:

$$z(\bar{x}) = N(\bar{x}) + w\Delta(\bar{x}) \quad (5.21)$$

where $N(\bar{x})$ denotes the total number of amplifiers corresponding to chromosome \bar{x} , $\Delta(\bar{x})$ is the maximum difference in DSC power at the hub node, and w is a small weighting factor. To consider constraints, we define a fitness function based on the objective function and the magnitude of constraint violations as follows:

$$f(\bar{x}) = z(\bar{x})^r + C(i) \sum_{q=1}^Q \delta_q(\bar{x}) [\phi_q(\bar{x})] \quad (5.22)$$

where r is an exponent for rewarding smaller $z(\bar{x})$, $C(i)$ is an increasing function with regard of iteration index i , $\delta_q(\bar{x})$ is 1 if constraint q (the total number of constraints is Q) is violated where the violations is presented as $\phi_q(\bar{x})$, otherwise 0. Initially the penalty parameter is small but increases over time so that infeasible solutions are not present in the final generations. Additionally, to avoid convergence to an infeasible solution with a negligible penalty, the magnitude of constraints violation is rounded up to the nearest integer number. In Fig. 5.12, we present the flowchart of our proposed GA.

Firstly, the algorithm initializes a population of size N_{pop} . Then, a group of top-performing individuals is identified based on the predefined elite rate ρ_y . In the following, a set of individuals is formed, consisting of offspring obtained through crossover ($N_{pop} \times \rho_c$) and mutation ($N_{pop} \times \rho_m$). To produce individuals using crossover, we use the biased random-key method proposed in [9]. In this method, top-fit individuals in a population are considered as elite and one of the parents for mating is always an elite individual. Besides, the offspring inherits more genes (when random-key probability is larger than a pre-fixed value) from its elite parent. Elite or non-elite parents are selected by the roulette wheel selection (RWS)

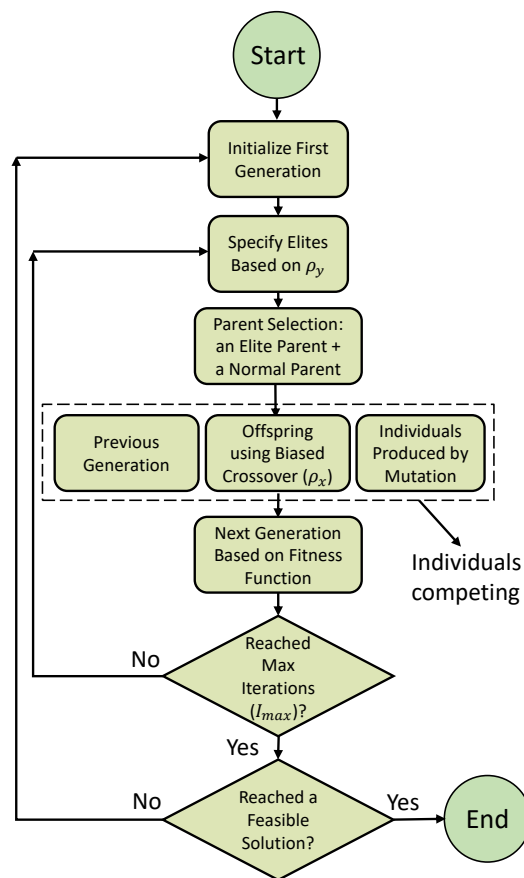


Fig. 5.12 Flowchart of the proposed GA.

method. Fig. 5.13 illustrates an example of producing an offspring using this approach. The parameter ρ_y shows that the top 25% most fit individuals are considered as elite. The uniform random-key generated is compared with the probability ρ_x to decide each gene comes from which parent. For instance, $\rho_x = 0.7$ indicates that the elite parent genes will be passed to the offspring with a 70% probability. With respect to individuals with mutation, for every section of a parent's the chromosome (splitters, combiners and amplifiers), N_m gene(s) are randomly substituted with a different gene. Next, offsprings, parents, and individuals created by mutation are sorted based on their fitness and the top N_{pop} individuals are selected to form the next generation. The process is repeated for a maximum of I_{max} iterations. However, if the most fitted solution is not feasible at the end of iterations, the algorithm restarts by starting another round of initialization.

Table 5.4 shows the P2MP transceiver parameter values, the Erbium-doped fiber amplifier (EDFA) characteristics, the splitter/combiner types, the network size and the fiber attenuation

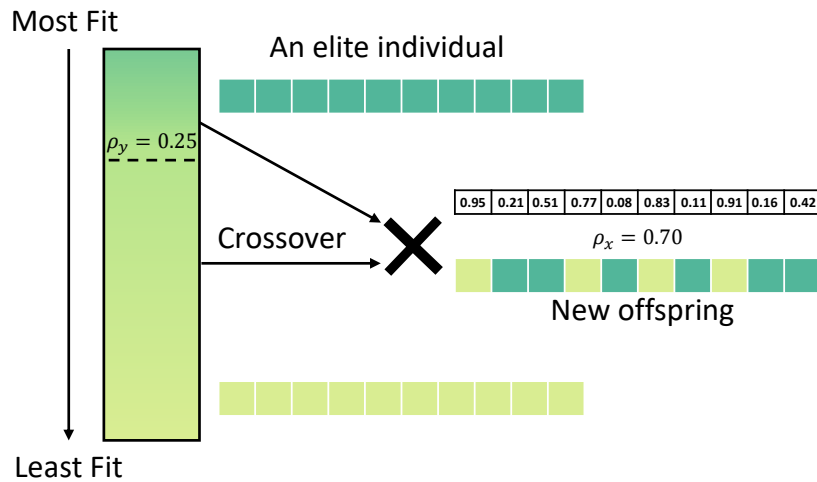


Fig. 5.13 Biased crossover approach, where one parent is an elite individual and the offspring inherits a greater number of genes from this parent [9].

coefficient. Note that the transceiver parameters are determined on the basis of the OpenZR+ MSA requirements [161].

5.6 Results and Discussion

In this section, we present results obtained with the proposed optimization framework. The first set of results is used to benchmark the algorithm's performance by comparing the solutions obtained with the optimal ones computed with the previous ILP model. Executing this comparison requires disabling the required OSNR threshold constraint. The second set of results provides a detailed analysis of results obtained with the GA when enabling all the constraints. Table 5.5 summarizes the parameters and values obtained through fine-tuning.

Incorporating splitters/combiners with a variety of power split/combine ratios into the network design affords greater flexibility; however, it also introduces planning complexity. We consider three distinct scenarios. In Scenario1, splitters/combiners with all ratios listed in Table 5.4 are available. In Scenario2, ratios are limited to [0.1, 0.3, 0.7, 0.9]. Finally, in Scenario3, only balanced (0.5/0.5) splitters/combiners are available. We use the data of real horseshoe topologies described in [142] to generate new horseshoes by fitting a log-normal distribution. The average link length is 13.2 km and the standard deviation is 5.6 km. Also, $C(i)$ is defined as $(1 + \frac{i}{I_{max}})^2$ and exponent r ranges between 1.3 and 2.5.

In Fig. 5.14a, we present the average number of amplifiers required in 50 network design instances in the case of using 16-QAM modulation format, comparing the ILP model results

Table 5.4 Network parameters and their corresponding values considered in this study ([C8] © 2023 IEEE).

Parameter	Value
Optical fiber loss	0.22 dB/km
Launch power	-12 dBm/SC
8-QAM, 16-QAM, 32-QAM power sensitivity	-26,-24,-22 dBm/SC
8-QAM, 16-QAM, 32-QAM required OSNR	9,12,16 dB/SC
Maximum DSCs power difference tolerance	8 dB
Non-linearity power threshold	-10 dB/SC
EDFA gain range	[0,6,7,...,20] dB
EDFA noise figure (NF)	7 dB
Splitters/combiners ratio set	[0.1,0.2,...,0.9]
Number of leaf nodes	10

Table 5.5 GA parameters and their corresponding values considered in this paper ([C8] © 2023 IEEE).

Parameter	Value
w : Objective function weighting factor	0.1
ρ_x : Elite genes inheritance probability	0.7
ρ_y : Elite rate	0.25
N_{pop} : Number of individuals per generation	200
I_{max} : Number of iterations	100
ρ_c : Crossover percentage	0.8
ρ_m : Mutation percentage	0.2
N_m : Number of mutations in each section of the chromosome	1
r : Objective exponent	1.3–2.5

with those of the proposed GA when OSNR constraints are not considered. Among the three scenarios examined, Scenario1 gives the lowest number of amplifiers, which is less than half of Scenario3. Scenario2 results in a slightly higher average number of amplifiers, utilizing only half of the available splitters/combiners ratios. Importantly, the results obtained with the GA are very close to those achieved by the ILP. The largest deviation is observed in Scenario2 and might indicate that in this case it is more difficult to escape local minimums in the solution search space.

The convergence plot in Fig. 5.14b depicts the changes in fitness value of the best individual in each iteration and its components; objective-related term, and penalty term (see Eq. 5.22) over the course of a single problem instance in Scenario1. While the fitness function is non-increasing, the objective-related and penalty terms exhibit fluctuations, albeit with an overall downward trend. Notably, the penalty term eventually becomes zero by

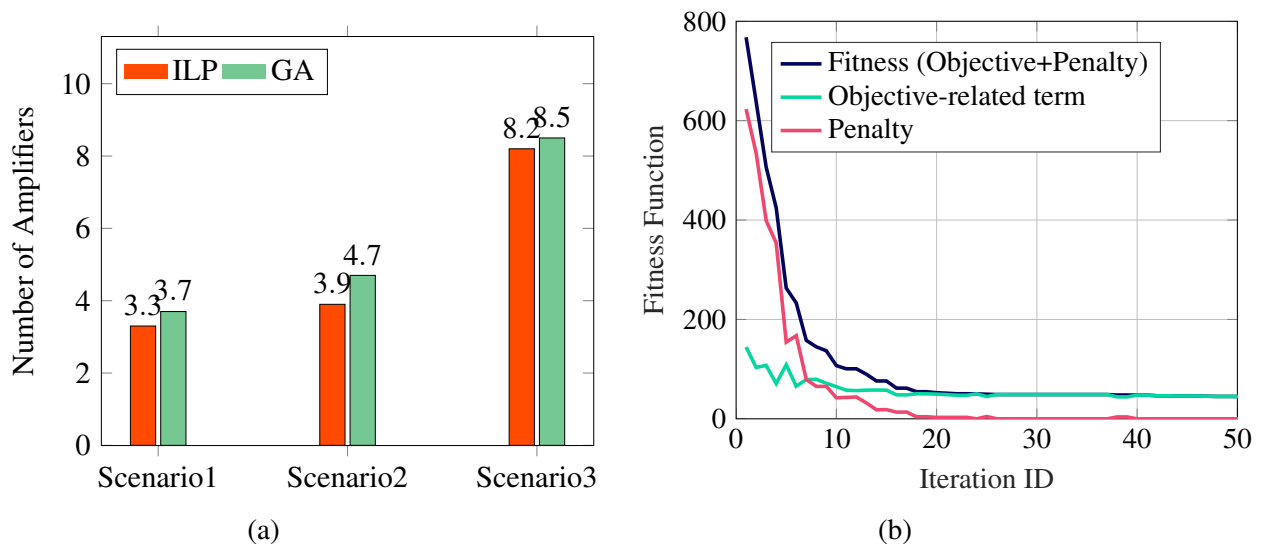


Fig. 5.14 (a) Average number of amplifiers using the ILP model and GA for three different splitters/combiners scenarios and 16-quadrature amplitude modulation (QAM) format, and (b) evolution of the fitness of the best individual of each generation and its components; objective-related term and the penalty for a single problem instance of Scenario1 ([C8] © 2023 IEEE).

iteration 40, indicating that the most fit individual is now feasible. It is worth noting that if the balance between the objective-related and penalty terms shifts drastically, the GA may either fail to identify a feasible solution or converge to a sub-optimal solution.

The modulation formats feature different trade-offs between capacity and performance requirements (e.g. power sensitivity and required OSNR). For instance, while the 32-QAM modulation format allows higher data rates, it has a more stringent required OSNR and power sensitivity than 16-QAM. Fig. 5.15a illustrates the average number of amplifiers obtained with the GA when all constraints are considered for three modulation formats and for the three described scenarios. Overall, the number of amplifiers required is higher for transceivers operating with 32-QAM than those when using 8-QAM or 16-QAM. Notably, the number of amplifiers required increases from Scenario1 to Scenario3. The reason is that having fewer splitters/combiners ratios limits the design and results in having to increase the number of amplifiers to meet all the constraints. Scenario1 with full splitters/combiner ratios granularity results in an amplifier count reduction that ranges between 40% and 60% of that with Scenario3. Scenario2 offers an interesting compromise by almost halving the number of different splitter/combiner ratios used, reducing the amount of different part numbers the operator needs to maintain, at the cost of an increase of amplifiers that does not exceed 10% when averaging the results for the three modulation formats.

Fig. 5.15b shows the maximum DSC power difference at the hub. This difference tends to increase from Scenario1 to Scenario2. However, Scenario3's design flexibility is limited

due to the use of only 50/50 splitters/combiners. As a result, adjusting amplifier gain is the only means of equalizing DSC power. Hence, the more amplifiers there are, the lower the maximum DSC power difference. The results indicate that the maximum DSC power difference is in most cases considerably lower than the 8 dB threshold, which means the hub's receiver can safely operate far from the threshold, allowing for accommodating occasional power fluctuations.

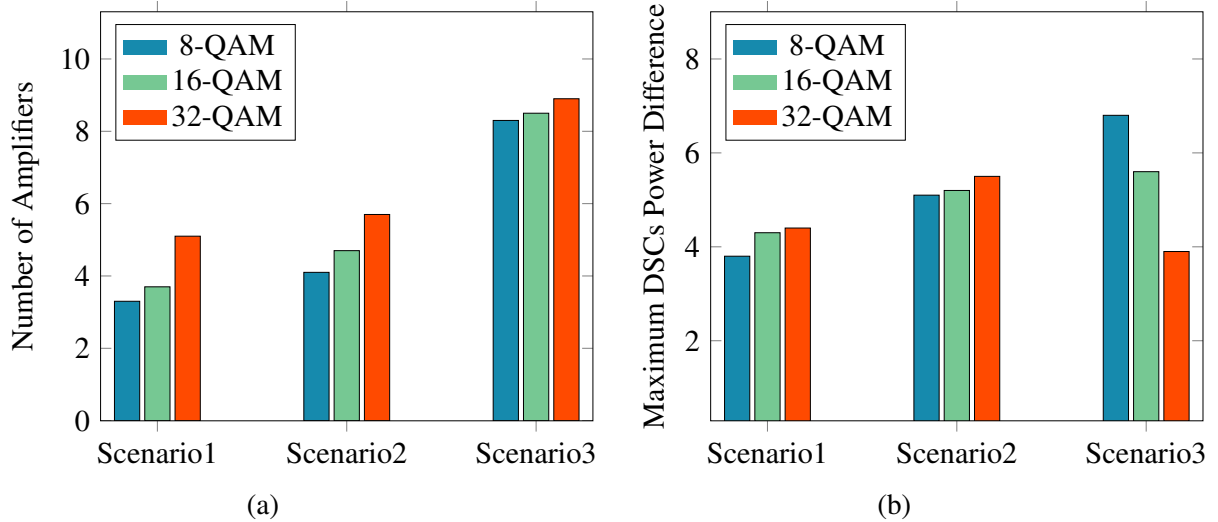


Fig. 5.15 (a) Average number of amplifiers for 50 networks optimized by the GA considering 8-QAM, 16-QAM and 32-QAM and (b) the average maximum DSC power difference ([C8] © 2023 IEEE).

5.7 Conclusion

In this chapter, an ILP optimization method has been developed for designing a filterless horseshoe architecture that supports P2MP transceivers. Different design criteria have been met through constraints in the ILP model. The results obtained for networks generated using statistical data showed that unbalanced splitters/combiners help manage power loss and consequently lead to a design with fewer EDFAs. In contrast, when using only balanced splitters/combiners, most of the leaf nodes need an amplifier. Besides, a GA-based optimization framework was proposed to tackle the nonlinear OSNR constraints.

Chapter 6

Conclusion and Future Works

6.1 Review of Thesis

This thesis focused on network planning and optimizations with the goal of the most efficient use of resources (capital, equipment, fibers, and so on). First, the well-known routing and wavelength assignment problems were partly investigated using heuristics, integer linear programming, and genetic algorithms. Integer linear programming was selected as the primary method of optimization in the rest of the thesis as it provides exact solutions efficiently when the size of problems is not too large. DSCM-based P2MP transceivers were discussed in terms of architecture and applications. ROADM-based and filterless architectures were optimized using reference networks. Besides, P2MP transceivers' multi-period planning was studied in which the optimization in a long period of time is considered instead of a single instance of time. Finally, a comprehensive filterless horseshoe architecture was introduced and optimized for the deployment of P2MP transceivers considering several key performance metrics such as receiver sensitivity and equalized SC power levels at receivers.

The key achievements of the thesis are as follows:

- Results demonstrated that optimized deployment of P2MP transceivers could reduce the cost of transceivers between 20% and 40% compared to conventional P2P transceivers.
- As long as the traffic pattern is hub-and-spoke, the saving of P2MP transceivers holds by upgrading 400G transceivers to higher data rates such as 800G and 1.2T.
- In the case of multi-period planning, if transceivers can be exchanged between leaf sites when upgrading network capacity, it can reduce the long-term CapEx at the expense of an increase in OpEx. There is a trade-off.

- Horseshoe metro-aggregation networks are designed in a filterless approach supporting P2MP transceivers. Using a flexible set of unbalanced splitters/combiners results in fewer amplifiers.
- A Genetic Algorithm based optimization framework has been proposed to tackle nonlinear constraints such as OSNR constraints for filterless horseshoe networks.

6.2 Future Work Direction

This section aims to shed light on the potential avenues of research and practical applications that can build upon the findings and contributions presented in the preceding chapters. As a culmination of extensive research and analysis, this section looks beyond the immediate scope of the thesis and explores the broader implications and future directions in the field of study.

- The thesis primarily relies on ILP and heuristic techniques, such as genetic algorithms, for conducting the majority of the work. It is highly advised to venture into alternative domains like machine learning for further investigation. However, it is crucial to exercise caution while implementing optimization frameworks, taking into account the inherent complexity of optimization problems.
- Understanding the power consumption of routers and switches is crucial when examining the electricity usage of internet transportation. While determining a precise value for the power consumption of routers may be challenging, accurately modeling power consumption across various scenarios, ranging from small to large routers and from partially loaded to fully loaded, can facilitate the analysis of IP layer power consumption.
- Conducting a thorough cost analysis of filterless networks using P2MP transceivers deployment is essential for understanding the benefits compared to ROADM-based P2P scenarios. This analysis should consider not only the cost of transceivers but also the costs associated with splitters/combiners and ROADMs, which need to be accurately modeled.
- Historical traffic data plays a vital role in multiperiod planning as it enables accurate predictions of future traffic growth. Accessing authentic traffic data from real networks presents exciting opportunities to conduct insightful simulations.

- Our research focused on P2MP transceivers and their characteristics, which are primarily influenced by industry standards. Introducing innovative features to these devices can lead to more versatile solutions. For example, we traditionally assumed that the subcarriers (SCs) of a P2MP transceiver must use the same modulation format. However, it is theoretically possible to enable individual SCs to operate on different modulation formats.

Author's Publications

Conference papers:

- C1 M. M. Hosseini, J. Pedro, N. Costa, A. Napoli, J. E. Prilepsky and S. K. Turitsyn, "Optimized Design of Metro-Aggregation Networks Exploiting Digital Subcarrier Routing," 2021 Asia Communications and Photonics Conference (ACP), 2021, pp. 1-3.
- C2 M. M. Hosseini, J. Pedro, A. Napoli, N. Costa, J. E. Prilepsky and S. K. Turitsyn, "Design of Survivable Metro-Aggregation Networks based on Digital Subcarrier Routing," 2021 IEEE Global Communications Conference (GLOBECOM), 2021, pp. 1-6, doi: 10.1109/GLOBECOM46510.2021.9685219.
- C3 M. M. Hosseini, J. Pedro, A. Napoli, N. Costa, J. E. Prilepsky and S. K. Turitsyn, "Optimization of Survivable Filterless Optical Networks Exploiting Digital Subcarrier Multiplexing," ICC 2022 - IEEE International Conference on Communications, 2022, pp. 5731-5736, doi: 10.1109/ICC45855.2022.9838887.
- C4 M. M. Hosseini, J. Pedro, N. Costa, A. Napoli, E. P. Jaroslaw and S. K. Turitsyn, "Optimized Physical Design of Metro Aggregation Networks using Point to Multipoint Transceivers," 2022 Optical Fiber Communications Conference and Exhibition (OFC), 2022, pp. 01-03.
- C5 M. M. Hosseini, J. Pedro, A. Napoli, N. Costa, J. E. Prilepsky and S. K. Turitsyn, "Long-Term Cost-Effectiveness of Metro Networks Exploiting Point-to-Multipoint Transceivers," 2022 International Conference on Optical Network Design and Modeling (ONDM), 2022, pp. 1-6, doi: 10.23919/ONDM54585.2022.9782846.
- C6 M. M. Hosseini, J. Pedro, N. Costa, A. Napoli, J. E. Prilepsky and S. K. Turitsyn, "Multi-period Planning in Metro-Aggregation Networks using Point-to-Multipoint Transceivers," GLOBECOM 2022 - 2022 IEEE Global Communications Conference, Rio de Janeiro, Brazil, 2022, pp. 2921-2926, doi: 10.1109/GLOBECOM48099.2022.10001405.
- C7 M. M. Hosseini, J. Pedro, N. Costa, A. Napoli, J. E. Prilepsky and S. K. Turitsyn, "Optimal Design of Filterless Horseshoe Networks Supporting Point-to-Multipoint Transceivers," 2023 Optical Fiber Communications Conference and Exhibition (OFC), San Diego, CA, USA, 2023, pp. 1-3, doi: 10.1364/OFC.2023.W2A.16.
- C8 M. M. Hosseini, J. Pedro, A. Napoli, N. Costa, J. E. Prilepsky and S. K. Turitsyn, "Meta-Heuristic Framework for Designing Filterless Horseshoe Networks with P2MP Transceivers," 2023 Photonics in Switching and Computing (Oral Presentation).

Journal papers:

- J1 M. M. Hosseini, J. Pedro, A. Napoli, N. Costa, J. E. Prilepsky and S. K. Turitsyn, "Optimization of survivable filterless optical networks exploiting digital subcarrier multiplexing," in *Journal of Optical Communications and Networking*, vol. 14, no. 7, pp. 586-594, July 2022, doi: 10.1364/JOCN.451182.

- J2 M. M. Hosseini, J. Pedro, A. Napoli, N. Costa, J. E. Prilepsky and S. K. Turitsyn, "Multi-period planning in metro-aggregation networks exploiting point-to-multipoint coherent transceivers," in *Journal of Optical Communications and Networking*, vol. 15, no. 3, pp. 155-162, March 2023, doi: 10.1364/JOCN.475902.
- J3 M. M. Hosseini, J. Pedro, A. Napoli, N. Costa, J. E. Prilepsky and S. K. Turitsyn, "Optimized design of filterless horseshoe networks exploiting point-to-multipoint coherent transceivers," in *Journal of Optical Communications and Networking*, vol. 15, no. 9, pp. 569-578, September 2023, doi: 10.1364/JOCN.494342.

References

- [1] T. F. O. Association, “Coherent fiber optic communications.” <https://www.thefoa.org/tech/ref/appln/coherent.html>, 2020.
- [2] C. Liu, J. Pan, T. Detwiler, A. Stark, Y.-T. Hsueh, G.-K. Chang, and S. E. Ralph, “Super receiver design for superchannel coherent optical systems,” in Next-Generation Optical Communication: Components, Sub-Systems, and Systems, vol. 8284, pp. 40–47, SPIE, 2012.
- [3] M. Jinno, H. Takara, Y. Sone, K. Yonenaga, and A. Hirano, “Multiflow optical transponder for efficient multilayer optical networking,” IEEE Communications Magazine, vol. 50, no. 5, pp. 56–65, 2012.
- [4] D. Welch, A. Napoli, J. Bäck, W. Sande, J. Pedro, F. Masoud, C. Fludger, T. Duthel, H. Sun, S. J. Hand, et al., “Point-to-multipoint optical networks using coherent digital subcarriers,” Journal of Lightwave Technology, vol. 39, no. 16, pp. 5232–5247, 2021.
- [5] F. Paolucci, R. Emmerich, A. Eira, N. Costa, J. Pedro, P. W. Berenguer, C. Schubert, J. Fischer, F. Fresi, A. Sgambelluri, et al., “Disaggregated edge-enabled C+ L-band filterless metro networks,” Journal of Optical Communications and Networking, vol. 12, no. 3, pp. 2–12, 2020.
- [6] M. Furdek, A. Muhammad, G. Zervas, N. Alloune, C. Tremblay, and L. Wosinska, “Programmable filterless network architecture based on optical white boxes,” in 2016 International Conference on Optical Network Design and Modeling (ONDM), pp. 1–6, IEEE, 2016.
- [7] FS, “How do different fiber optic couplers work?.” <https://community.fs.com/blog/how-do-different-fiber-optic-couplers-work.html>, Mar. 2021.
- [8] THORLAB, “Definition of 1x2 fused fiber optic coupler specifications.” <https://www.thorlabs.com>.
- [9] J. F. Gonçalves and M. G. Resende, “Biased random-key genetic algorithms for combinatorial optimization,” Journal of Heuristics, vol. 17, no. 5, pp. 487–525, 2011.
- [10] P. J. Winzer and D. T. Neilson, “From scaling disparities to integrated parallelism: A decathlon for a decade,” Journal of Lightwave Technology, vol. 35, no. 5, pp. 1099–1115, 2017.
- [11] T. Hatt and P. Jarich, “Global mobile trends 2021. navigating COVID-19 and beyond,” GSMA Intelligence, 2020.

- [12] N. Jones et al., “The information factories,” *Nature*, vol. 561, no. 7722, pp. 163–6, 2018.
- [13] N. Ghani, S. Dixit, and T.-S. Wang, “On IP-over-WDM integration,” *IEEE Communications magazine*, vol. 38, no. 3, pp. 72–84, 2000.
- [14] A. Eira, J. Pedro, and J. Pires, “Optimized design of multistage passive optical networks,” *Journal of Optical Communications and Networking*, vol. 4, no. 5, pp. 402–411, 2012.
- [15] GSMA, “The mobile economy 2022.” <https://www.gsma.com/mobileeconomy/wp-content/uploads/2022/02/280222-The-Mobile-Economy-2022.pdf>, May 2022.
- [16] C. Magazzino, D. Porrini, G. Fusco, and N. Schneider, “Investigating the link among ict, electricity consumption, air pollution, and economic growth in EU countries,” *Energy Sources, Part B: Economics, Planning, and Policy*, vol. 16, no. 11-12, pp. 976–998, 2021.
- [17] J. Berthold, A. A. Saleh, L. Blair, and J. M. Simmons, “Optical networking: Past, present, and future,” *Journal of lightwave technology*, vol. 26, no. 9, pp. 1104–1118, 2008.
- [18] D. K. Tripathi, P. Singh, N. Shukla, and H. Dixit, “Reconfigurable optical add and drop multiplexers a review,” *Electrical & Computer Engineering: An International Journal (ECIJ) Volume*, vol. 3, 2019.
- [19] T. I. T. Union, “Spectral grids for WDM applications: DWDM frequency grid.” file: <///C:/Users/hosseini/Downloads/T-REC-G.694.1-202010-I!!PDF-E.pdf>, Oct. 2020.
- [20] B. Ramamurthy, H. Feng, D. Datta, J. P. Heritage, and B. Mukherjee, “Transparent vs. opaque vs. translucent wavelength-routed optical networks,” in *OFC/IOOC. Technical Digest. Optical Fiber Communication Conference, 1999, and the International Conference on Integrated Optics and Optical Fiber Communication*, vol. 1, pp. 59–61, IEEE, 1999.
- [21] G. A. Beletsioti, G. I. Papadimitriou, and P. Nicopolitidis, “Energy-aware algorithms for IP over WDM optical networks,” *Journal of Lightwave Technology*, vol. 34, no. 11, pp. 2856–2866, 2016.
- [22] V. López, L. Velasco, et al., “Elastic optical networks,” *Architectures, Technologies, and Control*, Switzerland: Springer Int. Publishing, 2016.
- [23] S. Gorshe, “A tutorial on ITU-T G. 709 optical transport networks (OTN),” *PMCSierra white paper, personal communication*, 2010.
- [24] O. Gerstel, M. Jinno, A. Lord, and S. B. Yoo, “Elastic optical networking: A new dawn for the optical layer?,” *IEEE communications Magazine*, vol. 50, no. 2, pp. s12–s20, 2012.
- [25] J. Pedro, N. Costa, and S. Sanders, “Cost-effective strategies to scale the capacity of regional optical transport networks,” *Journal of Optical Communications and Networking*, vol. 14, no. 2, pp. A154–A165, 2022.

- [26] M. Jinno, H. Takara, B. Kozicki, Y. Tsukishima, Y. Sone, and S. Matsuoka, "Spectrum-efficient and scalable elastic optical path network: architecture, benefits, and enabling technologies," *IEEE communications magazine*, vol. 47, no. 11, pp. 66–73, 2009.
- [27] R. K. Ahuja, T. L. Magnanti, and J. B. Orlin, "Network flows," 1988.
- [28] C. H. Papadimitriou and K. Steiglitz, *Combinatorial optimization: algorithms and complexity*. Courier Corporation, 1998.
- [29] G. Dantzig, S. U. S. O. Laboratory, N. S. F. (U.S.), U. S. D. of Energy, and U. S. O. of Naval Research, *Origins of the Simplex Method*. Technical report (Stanford University. Systems Optimization Laboratory), Stanford University, Department of Operations Research, Systems Optimization Laboratory, 1987.
- [30] V. Klee and G. J. Minty, "How good is the simplex algorithm," *Inequalities*, vol. 3, no. 3, pp. 159–175, 1972.
- [31] M. Cuturi, "Linear programming and convex analysis, ellipsoid methods." <https://marcocuturi.net/Teaching/ORF522/lec11v2.pdf>, 2009.
- [32] R. Freund and C. Roos, "The ellipsoid method," *Optimization*, vol. 1, p. 26, 2007.
- [33] K. Frisch, "The logarithmic potential method of convex programming," *Memorandum, University Institute of Economics, Oslo*, vol. 5, no. 6, 1955.
- [34] J. Gondzio, "Interior point methods 25 years later," *European Journal of Operational Research*, vol. 218, no. 3, pp. 587–601, 2012.
- [35] R. M. Karp, "Reducibility among combinatorial problems," in *Complexity of computer computations*, pp. 85–103, Springer, 1972.
- [36] J. Hartmanis, "Computers and intractability: a guide to the theory of NP-completeness (michael r. Garey and david s. Johnson)," *Siam Review*, vol. 24, no. 1, p. 90, 1982.
- [37] E. Balas, S. Ceria, M. Dawande, F. Margot, and G. Pataki, "Octane: A new heuristic for pure 0–1 programs," *Operations Research*, vol. 49, no. 2, pp. 207–225, 2001.
- [38] F. Glover and M. Laguna, "General purpose heuristics for integer programming—part i," *Journal of Heuristics*, vol. 2, no. 4, pp. 343–358, 1997.
- [39] L. Bertacco, *Exact and heuristic methods for mixed integer linear programs*. PhD thesis, Ph. D. thesis, Universita degli Studi di Padova, 2006.
- [40] J. E. Kelley, Jr, "The cutting-plane method for solving convex programs," *Journal of the society for Industrial and Applied Mathematics*, vol. 8, no. 4, pp. 703–712, 1960.
- [41] A. H. Land and A. G. Doig, "An automatic method for solving discrete programming problems," in *50 Years of Integer Programming 1958-2008*, pp. 105–132, Springer, 2010.
- [42] J. E. Mitchell, "Branch-and-cut algorithms for combinatorial optimization problems," *Handbook of applied optimization*, vol. 1, no. 1, pp. 65–77, 2002.

- [43] X. Yu and M. Gen, Introduction to evolutionary algorithms. Springer Science & Business Media, 2010.
- [44] J. R. Koza, “Genetic programming as a means for programming computers by natural selection,” Statistics and computing, vol. 4, no. 2, pp. 87–112, 1994.
- [45] C. A. Kyriakopoulos, G. I. Papadimitriou, P. Nicopolitidis, and E. Varvarigos, “Energy-efficient lightpath establishment in backbone optical networks based on ant colony optimization,” Journal of Lightwave Technology, vol. 34, no. 23, pp. 5534–5541, 2016.
- [46] X. Wang, M. Brandt-Pearce, and S. Subramaniam, “Distributed grooming, routing, and wavelength assignment for dynamic optical networks using ant colony optimization,” Journal of Optical Communications and Networking, vol. 6, no. 6, pp. 578–589, 2014.
- [47] S. Li, H. Liu, Y. Du, et al., “An optimal resource allocation scheme for elastic applications in multipath networks via particle swarm optimization,” IAENG International Journal of Computer Science, vol. 47, no. 2, 2020.
- [48] F. R. Durand and T. Abrão, “Energy-efficient power allocation for WDM/OCDM networks with particle swarm optimization,” Journal of Optical Communications and Networking, vol. 5, no. 5, pp. 512–523, 2013.
- [49] C. Tremblay, F. Gagnon, B. Chatelain, E. Bernier, and M. P. Belanger, “Filterless optical networks: a unique and novel passive WAN network solution,” IEICE Proceedings Series, vol. 49, no. 12P-7, 2007.
- [50] O. Ayoub, O. Karandin, M. Ibrahimi, A. Castoldi, F. Musumeci, and M. Tornatore, “Tutorial on filterless optical networks,” Journal of Optical Communications and Networking, vol. 14, no. 3, pp. 1–15, 2022.
- [51] M. Ibrahimi, O. Ayoub, F. Albanese, F. Musumeci, and M. Tornatore, “Strategies for dedicated path protection in filterless optical networks,” in 2021 IEEE Global Communications Conference (GLOBECOM), pp. 01–06, IEEE, 2021.
- [52] D. Simon, Evolutionary optimization algorithms. John Wiley & Sons, 2013.
- [53] F. P. Kelly, “Blocking probabilities in large circuit-switched networks,” Advances in applied probability, vol. 18, no. 2, pp. 473–505, 1986.
- [54] A. E. Ozdaglar and D. P. Bertsekas, “Routing and wavelength assignment in optical networks,” IEEE/ACM transactions on networking, vol. 11, no. 2, pp. 259–272, 2003.
- [55] I. Chlamtac, A. Ganz, and G. Karmi, “Lightpath communications: An approach to high bandwidth optical wan’s,” IEEE transactions on communications, vol. 40, no. 7, pp. 1171–1182, 1992.
- [56] H. Zang, J. P. Jue, B. Mukherjee, et al., “A review of routing and wavelength assignment approaches for wavelength-routed optical WDM networks,” Optical networks magazine, vol. 1, no. 1, pp. 47–60, 2000.

- [57] D. T. Hai, "On solving the 1+ 1 routing, wavelength and network coding assignment problem with a bi-objective integer linear programming model," Telecommunication Systems, vol. 71, no. 2, pp. 155–165, 2019.
- [58] J. A. Bondy, U. S. R. Murty, et al., Graph theory with applications, vol. 290. Macmillan London, 1976.
- [59] B. C. Chatterjee, N. Sarma, P. P. Sahu, and E. Oki, "Priority-based routing and wavelength assignment scheme," in Routing and Wavelength Assignment for WDM-based Optical Networks, pp. 51–63, Springer, 2017.
- [60] G. Z. Marković, "Routing and spectrum allocation in elastic optical networks using bee colony optimization," Photonic Network Communications, vol. 34, no. 3, pp. 356–374, 2017.
- [61] Y. Wang, X. Cao, and Y. Pan, "A study of the routing and spectrum allocation in spectrum-sliced elastic optical path networks," in 2011 Proceedings Ieee Infocom, pp. 1503–1511, IEEE, 2011.
- [62] P. Lechowicz and K. Walkowiak, "Genetic algorithm for routing and spectrum allocation in elastic optical networks," in 2016 Third European Network Intelligence Conference (ENIC), pp. 273–280, IEEE, 2016.
- [63] B. C. Chatterjee, N. Sarma, and P. P. Sahu, "Review and performance analysis on routing and wavelength assignment approaches for optical networks," IETE Technical Review, vol. 30, no. 1, pp. 12–23, 2013.
- [64] B. C. Chatterjee, N. Sarma, P. P. Sahu, and E. Oki, Routing and wavelength assignment for wdm-based optical networks: quality-of-service and fault resilience, vol. 410. Springer, 2016.
- [65] X. Zhou, W. Lu, L. Gong, and Z. Zhu, "Dynamic rmsa in elastic optical networks with an adaptive genetic algorithm," in 2012 IEEE Global Communications Conference (GLOBECOM), pp. 2912–2917, IEEE, 2012.
- [66] K. Christodoulopoulos, I. Tomkos, and E. A. Varvarigos, "Elastic bandwidth allocation in flexible OFDM-based optical networks," Journal of Lightwave Technology, vol. 29, no. 9, pp. 1354–1366, 2011.
- [67] D. T. Hai and K. M. Hoang, "An efficient genetic algorithm approach for solving routing and spectrum assignment problem," in 2017 International Conference on Recent Advances in Signal Processing, Telecommunications & Computing (SigTelCom), pp. 187–192, IEEE, 2017.
- [68] F. Ilchmann et al., "Efficient and optimized network architecture: Requirements and reference scenarios," Strongest, 2010.
- [69] T. Ahmed et al., "Dynamic routing, spectrum, and modulation-format allocation in mixed-grid optical networks," Journal of Optical Communications and Networking, vol. 12, no. 5, pp. 79–88, 2020.

- [70] E. Archambault et al., “Routing and spectrum assignment in elastic filterless optical networks,” IEEE/ACM Transactions on Networking, vol. 24, no. 6, pp. 3578–3592, 2016.
- [71] A. L. Chiu, G. Choudhury, G. Clapp, R. Doverspike, M. Feuer, J. W. Gannett, J. Jackel, G. T. Kim, J. G. Klincewicz, T. J. Kwon, et al., “Architectures and protocols for capacity efficient, highly dynamic and highly resilient core networks,” Journal of Optical Communications and Networking, vol. 4, no. 1, pp. 1–14, 2012.
- [72] M. Gupta and S. Singh, “Greening of the internet,” in Proceedings of the 2003 conference on Applications, technologies, architectures, and protocols for computer communications, pp. 19–26, 2003.
- [73] A. Gati, F. E. Salem, A. M. G. Serrano, D. Marquet, S. L. Masson, T. Rivera, D.-T. Phan-Huy, Z. Altman, J.-B. Landre, O. Simon, et al., “Key technologies to accelerate the ICT green evolution—an operator’s point of view,” arXiv preprint arXiv:1903.09627, 2019.
- [74] G. Shen and R. S. Tucker, “Energy-minimized design for IP over WDM networks,” Journal of Optical Communications and Networking, vol. 1, no. 1, pp. 176–186, 2009.
- [75] J. Baliga, R. Ayre, K. Hinton, W. V. Sorin, and R. S. Tucker, “Energy consumption in optical IP networks,” Journal of Lightwave Technology, vol. 27, no. 13, pp. 2391–2403, 2009.
- [76] W. Van Heddeghem, F. Idzikowski, W. Vereecken, D. Colle, M. Pickavet, and P. Demeester, “Power consumption modeling in optical multilayer networks,” Photonic Network Communications, vol. 24, no. 2, pp. 86–102, 2012.
- [77] A. Andrae, “Total consumer power consumption forecast,” Nordic Digital Business Summit, vol. 10, p. 69, 2017.
- [78] Y. Zhang, P. Chowdhury, M. Tornatore, and B. Mukherjee, “Energy efficiency in telecom optical networks,” IEEE Communications Surveys & Tutorials, vol. 12, no. 4, pp. 441–458, 2010.
- [79] R. A. Butt, M. Faheem, M. W. Ashraf, and S. M. Idrus, “Sleep assistive dynamic bandwidth assignment scheme for passive optical network (PON),” Photonic Network Communications, vol. 36, no. 3, pp. 289–300, 2018.
- [80] J.-i. Kani, “Power saving techniques and mechanisms for optical access networks systems,” Journal of Lightwave Technology, vol. 31, no. 4, pp. 563–570, 2012.
- [81] S. Garg and A. Dixit, “Evaluating power saving techniques in passive optical access networks,” Photonic Network Communications, vol. 42, no. 1, pp. 1–14, 2021.
- [82] J. Borger, A. Ionescu-Graff, S. Kulkarni, and N. Raman, “Economics of ethernet over sonet/sdh,” Bell Labs Technical Journal, vol. 12, no. 1, pp. 187–206, 2007.
- [83] M. Maier, Optical switching networks. Cambridge University Press, 2008.

- [84] A. Bianco, T. Bonald, D. Cuda, and R.-M. Indre, "Cost, power consumption and performance evaluation of metro networks," Journal of Optical Communications and Networking, vol. 5, no. 1, pp. 81–91, 2013.
- [85] X. Dong, T. E. El-Gorashi, and J. M. Elmirghani, "On the energy efficiency of physical topology design for IP over WDM networks," Journal of Lightwave Technology, vol. 30, no. 12, pp. 1931–1942, 2012.
- [86] L. Guo, W. Hou, X. Wei, and S. Lv, "Power efficient grooming based on optical bypass reconfiguration in green optical networks," Optik, vol. 124, no. 5, pp. 437–445, 2013.
- [87] F. Idzikowski, S. Orłowski, C. Raack, H. Woesner, and A. Wolisz, "Saving energy in IP-over-WDM networks by switching off line cards in low-demand scenarios," in 2010 14th Conference on Optical Network Design and Modeling (ONDM), pp. 1–6, IEEE, 2010.
- [88] P.-K. Tseng and W.-H. Chung, "Near optimal link on/off scheduling and weight assignment for minimizing IP network energy consumption," Computer Communications, vol. 35, no. 6, pp. 729–737, 2012.
- [89] Y. Zhang, M. Tornatore, P. Chowdhury, and B. Mukherjee, "Energy optimization in IP-over-WDM networks," Optical Switching and Networking, vol. 8, no. 3, pp. 171–180, 2011.
- [90] E. Palkopoulou, D. A. Schupke, and T. Bauschert, "Energy efficiency and capex minimization for backbone network planning: Is there a tradeoff?," in 2009 IEEE 3rd International Symposium on Advanced Networks and Telecommunication Systems (ANTS), pp. 1–3, IEEE, 2009.
- [91] W. Van Heddeghem and F. Idzikowski, "Equipment power consumption in optical multilayer networks-source data," Photonic Network Comm, 2012.
- [92] I. Alimi, R. Patel, N. Silva, C. Sun, H. Ji, W. Shieh, A. Pinto, and N. Muga, "A review of self-coherent optical transceivers: Fundamental issues, recent advances, and research directions," Applied Sciences, vol. 11, no. 16, p. 7554, 2021.
- [93] D. Che, X. Chen, A. Li, Q. Hu, Y. Wang, and W. Shieh, "Optical direct detection for 100g short reach applications," in 2014 Asia Communications and Photonics Conference (ACP), pp. 1–3, IEEE, 2014.
- [94] K. Kikuchi, "Digital coherent optical communication systems: Fundamentals and future prospects," IEICE Electronics Express, vol. 8, no. 20, pp. 1642–1662, 2011.
- [95] Z. Jia and L. A. Campos, "Coherent optics ready for prime time in short-haul networks," IEEE Network, vol. 35, no. 2, pp. 8–14, 2021.
- [96] A. Shahpari, R. M. Ferreira, R. S. Luis, Z. Vujicic, F. P. Guiomar, J. D. Reis, and A. L. Teixeira, "Coherent access: A review," Journal of Lightwave Technology, vol. 35, no. 4, pp. 1050–1058, 2016.
- [97] Z. Jia and L. A. Campos, Coherent Optics for Access Networks. CRC Press, 2019.

- [98] M. Erkiñiç, D. Lavery, K. Shi, B. Thomsen, R. Killely, S. Savory, and P. Bayvel, “Bidirectional wavelength-division multiplexing transmission over installed fibre using a simplified optical coherent access transceiver,” *Nature communications*, vol. 8, no. 1, pp. 1–10, 2017.
- [99] W. Jin, X. Duan, M. Bolea, R. Giddings, N. Jing, C. Zhang, K. Qiu, and J. Tang, “New roadms with dsp-enabled dynamic and flexible operations for elastic optical networks,” in *2015 Optical Fiber Communications Conference and Exhibition (OFC)*, pp. 1–3, IEEE, 2015.
- [100] P. Pavon-Marino, M.-V. Bueno-Delgado, and J.-L. Izquierdo-Zaragoza, “Evaluating internal blocking in noncontentionless flex-grid roadms,” *Journal of Optical Communications and Networking*, vol. 7, no. 3, pp. A474–A481, 2015.
- [101] R. Casellas, R. Munoz, J. M. Fabrega, M. S. Moreolo, R. Martinez, L. Liu, T. Tsuritani, and I. Morita, “Design and experimental validation of a gmpls/pce control plane for elastic CO-OFDM optical networks,” *IEEE Journal on Selected Areas in Communications*, vol. 31, no. 1, pp. 49–61, 2012.
- [102] M. S. Moreolo, J. M. Fàbrega, L. Nadal, F. J. Vílchez, and G. Junyent, “Bandwidth variable transponders based on OFDM technology for elastic optical networks,” in *2013 15th International Conference on Transparent Optical Networks (ICTON)*, pp. 1–4, IEEE, 2013.
- [103] N. Sambo, P. Castoldi, A. D’Errico, E. Riccardi, A. Pagano, M. S. Moreolo, J. M. Fabrega, D. Rafique, A. Napoli, S. Frigerio, et al., “Next generation sliceable bandwidth variable transponders,” *IEEE Communications Magazine*, vol. 53, no. 2, pp. 163–171, 2015.
- [104] E. Riccardi, A. Pagano, E. Hugues-Salas, G. Zervas, D. Simeonidou, M. Bohn, A. Napoli, D. Rafique, A. D’Errico, N. Sambo, et al., “Sliceable bandwidth variable transponder: The idealist vision,” in *2015 European Conference on Networks and Communications (EuCNC)*, pp. 330–334, IEEE, 2015.
- [105] G. Meloni, T. Rahman, A. Napoli, F. Fresi, N. Sambo, A. D’Errico, D. Rafique, M. Nölle, H. de Waardt, M. Bohn, et al., “Experimental comparison of transmission performance for Nyquist WDM and time–frequency packing,” *Journal of Lightwave Technology*, vol. 33, no. 24, pp. 5261–5268, 2015.
- [106] V. López, B. de la Cruz, Ó. G. de Dios, O. Gerstel, N. Amaya, G. Zervas, D. Simeonidou, and J. P. Fernandez-Palacios, “Finding the target cost for sliceable bandwidth variable transponders,” *Journal of Optical Communications and Networking*, vol. 6, no. 5, pp. 476–485, 2014.
- [107] M. S. Moreolo, J. M. Fabrega, L. Nadal, F. J. Vílchez, A. Mayoral, R. Vilalta, R. Muñoz, R. Casellas, R. Martínez, M. Nishihara, et al., “Sdn-enabled sliceable bvt based on multicarrier technology for multiframe rate/distance and grid adaptation,” *Journal of Lightwave Technology*, vol. 34, no. 6, pp. 1516–1522, 2015.

- [108] Infinera, “Baud rate, modulation, and maximizing coherent optical performance.” <https://www.infinera.com/wp-content/uploads/Baud-Rate-Modulation-and-Maximizing-Coherent-Optical-Performance-0294-WP-RevA-0921.pdf>, 2021.
- [109] D. Krause, A. Awadalla, A. S. Karar, H. Sun, and K.-T. Wu, “Design considerations for a digital subcarrier coherent optical modem,” in *2017 Optical Fiber Communications Conference and Exhibition (OFC)*, pp. 1–3, IEEE, 2017.
- [110] M. Qiu, Q. Zhuge, M. Chagnon, Y. Gao, X. Xu, M. Morsy-Osman, and D. V. Plant, “Digital subcarrier multiplexing for fiber nonlinearity mitigation in coherent optical communication systems,” *Opt. Express*, vol. 22, pp. 18770–18777, Jul 2014.
- [111] H. Sun, M. Torbatian, M. Karimi, R. Maher, S. Thomson, M. Tehrani, Y. Gao, A. Kumpera, G. Soliman, A. Kakkar, et al., “800g DSP ASIC design using probabilistic shaping and digital sub-carrier multiplexing,” *Journal of lightwave technology*, vol. 38, no. 17, pp. 4744–4756, 2020.
- [112] A. Rashidinejad, A. Nguyen, M. Olson, S. Hand, and D. Welch, “Real-time demonstration of 2.4 tbps (200gbps/) bidirectional coherent DWDM-PON enabled by coherent Nyquist subcarriers,” in *Optical Fiber Communication Conference*, pp. W2A–30, Optica Publishing Group, 2020.
- [113] S. J. Savory, “Digital filters for coherent optical receivers,” *Optics express*, vol. 16, no. 2, pp. 804–817, 2008.
- [114] B. Spinnler, “Equalizer design and complexity for digital coherent receivers,” *IEEE Journal of Selected Topics in Quantum Electronics*, vol. 16, no. 5, pp. 1180–1192, 2010.
- [115] J. A. Hernández, M. Quagliotti, L. Serra, L. Luque, R. L. da Silva, A. Rafel, Ó. G. de Dios, V. López, A. Eira, R. Casellas, et al., “Comprehensive model for techno-economic studies of next-generation central offices for metro networks,” *Journal of Optical Communications and Networking*, vol. 12, no. 12, pp. 414–427, 2020.
- [116] A. Rashidinejad et al., “Real-time demonstration of 2.4tbps (200gbps/) bidirectional coherent DWDM-PON enabled by coherent Nyquist subcarriers,” in *2020 OFC*, Optical Society of America, 2020.
- [117] J. Bäck et al., “Capex savings enabled by point-to-multipoint coherent pluggable optics using digital subcarrier multiplexing in metro aggregation networks,” in *ECOC*, pp. 1–4, IEEE, 2020.
- [118] J. Pedro, A. Eira, and N. Costa, “Metro transport architectures for reliable and ubiquitous service provisioning,” in *2018 Asia Communications and Photonics Conference and Exhibition (ACP)*, pp. 1–3, IEEE, 2018.
- [119] FP7 IDEALIST Project Deliverable D1.1, “Elastic optical network architecture: Reference scenario, cost and planning.” <https://cordis.europa.eu/docs/projects/cnect/9/317999/080/deliverables/001-D11ElasticOpticalNetworkArchitecture.doc>.

- [120] J. Bäck, J. Pedro, T. Schaich, A. Napoli, P. Wright, A. Chase, D. Welch, and A. Lord, “Hubbedness: a metric to describe traffic flows in optical networks and an analysis of its impact on efficiency of point-to-multipoint coherent transceiver architectures,” in ECOC, pp. 1–4, IEEE, 2021.
- [121] The Boston Consulting Group, “Reforming europe’s telecoms regulation to enable the digital single market.” https://etno.eu/datas/publications/studies/BCG_ETNO_REPORT_2013.pdf.
- [122] M. R. Bussieck and A. Meeraus, “General algebraic modeling system (GAMS),” in Modeling languages in mathematical optimization, pp. 137–157, Springer, 2004.
- [123] I. Chlamtac and A. Gumaste, “Light-trails: A solution to IP centric communication in the optical domain,” in International Workshop on Quality of Service in Multiservice IP Networks, pp. 634–644, Springer, 2003.
- [124] A. Gumaste and I. Chlamtac, “Light-trails: a novel conceptual framework for conducting optical communications,” in Workshop on High Performance Switching and Routing, 2003, HPSR., pp. 251–256, IEEE, 2003.
- [125] B. Jaumard, Y. Wang, and N. Huin, “Optimal design of filterless optical networks,” in 2018 20th International Conference on Transparent Optical Networks (ICTON), pp. 1–5, IEEE, 2018.
- [126] J. Pedro and A. Eira, “Hybrid backup resource optimization for VNF placement over optical transport networks,” in 2019 International Conference on Optical Network Design and Modeling (ONDM), pp. 1–6, IEEE, 2019.
- [127] A. Itai and M. Rodeh, “The multi-tree approach to reliability in distributed networks,” Information and Computation, vol. 79, no. 1, pp. 43–59, 1988.
- [128] M. O. Ball, T. Magnanti, C. L. Monma, and G. L. Nemhauser, Handbooks in Operations Research and Management Science: Network Models. North-Holland, 1995.
- [129] J. Chen, S. Khanmohamadi, F. Abtahi, L. Wosinska, Z. Xu, A. Cassidy, C. Tremblay, P. Littlewood, S. Asselin, and M. P. Bélanger, “Passive wide area network solutions: Filterless and semi-filterless optical networks,” in 2011 13th International Conference on Transparent Optical Networks, pp. 1–1, IEEE, 2011.
- [130] T. P. Wright, “Factors affecting the cost of airplanes,” Journal of the aeronautical sciences, vol. 3, no. 4, pp. 122–128, 1936.
- [131] M. Bourreau, C. Cambini, and P. Doğan, “Access pricing, competition, and incentives to migrate from “old” to “new” technology,” International Journal of Industrial Organization, vol. 30, no. 6, pp. 713–723, 2012.
- [132] A. Odlyzko, “Internet pricing and the history of communications,” Computer networks, vol. 36, no. 5-6, pp. 493–517, 2001.
- [133] G. E. Moore et al., “Cramming more components onto integrated circuits,” 1965.

- [134] T. Barnett, S. Jain, U. Andra, and T. Khurana, “Cisco visual networking index (vni) complete forecast update, 2017–2022,” Americas/EMEAR Cisco Knowledge Network (CKN) Presentation, pp. 1–30, 2018.
- [135] E. Bonetto, E. Le Rouzic, L. Sadeghioon, P. Gavignet, B. Arzur, and O. Renais, “Facing the traffic explosion in metro transport networks with energy-sustainable architectures,” Photonic Network Communications, vol. 30, no. 1, pp. 29–42, 2015.
- [136] C. Kronberger, T. Schondienst, and D. A. Schupke, “Impact and handling of demand uncertainty in multiperiod planned networks,” in 2011 IEEE International Conference on Communications (ICC), pp. 1–6, IEEE, 2011.
- [137] T. Panayiotou and G. Ellinas, “Addressing traffic prediction uncertainty in multi-period planning optical networks,” in 2022 Optical Fiber Communications Conference and Exhibition (OFC), pp. 1–3, IEEE, 2022.
- [138] M. Geilen, T. Basten, B. Theelen, and R. Otten, “An algebra of pareto points,” Fundamenta Informaticae, vol. 78, no. 1, pp. 35–74, 2007.
- [139] T. Horvath, P. Munster, V. Oujezsky, and N.-H. Bao, “Passive optical networks progress: a tutorial,” Electronics, vol. 9, no. 7, p. 1081, 2020.
- [140] P. Pavon-Marino, N. Skorin-Kapov, M. Bueno-Delgado, J. Bäck, and A. Napoli, “On the benefits of point-to-multipoint coherent optics for multilayer capacity planning in ring networks with varying traffic profiles,” Journal of Optical Communications and Networking, vol. 14, no. 5, pp. B30–B44, 2022.
- [141] L. S. de Sousa and A. C. Drummond, “Metropolitan optical networks: A survey on single-layer architectures,” Optical Switching and Networking, p. 100719, 2022.
- [142] J. Bäck, A. Napoli, E. Riccardi, M. Quagliotti, M. Porrega, J. Pedro, T. A. Eriksson, F. Masoud, A. Mathur, and D. Welch, “A filterless design with point-to-multipoint transceivers for cost-effective and challenging metro/regional aggregation topologies,” in 2022 International Conference on Optical Network Design and Modeling (ONDM), pp. 1–6, IEEE, 2022.
- [143] D. Uzunidis, M. Presi, A. Sgambelluri, F. Paolucci, A. Stavdas, and F. Cugini, “Bidirectional single-fiber filterless optical networks: modeling and experimental assessment,” Journal of Optical Communications and Networking, vol. 13, no. 6, pp. C1–C9, 2021.
- [144] F. Cugini, C. Porzi, N. Sambo, A. Bogoni, and P. Castoldi, “Receiver architecture with filter for power-efficient drop&waste networks,” in Optical Fiber Communication Conference, pp. W2A–41, Optical Society of America, 2016.
- [145] G. Serafino, A. Malacarne, C. Porzi, F. Fresi, G. Meloni, P. Velha, L. Potì, A. Bogoni, and F. Cugini, “Semi filter-less drop & waste network demonstration with integrated soi optical filter,” in 2017 European Conference on Optical Communication (ECOC), pp. 1–3, IEEE, 2017.
- [146] N. Deo, Graph theory with applications to engineering and computer science. Courier Dover Publications, 2017.

- [147] Z. Xu, E. Archambault, C. Tremblay, J. Chen, L. Wosinska, M. P. Bélanger, and P. Littlewood, “1+ 1 dedicated optical-layer protection strategy for filterless optical networks,” IEEE communications letters, vol. 18, no. 1, pp. 98–101, 2013.
- [148] S. Khanmohamadi, J. Chen, F. Abtahi, L. Wosinska, A. Cassidy, É. Archambault, C. Tremblay, S. Asselin, P. Littlewood, and M. Bélanger, “Semi-filterless optical network: a cost-efficient passive wide area network solution with effective resource utilization,” in 2011 Asia Communications and Photonics Conference and Exhibition (ACP), pp. 1–3, IEEE, 2011.
- [149] N. Amaya, G. Zervas, and D. Simeonidou, “Introducing node architecture flexibility for elastic optical networks,” Journal of Optical Communications and Networking, vol. 5, no. 6, pp. 593–608, 2013.
- [150] X. Mu, S. Wu, L. Cheng, and H. Fu, “Edge couplers in silicon photonic integrated circuits: A review,” Applied Sciences, vol. 10, no. 4, p. 1538, 2020.
- [151] C. Kopp, S. Bernabe, B. B. Bakir, J.-M. Fedeli, R. Orobtchouk, F. Schrank, H. Porte, L. Zimmermann, and T. Tekin, “Silicon photonic circuits: on-cmos integration, fiber optical coupling, and packaging,” IEEE Journal of selected topics in quantum electronics, vol. 17, no. 3, pp. 498–509, 2010.
- [152] J. Teng, J. Yang, C. Lv, T. Chen, J. Guo, J. Feng, and P. Wu, “Guidelines for design and fabrication of fused fiber coupler based wavelength division multiplexings,” Optical Fiber Technology, vol. 20, no. 3, pp. 239–244, 2014.
- [153] É. Archambault, D. O’Brien, C. Tremblay, F. Gagnon, M. P. Bélanger, and É. Bernier, “Design and simulation of filterless optical networks: Problem definition and performance evaluation,” Journal of Optical Communications and Networking, vol. 2, no. 8, pp. 496–501, 2010.
- [154] I. Cale, A. Salihovic, and M. Ivekovic, “Gigabit passive optical network-GPON,” in 2007 29th International Conference on Information Technology Interfaces, pp. 679–684, IEEE, 2007.
- [155] A. Agata and Y. Horiuchi, “PON network designing algorithm for suboptimal deployment of optical fiber cables,” in 2009 Asia Communications and Photonics conference and Exhibition (ACP), vol. 2009, pp. 1–6, IEEE, 2009.
- [156] A. Kawakita, K. Hara, Y. Kimura, K. Horikawa, H. Furukawa, Y. Suzuki, and S. Ikeda, “Design for long-reach coexisting PON in consideration of area characteristics with wavelength selective asymmetrical splitters,” in 2019 24th OptoElectronics and Communications Conference (OECC) and 2019 International Conference on Photonics in Switching and Computing (PSC), pp. 1–3, IEEE, 2019.
- [157] K. Grobe and J.-P. Elbers, “PON in adolescence: from TDMA to WDM-PON,” IEEE Communications Magazine, vol. 46, no. 1, pp. 26–34, 2008.
- [158] Y. Park, C. Lim, and I. Jung, “Onu power equalization of ethernet PON systems,” IEEE Photonics Technology Letters, vol. 16, no. 8, pp. 1984–1986, 2004.

-
- [159] M. Dalla Santa, C. Antony, G. Talli, and P. D. Townsend, “Variable gain soa pre-amplifier for optical equalization of a 25gb/s burst-mode PON upstream with 10g optics,” in 2019 Optical Fiber Communications Conference and Exhibition (OFC), pp. 1–3, IEEE, 2019.
- [160] J. A. Besley, J. D. Love, and W. Langer, “A multimode planar power splitter,” Journal of lightwave technology, vol. 16, no. 4, pp. 678–684, 1998.
- [161] “Openzr+ 400g digital coherent optics for multi-haul.” https://openzrplus.org/site/assets/files/1074/openzrplus_whitepaper_-_sept_29_2020_final.pdf.
- [162] S. Katoch et al., “A review on genetic algorithm: past, present, and future,” Multimedia Tools and Applications, vol. 80, pp. 8091–8126, 2021.
- [163] G. D’Angelo and F. Palmieri, “GGA: A modified genetic algorithm with gradient-based local search for solving constrained optimization problems,” Information Sciences, vol. 547, pp. 136–162, 2021.
- [164] D. W. Coit and A. E. Smith, “Penalty guided genetic search for reliability design optimization,” Computers & industrial engineering, vol. 30, no. 4, pp. 895–904, 1996.
- [165] Z. Michalewicz and M. Schoenauer, “Evolutionary algorithms for constrained parameter optimization problems,” Evolutionary computation, vol. 4, no. 1, pp. 1–32, 1996.
- [166] N. Fan and M. Golari, “Integer programming formulations for minimum spanning forests and connected components in sparse graphs,” in International Conference on Combinatorial Optimization and Applications, pp. 613–622, Springer, 2014.

Appendix A

How to Formulate ILP Problems Using GAMS

A.1 What is GAMS

GAMS is a modelling system for high-level mathematical programming and optimization. It is made up of a language compiler and a number of associated solvers such CPLEX.

A.2 Minimum Spanning Tree Problem

Given an undirected graph $G(V, E)$, where V is the vertex set with cardinality $|V| = n$, and E is the edge set. A tree is a subgraph of G , which has no cycle. A minimum spanning tree (MST) is a tree that spanned to all nodes and has the minimum total edge weight. There are several algorithms for finding this tree such as Prim's algorithm and Kruskal's algorithm. Figure. A.1 illustrates an undirected graph with 6 nodes and 8 links and its MST obtained by a MATLAB function. The total weights on this MST is 14.

Listing A.1 MATLAB code for minimum spanning tree

```
1 clear
2 clc
3 %%%%%%%%%%%%%%%%%%%%%%%%%%%%%%%%%%%%%%%%%%%%%%%%%%%%%%%%%%%%%%%%%%%%%%%%%
4 s = [1 2 3 4 5 5 6 6]; %% Source nodes
5 t = [2 3 4 5 3 6 2 1]; %% Destination nodes
6 w = [4 3 5 1 4 6 2 6]; %% Weights
7 h = graph(s,t,w); %% Building undirected graph
8 plot(h) %% Plot the graph
9 MST = minspantree(h); %% Minimum Spanning Tree
```

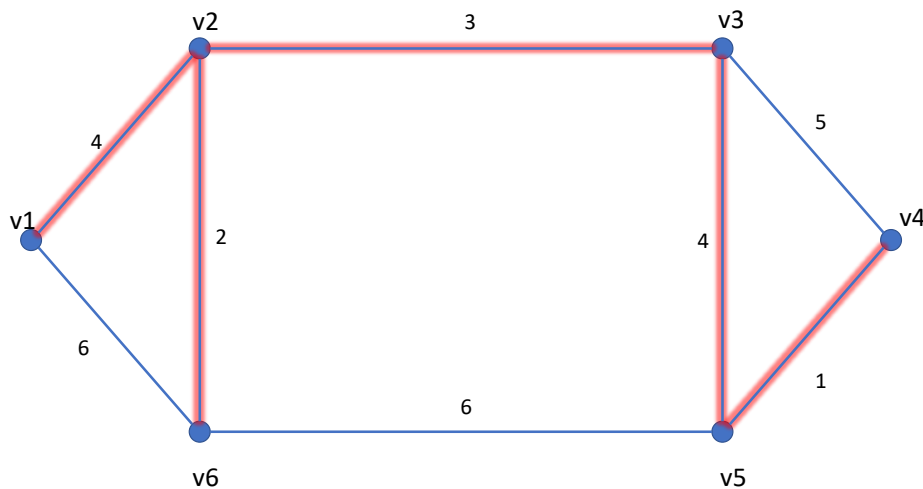


Fig. A.1 An undirected graph and its MST

A.3 ILP formulation Using GAMS

We can solve this problem using integer linear programming. A spanning tree is an undirected simple graph T (with n vertices) that satisfies any one of the following equivalent conditions:

- T has no simple cycles and has $n - 1$ edges.
- T is connected and has $n - 1$ edges.

The MST problem (like many other problems) can be represented differently considering the above properties. For example, the subtour elimination formulation is based on the fact that G has no simple cycles and has $n - 1$ edges [166].

Single commodity flow formulation is based on the fact that G is connected and has $n - 1$ edges. Let's assume $x_{ij} \in \{0, 1\}$ denotes whether edge $(i, j) \in E$ is selected into tree if $x_{ij} = 1$ or not if $x_{ij} = 0$. The ILP formulation can be presented:

$$\min \sum_{(i,j) \in E} w_{ij} x_{ij} \quad (\text{A.1})$$

subject to:

$$\sum_{(i,j) \in E} x_{ij} = n - 1 \quad (\text{A.2})$$

$$\sum_j f_{j1} - \sum_j f_{1j} = n - 1 \quad (\text{A.3})$$

$$\sum_j f_{j1} - \sum_j f_{1j} = 1, \quad \forall i \in V, i \neq 1 \quad (\text{A.4})$$

$$f_{ij} \leq (n-1)x_{ij}, \quad \forall (i, j) \in E \quad (\text{A.5})$$

$$f_{ji} \leq (n-1)x_{ij}, \quad \forall (i, j) \in E \quad (\text{A.6})$$

$$f_{ji} \geq 0, \quad \forall (i, j) \in E \cup E' \quad (\text{A.7})$$

$$x_{ij} \in 0, 1, \quad \forall (i, j) \in E \quad (\text{A.8})$$

Equation (A.1) is the objective function that has to be minimized. Constraint (A.2) ensures the size of tree must be $n - 1$. According to constraint (A.3), $n - 1$ units of flows generated at node v_1 and all other nodes receive only one unit based on constrain (A.4). Constraints (A.5) and (A.6) enforces that flows only existed on treed and do not exceed the maximum flow i.e. $n - 1$. Constrain (A.7) ensures that flows are positive where E' denotes set of edges with opposite direction for edges in E . x_{ij} is binary variable according to constraint (A.8).

To formulate this in GAMS we implement three different steps:

1. Introducing sets
2. Introducing input parameters
3. Introducing variable
4. Writing constraints as equations
5. Creating a model and selecting a solver and its options

We usually use sets for defining objects in our problems that correspond exactly to the indices in the algebraic representations. Here, we have a set of nodes and a set of links. Input parameters are often attributed to objects. They can be scalars, vectors, or tables. In MST problem, the weights of links are input parameters. There is always a free range variable that needs to be optimized. The other decision variables depend on the way of ILP formulation. Variables are specified by type: FREE, POSITIVE, NEGATIVE, BINARY, or INTEGER. In our considered example, x_{ij} and f_{ij} are binary and positive variables, respectively. Equations present the objective and constraint functions using all those input parameters and variables.

They are first declared by giving them names. Then their general algebraic formulae are described. Finally, solve statement is used to pick the right solver to solve the model. Below is the ILP for MST problem in the GAMS environment.

Listing A.2 GAMS ILP formulation for MST problem

```

3  set i index of nodes /v1*v6/;
4  Alias (i, j);
5  set nonroot(i) v1 is the root of tree /v2*v6/;
6  set e(i, j) index of links /v1.v2
7                                v2.v3
8                                v3.v4
9                                v4.v5
10                               v5.v3
11                               v5.v6
12                               v6.v2
13                               v6.v1/;

15  ***** Inputs *****
16  Parameters
17  w(i, j) set of weights /v1.v2 4
18                                v2.v3 3
19                                v3.v4 5
20                                v4.v5 1
21                                v5.v3 4
22                                v5.v6 6
23                                v6.v2 2
24                                v6.v1 6/;
25  scalar n number of nodes;
26  n = card(i);
27  ***** Optimization variables *****
28  variable z optimization variable;
29  positive variable f(i, j) flow on links;
30  binary variable x(i, j) selection of links;

32  ***** Obj fun & constraints *****
33  Equations
34  ObjFun      **minimization of tree**

36  cons1      **size of tree**
37  cons2      **flow at root**
38  cons3(i)   **flow at other nodes**

```



```

39 cons4(i,j)  **bounds of flows**
40 cons5(i,j)  **bounds of flows**
41 ;

43 ObjFun      ..z =e= sum((i,j)$e(i,j), w(i,j)*x(i,j));

45 cons1      ..sum((i,j)$e(i,j) ,x(i,j)) =e= n-1;
46 cons2      ..sum(j ,f('v1',j)) - sum(j,f(j,'v1')) =e= n
              -1;
47 cons3(i)    $nonroot(i)  ..sum(j ,f(j,i)) - sum(j,f(i,j)) =e= 1;
48 cons4(i,j)  $e(i,j)      ..f(i,j) =l= (n-1)*x(i,j);
49 cons5(i,j)  $e(i,j)      ..f(j,i) =l= (n-1)*x(i,j);
50 %%%%%%%%%%%%% modelling & solving %%%%%%%%%%%%%
51 model MST /all/;
52 solve MST using MIP minimizing z;
53 option MIP = CPLEX;
54 Display x.l,z.l,f.l;

```

Note that constraints (A.7) and (A.8) already considered when defining variables in lines 27 and 28.

A.4 Integer Linear Programming Techniques

Converting real problems to ILP formulations can be challenging. Usually, there is more than one way to implement an ILP formulation. In this section, some guidance on formulation is provided.

A.4.1 sets

As discussed earlier, in the context of optical networks, we might have a set of links, a set of nodes, a set of frequency slots, a set of amplifier types, a set of splitter/combiner types, a set of locations, etc. These sets must have specified by indices. For instance, we have 3 types of amplifiers, namely a_1 , a_2 , and a_3 ; then, we formulate it by giving a name (index) to set and specify the elements inside the set as follows:

```

1 set a /a1, a2, a3/;

```

Sometimes it is necessary to create two or more sets representing the same entity. This is usually helpful in defining nodes. For instance, if there are 5 nodes, we can create two same sets as follows:

```

1 set v /v1, v2, v3, v4, v5/;
2 Alias (v, u);

```

Sometimes, two or more sets have some inter-dependency. For example, links in optical networks always are terminated by nodes. So, the set of links can be defined using indices used in defining nodes:

```

1 set e (u, v) /v1.v2, v2.v3, v3.v4, v4.v5, v5.v6/;

```

where these sets of nodes and links present a ring graph(network).

A.4.2 Variables

Variables are those values that we are interested in finding through solving the ILP program. They are usually describing or counting resources. Binary variables only can take 0 or 1. This makes it suitable for presenting the state of an entity, such as "active" or "not active", "occupied" or "not occupied", and "selected" or "not selected". On the other hand, positive integer variables are used mainly for counting. Free variables that can take any values are used for objective functions. Let's say optical links have 80 channels, and channels are represented by index (set) f , the state of channel f on link (u, v) can be presented by binary variables $x(f, u, v)$. 1 means it is occupied and 0 means the channel is free. Note that sometimes it is helpful to define intermediate variables. We are not directly interested in these variables, but these help more straightforward formulation and finding values of variables of interest.

A.4.3 Constraints

Constraints are our preferences, physical limitations, and design interests that are presented as linear (nonlinear in the case of nonlinear programming) equations or inequalities. Constraints define the space of the solution, and solvers look for the optimized solutions within this search space. For instance, we are interested in not using more than 50 channels of spectrum capacity of all links. This constraint can be written as:

$$\sum_f x_f^{uv} \leq 50 \quad \forall (u, v) \in E \quad (\text{A.9})$$

and formulated in GAMS program as:

```

1 cons1 (u, v) $e (u, v) .. sum (f, x (f, u, v)) =l= 50;

```

where *cons1* is the constraint name, $Se(u, v)$ limits the constraint only to defined links.

Another great technique is MinMax or MaxMin optimization. This is helpful when we want to maximize the minimum of a variable and vice versa. For example, maximizing the quality of service in the worst scenario. Let us say we are interested in maximizing the minimum values of variable *y*. We can define an assist variable *k*. Using the below constraint, *w* will present a lower bound of *y*:

```
1 cons      ..k =l= y;
```

and the objective function will be:

```
1 obj      ..z = k;
```

A.4.4 Objective Function

The objective function (variable) is the final goal of the program. However, objectives are not always clear, and there are multiple objectives. In such cases, objectives can be combined to have a single objective: the more weighting factor, the more emphasis. Let us consider that we have two objectives, *M* and *N*. We can combine this like:

```
1 obj      ..z = w_1 * M + w_2 * N;
```

One can play with parameter w_2 to achieve the best scenario or do an extensive analysis on a large range of w_2 . If w_2 is small enough (depending on the relative values of *M* and *N*), the maximization program translated to optimizing *M* first and then optimizing *N*.

A.5 Connecting MATLAB and GAMS

Although MATLAB can solve optimization problems, it is not practical to use for large-scale problems (especially for non-linear programming). However, MATLAB has a solid and wide variety of capabilities to manipulate and plot the data. Therefore, the combination of GAMS and MATLAB can be advantageous. GAMS (version 2021) has MATLAB callable functions that can efficiently import and export data to and from GAMS through GDX (GAMS Data eXchange) files. GDX provides basic functionalities for exchanging GAMS data, such as reading and writing (for more about GDX see Link).

First of all, it is necessary to install both MATLAB and GAMS on your machine. Then set the MATLAB path to the GAMS directory (where GAMS is installed). A GAMS file and a MATLAB file have to be created and saved in this directory (other methods like setting

environment variables are also possible). We explain the procedure by solving the minimum spanning tree program in Appendix A. However, we give the values for length of the links from MATLAB and also returning the values of variable after optimization to the MATLAB.

Compared to the GAMS program in Appendix A, lines 1, 25-27, and 54-59 are newly added. Line 1 determines the variable for exporting to MATLAB. Lines 25-27 gets the values for w . When this model is executed, another file 'matsol.gdx' will be created because of the `execute_unload` statement in the last line of the model.

Listing A.3 Example program for interfacing GAMS and MATLAB: GAMS part

```

1 $set matout "'matsol.gdx', z, x, returnStat";

3 set i index of nodes /v1*v6/;
4 Alias (i, j);
5 set nonroot(i) v1 is the root of tree /v2*v6/;
6 set e(i,j) index of links /v1.v2
7                               v2.v3
8                               v3.v4
9                               v4.v5
10                              v5.v3
11                              v5.v6
12                              v6.v2
13                              v6.v1/;

15 ***** Inputs *****
16 Parameters
17 w(i,j) set of weights;
18 scalar n number of nodes;
19 n = card(i);
20 ***** Optimization variables *****
21 variable z optimization variable;
22 binary variable x(i,j) selection of links;
23 positive variable f(i,j) flow on links;
24 ***** Import from MATLAB via GDX *****
25 $gdxin Optional_name.gdx
26 $load w
27 $gdxin
28 ***** Obj fun & constraints *****
29 Equations
30 ObjFun      **minimization of tree**

32 cons1      **size of tree**
33 cons2      **flow at root**
34 cons3(i)   **flow at other nodes**

```

```

35 cons4(i,j)  **bounds of flows**
36 cons5(i,j)  **bounds of flows**
37 ;

39 ObjFun      ..z =e= sum((i,j)$e(i,j), w(i,j)*x(i,j));

41 cons1      ..sum((i,j)$e(i,j) ,x(i,j)) =e= n-1;
42 cons2      ..sum(j ,f('v1',j)) - sum(j,f(j,'v1')) =e= n-1;
43 cons3(i)    $nonroot(i) ..sum(j ,f(j,i)) - sum(j,f(i,j)) =e= 1;
44 cons4(i,j)  $e(i,j)     ..f(i,j) =l= (n-1)*x(i,j);
45 cons5(i,j)  $e(i,j)     ..f(j,i) =l= (n-1)*x(i,j);
46 *%%%%%%%%%%%%%% modelling & solving %%%%%%%%%%%%%%%
47 model MST /all/;
48 solve MST using MIP minimizing z;
49 option MIP = CPLEX;
50 Display x.l,z.l,f.l;

52 *%%% Exporting the value of variables defined in the first line %%%

54 Set stat / modelStat, solveStat /;

56 Parameter returnStat(stat);
57 returnStat('modelStat') = MST.modelstat;
58 returnStat('solveStat') = MST.solvestat;
59 execute_unload %matout%;

```

In the MATLAB file, all necessary inputs for the GAMS program have to be defined as structures. Then, it is written to the same.gdx file called from GAMS (Optional_name.gdx). The "System" command calls the operating system to execute the specified command. The operation waits for the command to finish execution before returning the exit status of the command to the status variable. Finally 'gams' command (line 21) imports the variables defined in the first line of the GAMS program (z, x). Lines 30 and 31 extracts the source and destination of links from the structure x .

Listing A.4 Example program for interfacing GAMS and MATLAB: MATLAB part

```

2 clear
3 clc
4 %%%%%%%%%%%%%%% Inputs to GAMS %%%%%%%%%%%%%%%
5 %% The parameters have to be a MATLAB structure for sending to GAMS
6 lengths.name = 'w';    %% Parameter that we want to send to GAMS

```

```

8 lengths.type = 'parameter';    %% Type of parameter (either "scalar" or "
    parameter")
9 lengths.val = [0 4 0 0 0 0;    %% values
10              0 0 3 0 0 0;
11              0 0 0 5 0 0;
12              0 0 0 0 1 0;
13              0 0 4 0 0 6;
14              6 2 0 0 0 0];
15 lengths.form = 'full';
16 lengths.dim = 2;    %% 0 if scalar, 1 if vector and 2 if parameter (
    including tables)
17 lengths.uels = {'v1' 'v2' 'v3' 'v4' 'v5' 'v6'}, {'v1' 'v2' 'v3' 'v4' 'v5'
    'v6'};
18 wgdxd('Optional_name.gdx', lengths);    %% write created input to a GDX
    file
19 %%%%%%%%% Command to GAMS to Solve the program in MST %%%%%%%%%
20 system(('gams MST lo=2 --TRIP='));    %% Tell the operating system to run
    "MST"
21 [z,x] = gams('MST');    %% Returning values from GAMS to MATLAB
22 z.val    %% show the objective value

24 %%%%%%%%%%%%%%% Higlighting the Tree %%%%%%%%%%%%%%%
25 s = [1 2 3 4 5 5 6 6];    %% Source nodes
26 t = [2 3 4 5 3 6 2 1];    %% Destination nodes
27 w = [4 3 5 1 4 6 2 6];    %% Weights
28 h = graph(s,t,w);    %% Biulding undirected graph
29 graph_plot = plot(h)    %% Plot the graph
30 s_tree = x.val(:,1);
31 t_tree = x.val(:,2);
32 highlight(graph_plot,s_tree,t_tree)    %% Minimum Spanning Tree

```
